MONTHLY NOTICES

OF THE

ROYAL ASTRONOMICAL SOCIETY

Volume 119 No. 5 1959

Published and Sold by the

ROYAL ASTRONOMICAL SOCIETY
BURLINGTON HOUSE
LONDON, W.1

Price £1 0s. 0d.; *in U.S.A.* $3

Annual Subscription for volume of six numbers: £5 5s. 0d.; *in U.S.A.* $16

Recent publications of the Society

MEMOIRS

of the

Royal Astronomical Society

Vol. LXVIII, Part II

Price 12*s.* 0*d.; in U.S.A.* $1.90

CONTENTS

OCCASIONAL NOTES

of the

Royal Astronomical Society

Vol. 3, No. 21

Price 5*s.* 0*d.; in U.S.A.* $0.90

CONTENTS

Orders should be addressed to

THE ASSISTANT SECRETARY,

ROYAL ASTRONOMICAL SOCIETY, BURLINGTON HOUSE, LONDON, W.1, ENGLAND.

MONTHLY NOTICES

OF THE

ROYAL ASTRONOMICAL SOCIETY

Vol. 119 No. 5

MEETING OF 1959 MARCH 13

Professor R. O. Redman, President, in the Chair

The election by the Council of the following Fellows was duly confirmed:—

Donald van-Burren Dun, 17 Victoria Gardens, London W.11 (proposed by W. B. Caunter); and

Anthony Fynn, S.J., Riverview College Observatory, Riverview, Sydney, Australia.

The election by the Council of the following Junior Members was duly confirmed:—

Thornsteinn Saemundsson, University of London Observatory, Mill Hill Park, London, N.W.7 (proposed by C. W. Allen);

Nigel Oscar Weiss, University Dept. of Geodesy and Geophysics, Cambridge (proposed by N. M. Hill); and

Bernard Douglas Yallop, Mathematics Dept., Imperial College, London, S.W.7 (proposed by G. J. Whitrow).

Seventy-seven presents were announced as having been received since the last meeting, including:—

G. Alter: *Two renaissance astronomers: David Gans — Joseph Delmedigo* (presented by the author);

A. Becvar: *Atlas eclipticalis* 1950.0 (presented by the Czech Academy of Sciences); and

M. Waldmeier: *Leitfaden der astronomischen Orts-und Zeitbestimmung*, 2nd edition (presented by the author).

MEETING OF 1959 APRIL 10

Professor R. O. Redman, President, in the Chair

The President announced that the Council had elected the following Associates of the Society:—

Nicholas Ulrich Mayall, Lick Observatory, Mount Hamilton, California, U.S.A.;

William Wilson Morgan, Yerkes Observatory, Williams Bay, Wisconsin, U.S.A.; and

Alexi Boriseivitch Severny, Crimean Astrophysical Observatory of Academy of Sciences U.S.S.R., Pochtove, Crimea, U.S.S.R.

Recent publications of the Society

MEMOIRS

of the

Royal Astronomical Society

Vol. LXVIII, Part II

Price 12*s.* 0*d.*; *in U.S.A.* $1.90

CONTENTS

OCCASIONAL NOTES

of the

Royal Astronomical Society

Vol. 3, No. 21

Price 5*s.* 0*d.*; *in U.S.A.* $0.90

CONTENTS

Orders should be addressed to

THE ASSISTANT SECRETARY,

ROYAL ASTRONOMICAL SOCIETY, BURLINGTON HOUSE, LONDON, W.1, ENGLAND.

MONTHLY NOTICES

OF THE

ROYAL ASTRONOMICAL SOCIETY

Vol. 119 No. 5

MEETING OF 1959 MARCH 13

Professor R. O. Redman, President, in the Chair

The election by the Council of the following Fellows was duly confirmed:—

Donald van-Burren Dun, 17 Victoria Gardens, London W.11 (proposed by W. B. Caunter); and

Anthony Fynn, S.J., Riverview College Observatory, Riverview, Sydney, Australia.

The election by the Council of the following Junior Members was duly confirmed:—

Thornsteinn Saemundsson, University of London Observatory, Mill Hill Park, London, N.W.7 (proposed by C. W. Allen);

Nigel Oscar Weiss, University Dept. of Geodesy and Geophysics, Cambridge (proposed by N. M. Hill); and

Bernard Douglas Yallop, Mathematics Dept., Imperial College, London, S.W.7 (proposed by G. J. Whitrow).

Seventy-seven presents were announced as having been received since the last meeting, including:—

G. Alter: *Two renaissance astronomers: David Gans — Joseph Delmedigo* (presented by the author);

A. Becvar: *Atlas eclipticalis* 1950.0 (presented by the Czech Academy of Sciences); and

M. Waldmeier: *Leitfaden der astronomischen Orts-und Zeitbestimmung*, 2nd edition (presented by the author).

MEETING OF 1959 APRIL 10

Professor R. O. Redman, President, in the Chair

The President announced that the Council had elected the following Associates of the Society:—

Nicholas Ulrich Mayall, Lick Observatory, Mount Hamilton, California, U.S.A.;

William Wilson Morgan, Yerkes Observatory, Williams Bay, Wisconsin, U.S.A.; and

Alexi Boriseivitch Severny, Crimean Astrophysical Observatory of Academy of Sciences U.S.S.R., Pochtove, Crimea, U.S.S.R.

The election by the Council of the following Fellows was duly confirmed:—

Fazal Ahmed, Royal Observatory, Edinburgh (proposed by H. A. Brück);
Edward Doylerush, Tyn Leydiant, Roewen, Conway, Caerns. (proposed by J. Davis);
Jan A. Högbom, 25 Victoria Street, Cambridge (proposed by M. Ryle);
J. D. North, 35 North Way, Headington, Oxford (proposed by C. W. Allen);
Dennis John Pearson, 40 Beechwood Road, Uplands, Swansea (proposed by B. E. Featherstone);
John Roland Shakeshaft, Cavendish Laboratory, Cambridge (proposed by M. Ryle);
Harry Sykes, Central Electricity Board, Butterworth, Malaya (proposed by A. F. O'D. Alexander);
Arthur George Tearle, 26 Wilsden Avenue, Luton, Beds. (proposed by H. C. King); and
Alan Burgess, Physics Department, University College, London, W.C.1 (proposed by M. J. Seaton).

The election by the Council of the following Junior Member was duly confirmed:—

John Edward Basil Ponsonby, 26 Upper High Street, Thame, Oxon (proposed by J. Heywood).

Eighty-five presents were announced as having been received since the last meeting, including:—

Royal Astronomical Society: *Franklin Adams Charts* (presented by Mrs. Wilfred Merton); and
G. J. Whitrow: *The structure and evolution of the universe* (presented by the author).

MEETING OF 1959 MAY 8

Professor R. O. Redman, President, in the Chair

The election by the Council of the following Fellows was duly confirmed:—

Simon Fairfax Humphrey John Archer, Norman Lockyer Observatory, Sidmouth, Devon (proposed by D. R. Barber);
Serge Colombo, Institut Henri-Poincaré, Paris, France (proposed by V. C. A. Ferraro);
John Aldworth Gould, 24 Salisbury Street, Swindon (proposed by A. P. Lenham);
Donald Harvey Tarling, 35 Thornhill Road, Sparkhill, Birmingham 11 (proposed by J. M. Bruckshaw); and
Wilfred Wallbank, 6 Waterside Cottages, Everton, Chorley, Lancs. (proposed by W. Granger).

The election by the Council of the following Junior Members was duly confirmed:—

Petros Serghiou Florides, Royal Holloway College, Englefield Green, Surrey (proposed by W. H. McCrea); and

Gillian Peach, Royal Holloway College, Englefield Green, Surrey (proposed by M. R. C. McDowell).

Eighty-two presents were announced as having been received since the last meeting, including:—

International Astronomical Union: ***Second conference on co-ordination of galactic research*** (presented by I.A.U.); and

R. D. Davies and H. P. Palmer: ***Radio studies of the universe*** (presented by Routledge & Kegan Paul Ltd.).

A NEW DETERMINATION OF THE CENTRE TO LIMB CHANGE IN SOLAR WAVE-LENGTHS

M. G. Adam

(Communicated by the Director, University Observatory, Oxford)

(Received 1959 May 4)

Summary

The centre to limb increase in wave-length, which is observed for medium strength solar lines, occurs almost wholly over the last 10 per cent of the way across the disk. So far, measurements have not been made in this region with nearly high enough disk resolution. The Oxford 35 m telescope, which gives a solar image of radius 165 mm, is used to make detailed observations of limb effect for 261 disk points in latitudes near to the solar equator. The observed points all lie close to the limb, at radial distances from the centre between 85 and 100 per cent of the disk radius. The individual observations show considerable fluctuations about a mean curve, which are attributed to the local velocity fields which are known to exist on the Sun. The systematic differences which appear in the measures from the east limb and the west limb, for radial distances greater than 98 per cent of the disk radius, are shown to be the result of light scattering. In the observational determination of the limb-effect curve it is most important that distortions, due to velocity fields and scattered light, should be taken into account.

The new limb-effect curve is in fair agreement with the old determinations, over the range in common. At the extreme limb there is a shift with respect to the centre wave-lengths which, expressed as a Doppler velocity, amounts to 0·53 km sec^{-1}. This indicates at the extreme limb a red shift of 0·84 km sec^{-1} compared with the Einstein shift of 0·636 km sec^{-1}.

Introduction.—Following Evershed's pioneer work on the change in wave-lengths across the solar disk (**8**), detailed observations have been made at Potsdam (**9**) and at Oxford (**1**), and these have formed the basis of theoretical discussions of the subject. Although the two series of observations are in good agreement, there are still peculiarities and deficiencies in the observational relation between wave-length and disk position, which make further measurements a matter of some importance for the problem of solar wave-lengths. On the visible disk the Fraunhofer line wave-lengths do not differ from their centre values by as much as 0·001 A until 85–90 per cent of the way towards the limb, and after this they increase rapidly to become some 0·007 A longer than the centre wave-lengths. Fig. 1 shows this centre to limb behaviour, for medium-strength lines, as observed at Oxford in 1948. The 'limb effect' $\Lambda(\theta^*)$, by which we mean now wave-length observed at disk position θ^* minus wave-length observed at the disk centre, is expressed as a Doppler velocity in km sec^{-1} and is plotted against cosine θ^*, where θ^* is the angle between the line of sight and the solar radius at the point of observation. This representation of limb effect is strictly relevant to the radial streaming interpretation, and is more suitable for Freundlich's path length interpretation than the usual plot of $\Lambda(\theta^*)$ with sin θ^*. The vertical lines through the observed

points in Fig. 1 show the estimated uncertainty in $\Lambda(\theta^*)$, and the horizontal lines show the range in cosine θ^* covered by each observed point.

The first necessity in improving the observations is obviously to work with much higher resolution on the solar disk, and thus to reduce the range in cosine θ^* covered by each observed point. The Potsdam observations were made with a resolution probably comparable with that shown in Fig. 1, and the number of observed points is the same. In making more precise observations it is important to take into account the recent work on motions in the solar photosphere (11), (12), (15), (17); this work shows the existence of long-lived small scale and large scale velocity fields on the Sun, which will superpose Doppler shifts on the limb effect observed at any point. Such velocity-field effects may be reduced by making observations at many close points on the disk, and by combining observations from several different regions on the Sun.

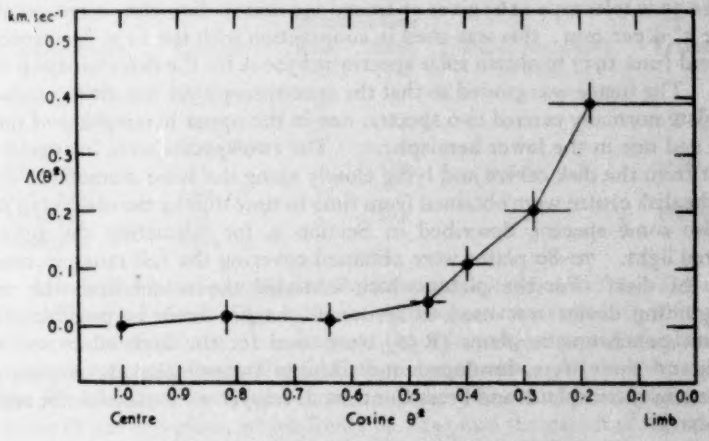

FIG. 1.—*Solar limb effect as observed in* 1948
Wave-length region 6100 *A.* 14 *lines: mean Rowland number* 6.

For the theoretical interpretation of limb effect, it is observations near to the solar limb, and particularly at $\theta^* = \pi/2$, which provide the most sensitive test. We see that in Fig. 1 the extreme point covers the range in cos θ^* 0·25 − 0·00, and it is here especially that high disk resolution is desirable. But this 25 per cent range in cos θ^* with which we are particularly concerned corresponds to a range of only 3 per cent in the distance from limb to centre, and detailed observations can only be made in this region with a very large solar image. Moreover it is the region within which the disk intensity drops very sharply from 60 per cent to zero, and this means that the observations are very susceptible to any effects introduced by the scattering of light, instrumentally or by the Earth's atmosphere.

The Oxford 35 m telescope, with its large solar image, and the associated high-dispersion grating spectroscope form excellent equipment for a redetermination of the limb effect curve. The paper gives an account of the first results for solar latitudes near to the equator, and cosine θ^* values between 0·5 and 0·0. The measures are differential and give only the change in wave-length from centre to limb. The new observational material and its measurement and reduction to give the observed limb effect are described in Section 1. These results show that the

scattering of light must be taken into account in deriving the limb effect for cosine $\theta^* < 0{\cdot}2$, and this problem is investigated in Section 2. The paper concludes with a short comparison of the final limb-effect curve with theoretical predictions.

1. *The observational material, measurement and reduction*

1.1. *Solar spectra.*—For the detailed point-to-point observations on the solar disk which we now wish to make, it is essential to adopt the method of measuring the solar lines against telluric lines in the same wave-length region. Only in this way can we avoid spurious displacements arising from any differences in collimator illumination. The new grating spectroscope gives sufficient dispersion to work in the red at 6300 A with atmospheric oxygen lines as standards. This is a favourable region in which to measure medium-strength solar lines, and the constant strength of the oxygen lines gives them a considerable advantage over the water vapour lines for our purpose.

The 35 m telescope (**16**) gives an image 330 mm in diameter, corresponding to a scale 5″·9 per mm; this was used in conjunction with the 11 m spectroscope in May and June 1957 to obtain solar spectra at 6300 A for the determination of limb effect. The image was guided so that the spectroscope slit was always radial, and each plate normally carried two spectra, one in the upper hemisphere of the solar image and one in the lower hemisphere. The two spectra were for points equidistant from the disk centre and lying closely along the same diameter. Spectra from the disk centre were obtained from time to time during the observing period, and also some spectra, described in Section 2, for estimating the amount of scattered light. 70–80 plates were obtained covering the full range in cosine θ^* across the disk. For the plates which included the actual limb the rocking plate guiding device was used to secure as sharp a limb as possible. Ilford half-tone panchromatic plates (R 50) were used for the limb effect and centre spectra and these were developed in Parkhurst two-solution developer; Ilford R 40 panchromatic plates and Press Contrast developer were used for the scattered light plates.

Because of the rotation of the solar image the full series of plates covers a wide range of latitudes in the two hemispheres. For a first investigation measurements have been confined to six heavily exposed limb spectra which were especially favourable for measurements close to the extreme limb. These were obtained fairly close to the solar equator, and include the limb and about 20 mm on to the disk; the range in cosine θ^* is 0·0 to 0·5. The details for these six spectra are given in Table I: ten centre spectra obtained on seven days have also been measured, and three of the scattered light spectra

TABLE I

Details of measured limb plates

Plate No.	Date U.T. 1957	Exp.	Region	Solar latitude in degrees
18a	May 22·5906	40 secs.	East limb	−11·53 to −12·36
18b	22·5946	40 secs.	West limb	+11·09 to +13·73
19a	22·6036	40 secs.	West limb	+13·85 to +16·92
19b	22·6081	40 secs.	East limb	−16·99 to −18·62
20a	22·6165	40 secs.	East limb	−19·66 to −21·70
20b	22·6211	40 secs.	West limb	+19·23 to +23·21

The Bausch and Lomb grating was used in the spectroscope in the first order, giving a dispersion of 1·4 mm A^{-1} at 6300 A, or in terms of Doppler velocities

33·98 km sec^{-1} per mm shift on the plate. Following preliminary measurements in the region it was decided to work with seven lines, four oxygen lines to serve as standards, and three solar lines. The selected lines are shown in Table II: the oxygen lines alternate with the solar lines and span the whole wave-length range. An analysis of the measurements on the east and west limbs, showed that these oxygen lines were apparently free from blends with unsuspected solar lines. The I.A.U. 1928 tables contain wave-lengths for six of the seven lines: the wave-length given for the oxygen line 6302·0 A is a mean value from Babcock's measures (4) and the Allegeheny Observatory—Bureau of Standards wave-lengths (6). The Rowland numbers of the lines are given in column three, and for the iron lines we have also shown the multiplet number and lower state excitation potential as given in Miss Moore's Multiplet Table (1945).

TABLE II

Measured lines

I.A.U. wave-length in A	Element	Row. No:	Mult. No:	Excit. pot. (low) in volts	Transition
6295·960	Atm. O_2	3			
6297·799	Fe	5	62	2·21	a^5P–y^5D^0
6299·228	Atm. O_2	3			
6301·508	Fe	7	816	3·64	z^5P^0–e^5D
[6302·000]	Atm. O_2	2			
6302·499	Fe	5	816	3·67	z^5P^0–e^5D
6302·764	Atm. O_2	2			

1.2. *Micrometer measurements and the determination of line shifts.*—The spectra have been measured with a Hilger photomeasuring micrometer which is fitted with a transverse motion on the plate stage (15); this motion greatly facilitates the measurements at many close points in the same spectrum. All the measurements of centre, limb, and scattered light spectra have been made with a diaphragm in the focal plane of the eye-piece, which limits to 0·145 mm the extent of the spectrum which is visible, perpendicular to the dispersion.

The measurements in the limb spectra were designed to give a uniform spread in cosine θ^* values. This means that the measured points were very close together near to the extreme limb and at gradually increasing intervals further in on the disk. The limb plates were marked, perpendicular to the dispersion, with fine scratches at mm intervals from the inner edge of the spectrum. Two sets of marks were made, one to the red of the wave-length region at 6337 A and the other to the violet at 6278 A. The limb formed the other edge of the spectrum, and its position was estimated visually with respect to the mm marks. The results from the two ends showed an uncertainty of the order of 0·04 mm in its position. In a normally exposed spectrum Miss Hart (11) has found that visual estimates agree well with photometric determinations. But, as Dr Treanor has pointed out, there may be systematic displacements with heavy exposures. The R 50 plates, however, have a very steep characteristic curve, which would reduce any such effect and the fair agreement of the estimates from the two ends of the plate, where the photographic density is noticeably different, indicate that it is small. Measurements parallel to the dispersion were made as soon as the photographic density at the limb edge of the spectrum permitted it; this gave measurements for four or five points in the scattered sky light beyond the estimated limb. The first 10 measured points

were at 0·1 mm intervals, the next 10 at 0·2 mm intervals, then 10 at 0·5 mm intervals and the remaining 13 or 14 at 1 mm intervals. This arrangement gives a fairly uniform spread in cosine θ^* values; we now have 24 measured points in the region covered by the first observed point in Fig. 1. For the six limb spectra measurements were made in all at 261 points on the disk.

Disk positions were calculated in terms of ρ the radial distance of the measured point from the disk centre, and ρ_0 the disk radius. We obtain $\rho_0-\rho$ from the estimated limb position and the particular point of measurement, both known with respect to the mm scratches. The image radius ρ_0 at the time of observation was obtained from a series of direct measures on the solar image which gave $\rho_0 = 167{\cdot}1$ mm in the spectroscope slit plane, for an angular radius of 16′. The spectroscope magnification can be assumed to be unity.

In deducing line shifts from the micrometer measurements we have followed the procedure as described by Professor Plaskett (**15**). The measurements in the centre spectra were used to set up 'standard' micrometer readings for the seven lines. The solar lines were first of all corrected for the observer's motion with respect to the solar centre, and the mean reading from the ten spectra was then taken as the standard setting for any line. For the solar lines this reduces the effect of velocity fields on the Sun; the standard error of the mean reading for a solar line was equivalent to a velocity of 0·04 km sec^{-1} (average value for the three lines). This estimate includes measurement errors in the solar and oxygen lines as well as any real variations due to velocity fields, though estimates of the measurement errors showed that the scatter was chiefly due to field effects.

For the limb spectra the micrometer measurements of the oxygen lines in each spectrum were used to set up a correction curve for the spectrum, to reduce the solar measurements to the dispersion of the standard settings. The correction curve was assumed to be linear over the very short wave-length range with which we are concerned. The corrected shifts for the solar lines were then coverted into Doppler velocities with factors 34·00, 33·99 and 33·97 km sec^{-1} per mm shift for the three lines in the order of Table II. The three velocity shifts were then used to form a mean velocity shift for the disk point. In order to point out the main features of the observational problem, we show in Fig. 2 the mean velocities so obtained for the east limb spectrum and the west limb spectrum, from Plate 18 in Table I. The velocities shown include solar rotation and limb effect and also effects due to the observer's motion; these last change only very slightly over the observed range in ρ/ρ_0. On the east limb we see that solar rotation and limb effect combine to give a nearly constant observed velocity, whereas on the west limb both effects give a red shift, and the observed velocity increases steeply as we approach the limb. An outstanding feature of the observations is the fluctuation, which increases with distance from the limb, about the general form of the two curves. In the light of the work on photospheric motions which we have quoted earlier, it appears that we are again observing the phenomenon of velocity fields on the solar surface. An analysis of the departures of the individual line velocities from the mean for any one disk point, gives 0·08 km sec^{-1} for the standard error of a single line velocity. From an examination of these residuals we conclude that there are no systematic differences in the centre-limb behaviour of individual lines within $\pm$ 0·03 km sec^{-1}. Assuming that measurement errors in the solar and oxygen lines are comparable in size, we then estimate fluctuations due to this cause at 0·06 km sec^{-1}, (standard error of a

single disk-point velocity). We see that the observed fluctuations are definitely greater than this and must indicate real variations from point to point on the solar disk.

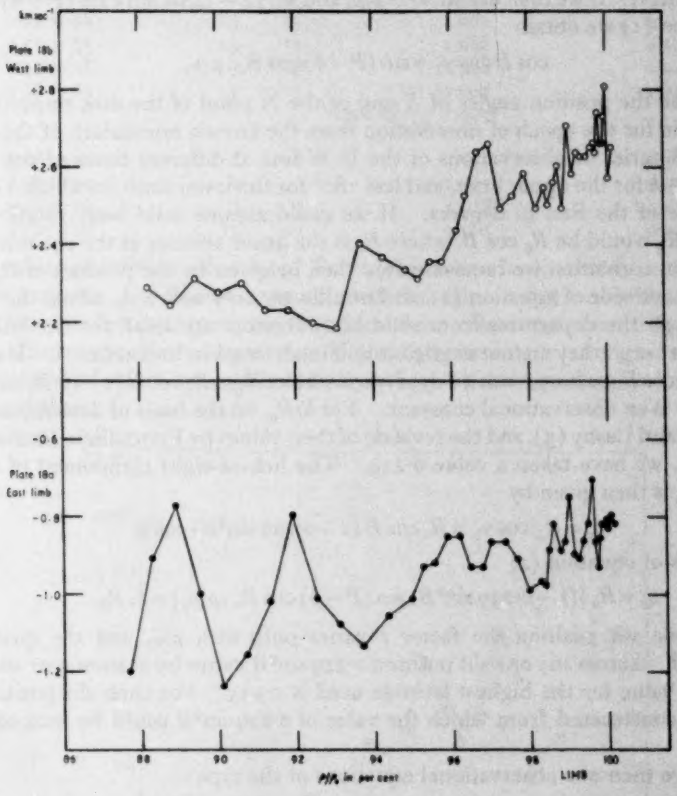

FIG. 2.—*Velocities observed on the east and west solar limbs (Plate* 18).
Open circles—west limb.
Filled circles—east limb.

1.3. *Correction for Earth's motion and solar rotation.*—In the correction for Earth's motion and the calculations for solar rotation we have followed very closely the scheme set out by Professor Plaskett (14). In almost all these calculations it was possible to work at representative values of ρ/ρ_0 across the slit, for the epoch of exposure, and then use interpolated values for the 44 measured points. The corrections for Earth's motion were found to vary linearly across the slit, and all the disk-point velocities obtained as described in the previous section were first of all reduced to velocities on the Sun (v_{obs}), by applying this correction.

We assume that $v_{obs.}$ at any point X on the disk is due wholly to solar rotation and limb effect $\Lambda(\theta^*)$. The component of solar rotation along the line of sight will be $R_B \cos\gamma_1$ where R_B is the linear velocity of solar rotation at the latitude B of X, and γ_1 is the angle between the line of sight and the direction of solar rotation at X. Then from Section 3·3 in (14) we have

$$\cos\gamma_1 = \sin(L - L_0)\cos B_0 \sin\theta^* \operatorname{cosec}\theta \qquad (1)$$

in which $(L-L_0)$ is the difference between the solar longitude of X, and L_0 the longitude of the centre of the projected disk, and B_0 is the latitude of the disk centre, θ is the angle between the line of sight to the disk centre and the solar radius to the point X. If we then use $\sin\theta^* \simeq \rho/\rho_0$ and $\sin(L-L_0) = \sin\theta \sin(P-\phi)\sec B$ in equation (1) we obtain

$$\cos B \cos\gamma_1 = \sin(P-\phi)\cos B_0 \,.\, \rho/\rho_0 \qquad (2)$$

ϕ and P are the position angles of X and of the N point of the disk respectively. ϕ we obtain for the epoch of observation from the known orientation of the solar image. A series of observations of the E–W line at different times of day gave $\phi = 231{\cdot}2 + h$ for the upper limb, and less 180° for the lower limb, in which h is the hour angle of the Sun in degrees. If we could assume solid body rotation for the Sun, R_B would be $R_0 \cos B$, where R_0 is the linear velocity at the equator, and the rotation correction we require would then be given by the product of R_0 and the right hand side of equation (2), and would vary only with ρ/ρ_0, across the slit.

Although the departures from solid body rotation are small for our latitude range of 12°–23°, they are not negligible and must be taken into account. Instead of $R_B = R_0 \cos B$ we have, with a Faye type formula, $R_B = R_0 \cos B\,(1-(b/R_0)\sin^2 B)$ in which b is an observational constant. For b/R_0, on the basis of determinations by Adams and Lasby (**3**), and the revision of their values by Freundlich, Brunn and Brück (**9**), we have taken a value 0·229. The line-of-sight component of solar rotation v_r is then given by

$$v_r = R_B \cos\gamma_1 = R_0 \cos B\,(1-0{\cdot}229\sin^2 B)\cos\gamma_1$$

or in terms of equation (2)

$$v_r = R_0\,[(1-0{\cdot}229\sin^2 B)\sin(P-\phi)\cos B_0 \,.\, \rho/\rho_0] = f\,.\,R_0. \qquad (3)$$

For any one slit position the factor f varies only with ρ/ρ_0 and the quantity $0{\cdot}229\sin^2 B$. Across any one slit position $0{\cdot}229\sin^2 B$ varies by at most 0·01 and its maximum value for the highest latitude used is 0·035. For each slit position a curve was constructed from which the value of $0{\cdot}229\sin^2 B$ could be read off for each ρ/ρ_0.

We have then 261 observational equations of the type

$$v_{obs.} = f\,.\,R_0 + \Lambda(\theta^*)$$

in which the unknowns are R_0 and $\Lambda(\theta^*)$.* $\Lambda(\theta^*)$ is a function of ρ/ρ_0, the form of which we are investigating, and in order to obtain R_0 we must combine equations at the same value of ρ/ρ_0. In order to reduce velocity-field effects and to use the directly observed velocities we have made solutions for R_0 combining observations over short ranges in ρ/ρ_0. We know that $\Lambda(\theta^*)$ varies only very slowly for our inner disk points, and further out, where $\Lambda(\theta^*)$ changes more rapidly, we must restrict ourselves to very short ranges in ρ/ρ_0. We then obtain R_0 from each range and a mean value for $\Lambda(\theta^*)$ over the range. Table III shows the result of least squares solutions of the observational equations for R_0 and $\Lambda(\theta^*)$; the range in ρ/ρ_0 we have given in terms of cosine θ^*, and we have also shown the number of observational equations used from each limb. In the lower half of the table we give the results obtained very close to the limb: the number of observational equations is reduced because of the small range in cos θ^*. As we shall see in the next section it appears that these results, obtained so near to the limb, are affected by scattered light. The purpose of our present calculations is to obtain a value for R_0 which we can then use to find $\Lambda(\theta^*)$ with high disk resolution: we see that the

TABLE III

Least squares solutions for R_0 and $\Lambda(\theta^*)$

Range in cos θ^*	No. of obs: vel: E	W	R_0 km sec^{-1}	$\Lambda(\theta^*)$ km sec^{-1}
0·47–0·42	15	15	2·002	0·156
0·41–0·35	15	15	1·986	0·186
0·33–0·28	15	15	1·992	0·248
0·28–0·22	15	15	2·007	0·354
		Mean val:	1·997	
0·08–0·06	8	7	1·946	0·384
0·06–0·04	4	3	1·941	0·398
0·04–0·02	3	3	1·918	0·456
0·02–0·00	12	11	1·901	0·443

mean values of $\Lambda(\theta^*)$ in column 4 of Table III increase fairly steadily in the way we should expect. For R_0 we have adopted the value 1·997 km sec^{-1}, the mean value from the first four groups in the table: these values come from a region of the disk unlikely to be affected by scattered light, and where $\Lambda(\theta^*)$ changes only slowly. The individual values are each based on 30 observational equations and they agree well together.

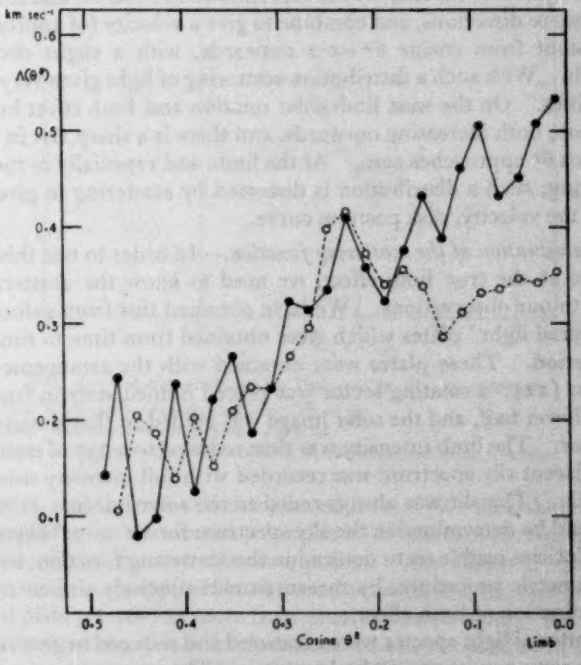

FIG. 3.—*The observed limb effect.*
Open circles—west limb.
Filled circles—east limb.

1.4. *The observed limb effect.*—With this value of R_0 and the appropriate f factors we have derived a value of $\Lambda(\theta^*)$ for each of our 261 points. The resulting limb effect curves for the east limb and the west limb are shown in Fig. 3. For

each limb the values of $\Lambda(\theta^*)$ from the three plates have been grouped together in intervals of 0·02 in cosine θ^* to give a mean value for the interval. Comparing Fig. 3 with Fig. 2 we see that the velocity-field effects are much reduced by this combination of the observations. From $\cos\theta^* = 0{\cdot}5$ to 0·2 the east and west limb curves agree well together, but the anomalous feature of the new measures is the steadily increasing difference between the two curves from $\cos\theta^* = 0{\cdot}2$ to 0·0, which amounts to 0·2 km sec^{-1} at the extreme limb.

2. *The effect of scattered light on the observed curve*

Further in on the disk, the differences between the east and west limb observations in Fig. 3 might be attributed to local velocity fields persisting in the mean from three different disk positions. But from $\cos\theta^* = 0{\cdot}2$ to the extreme limb we cover $1{\cdot}4 \times 10^5$ km on the Sun, which corresponds to 190″ at the disk centre, so that in view of their estimated sizes, we must be averaging out field effects. The plates 18, 19, 20 were taken in that order over an interval of 40 minutes, during which the sky conditions, although reasonably good, were noted to be deteriorating, and we find that the departures of the west limb curves from the east limb curves increase in the same order. There seems little doubt that the peculiarities in the observations for points further out than $\cos\theta^* = 0{\cdot}2$, must be the result of scattered light.

We saw in Section 1.2 that on the east limb solar rotation and limb effect give shifts in opposite directions, and combine to give a velocity (of approach) which is almost constant from cosine $\theta^* = 0{\cdot}2$ outwards, with a slight decrease at the extreme limb. With such a distribution scattering of light gives very little change in the velocities. On the west limb solar rotation and limb effect both act in the same direction, both increasing outwards, and there is a sharp rise in the resultant velocity as $\cos\theta^*$ approaches zero. At the limb, and especially in the presence of limb darkening, such a distribution is distorted by scattering to give a less steep gradient for the velocity, disk position curve.

2.1. *Determination of the scattering function.*—In order to test this explanation and to arrive at the true limb effect, we need to know the scattering function appropriate to our observations. We have obtained this from velocity measures in the 'scattered light' plates which were obtained from time to time during the observing period. These plates were obtained with the arrangement described by Miss Hart (11): a rotating sector was placed immediately in front of the slit to cover the lower half, and the solar image was guided so that the upper limb fell over the sector. The limb intensity was thus reduced to 0·035 of its normal value, while the adjacent sky spectrum was recorded with full intensity using the upper half of the slit. The slit was always radial to the solar image. In these spectra velocities could be determined in the sky spectrum for 10″ to 70″ beyond the limb, and these velocities enable us to determine the scattering function, independently of any photometric procedure, by measurements precisely similar to those used in the determination of limb effect.

Three scattered light spectra were measured and reduced to give velocity shifts in exactly the same way as the six limb spectra. The measurements were made at three points on the disk and nine or ten points in the sky spectrum, the furthest measured point being 76″ from the solar limb. Fig. 4 shows for two of the plates the measured velocities as a function of ρ/ρ_0; the shifts are corrected for Earth's motion, assuming that the scattered sky light requires the same correction as the limb points on the solar disk. The smooth curves show, for each of the plates, the

velocity distribution on the disk as calculated from a combination of solar rotation v_r and limb effect $\Lambda(\theta^*)$ at each point. v_r was obtained using the value of R_0 as in Section 1·3 assuming, for our present purpose, that we have solid body rotation: as a best approximation to the true value, $\Lambda(\theta^*)$ was taken as observed on the east limb. The scattered light spectra are all for the west limb, approximately 30°

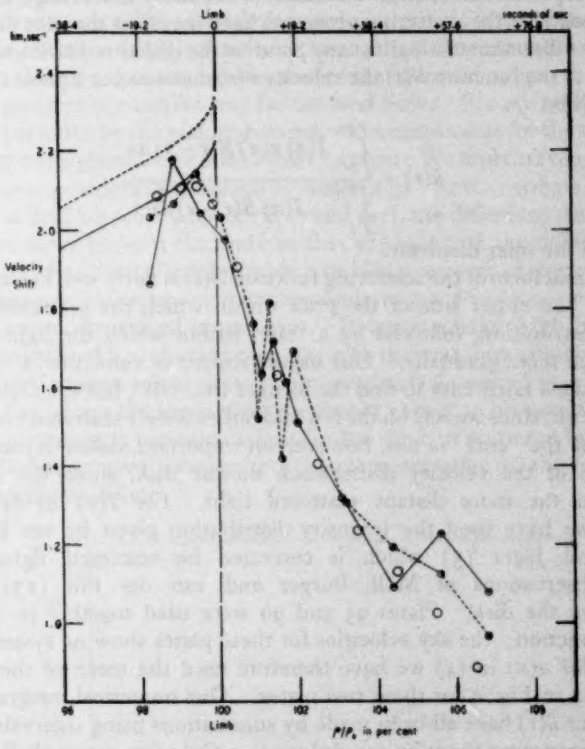

FIG. 4.—*Velocity shifts at the limb and in the sky spectrum.*
Half filled circles—continuous line: Plate 95.
Half filled circles—dotted line: Plate 96.
Open circles: calculated points using the deduced scattering function.

from the equator, and the two velocities are additive. We seek then a scattering function which, from the unsmeared velocities of the smooth curves, will produce the distribution shown by the observed points. The plates 95 and 96 were regarded as approximately typical for sky conditions during the observing period, while the third plate referred to more than usual scattered light. We see that the velocities observed on the disk fall below what we should predict in the absence of scattering by amounts comparable with the difference between the two limbs shown in Fig. 3. The third plate showed that the departure from the predicted curve becomes greater as the sky conditions became worse.

To find the effect of scattering on the measured velocities we assume that the velocity observed at any disk position is a weighted mean velocity of the light scattered to that position; the velocity contributions from neighbouring points

being weighted according to the disk intensity at those points. This is an assumption that has been tested observationally by Miss Hart (**11**). Our observed points are all fairly close to the limb and we therefore neglect the curvature of the image. If $I(x)$ is the intensity at a point whose radial distance from the limb, is x and $u(x)$ is the line-of-sight velocity at that point, we assume that $I(x)$ and $u(x)$ remain unaltered perpendicular to the x direction for the fairly short range with which we are concerned. If the scattering processes have the effect that, for distances measured in the x direction, the light at any point on the disk is redistributed in distance s according to the function $S(s)$ the velocity $\bar{u}(r)$ measured at a point distant r from the limb will be

$$\bar{u}(r) = \frac{\int_0^{2\rho_0} I(x)\,u(x)\,S(r-x)\,dx}{\int_0^{2\rho_0} I(x)\,S(r-x)\,dx} \qquad (4)$$

where $2\rho_0$ is the solar diameter.

The general form of the scattering function $S(s)$ is fairly well known; there is a region 2″–5″ on either side of the peak within which the scattered light has a Gaussian distribution, followed by a 'tail' within which the light distribution falls off much more gradually. Our measurements of velocities in the scattered sky light make it fairly easy to find the form of the 'tail', but the Gaussian 'core' is more difficult, since we rely on the few and rather widely scattered limb velocities. The form of the 'core' is not, however, an important matter in considering the modification of the velocity distribution on the disk, since the effects come chiefly from the more distant scattered light. For $I(x)$ in (4), the limb darkening, we have used the intensity distribution given by ten Bruggencate, Gollnow and Jäger (**5**) which is corrected for scattered light, combined with the observations of Moll, Burger and van der Bilt (**13**) for points further in on the disk. Plates 95 and 96 were used together in deriving the scattering function; the sky velocities for these plates show no systematic differences, and for $u(x)$ in (4) we have therefore used the mean of the continuous curves shown in Fig. 4 for these two plates. Our numerical integrations in the expression for $\bar{u}(r)$ have all been made by summations using intervals of 0·002 in ρ/ρ_0. The scattering function we deduce is a Gaussian curve (half, half-width 3″·5) out to 5″ from the peak value, after which it decreases more slowly to 1 per cent of the peak intensity at a distance of 30″. We have carried the 'tail' out to 110″ from the peak and then assumed that just under 1 per cent (0·78 per cent) of the total light is scattered on each side beyond this. In deducing the light *arriving* at any point on account of scattering, we have assumed that this small fraction of light, scattered from great distances, has the mean properties of light from the centre of the disk.

We first of all tested the deduced scattering function by applying it back again to the plates 95 and 96, using again the mean predicted $u(x)$ curve for these plates. The open circles in Fig. 4 show the velocities we then expect to observe in the scattered light plates. We see that the agreement with the disk point observations is quite fair, and that in the sky spectrum we can account for the observations very well out to 50 or 60″; the departures after this are presumably due to the artificial simplification of the function for large distances.

2.2. *Application of the scattering function: the final limb effect curve.*—As a first step we have so far assumed that the east-limb observed velocities are affected

to a negligible extent by scattered light. We must now apply our scattering function to test this assumption, and if necessary proceed to the true limb effect by iteration. On the east limb we have accordingly calculated $\bar{u}(r)$ in equation (4) over the whole observed range in ρ/ρ_0, using for $u(x)$ the mean of the observed velocities from the east limb spectra, after each has been corrected for the Earth's motion. $u(x)$ had to be extended beyond the range of the observations for these calculations, but this is a fairly straightforward matter. It is found that scattering has very little effect on the velocity distribution, the differences between $\bar{u}(r)$ and $u(x)$ not exceeding 0·02 km sec^{-1} at any part of the observed range.

We next proceed in a similar way for the west limb. For $u(x)$ we now use the sum of $\Lambda(\theta^*)$ as given by the east limb curve, and a mean value for the three spectra (1·2) of the line of sight velocity due to solar rotation. We find that the velocity distribution is now considerably modified by scattering. At the extreme limb there is a difference of 0·18 km sec^{-1} between $u(x)$ and $\bar{u}(r)$, the difference decreases quite rapidly as we move in from the limb, so that at $\rho/\rho_0 = 0{\cdot}98$ the difference is only 0·04 km sec^{-1}. For limb effect, however, this last 2 per cent of the way across the disk is of considerable interest; it corresponds to $\cos\theta^* = 0{\cdot}20 - 0{\cdot}00$, which is just the region of theoretical importance. If our scattered light explanation is correct this calculated $\bar{u}(r)$ should now agree with the west limb observed velocities. The agreement between calculation and observation is shown in Fig. 5, in which the continuous line shows the limb-effect we should expect to observe for west limb disk points according to our calculations for the effect of scattered light. We see that the calculated curve gives quite a fair representation of the limb effect as measured on the west limb.

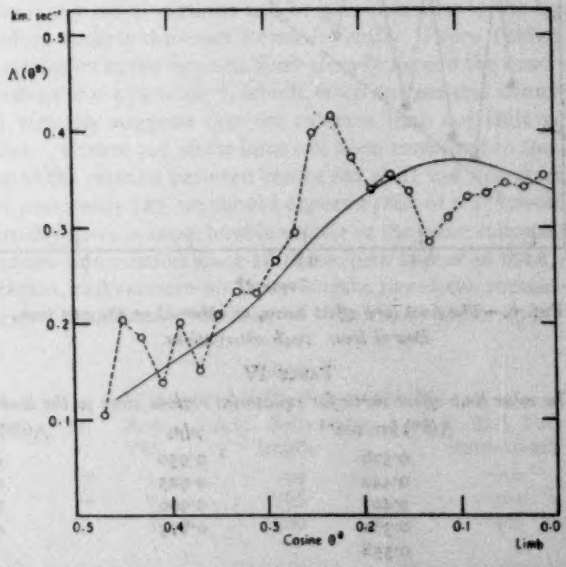

FIG. 5.—*The calculated and observed limb effect for disk positions on the west limb.*

Ideally we should now invert the order of our calculations to pass from the observed $\bar{u}(r)$ to the unsmeared velocity distribution $u(x)$ on each limb. The

calculations above show, however, that such a procedure would give limb-effect curves for the two limbs in substantial agreement, since light scattering accounts adequately for the differences between the two observed curves. In view of our ignorance of the exact scattering function appropriate to the actual limb spectra, we shall do best to accept now the limb effect as given by the east-limb spectra, the errors we predict are only of the order of 0·02 km sec^{-1}, and we cannot correct for these with any reality.

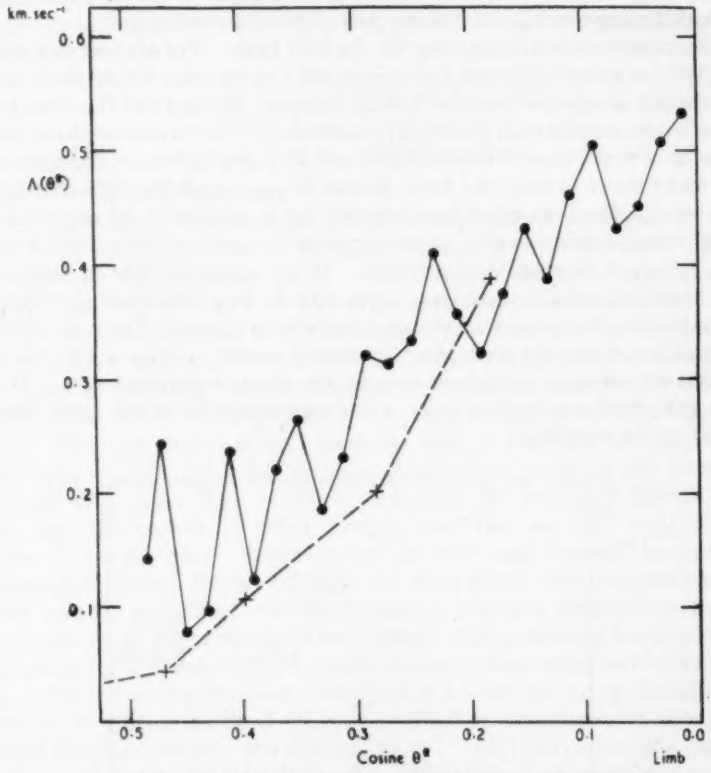

FIG. 6.—*The final limb effect curve, as observed on the east limb. Dotted line:* 1948 *observations.*

TABLE IV

The solar limb effect curve for equatorial regions close to the limb

ρ/ρ_0	$\Lambda(\theta^*)$ km sec^{-1}	ρ/ρ_0	$\Lambda(\theta^*)$ km sec^{-1}
1·000	0·526	0·950	0·263
0·995	0·442	0·925	0·206
0·990	0·407	0·900	0·159
0·985	0·381	0·875	0·118
0·980	0·358	...	...
0·975	0·339	...	...
0·970	0·321	0·000	0·000

The east-limb observations from Fig. 3 are shown again in Fig. 6, and in Table IV we give, as a function of ρ/ρ_0, the values of $\Lambda(\theta^*)$ which are obtained

from a smooth curve drawn through the observed points in the figure. The 1948 limb-effect curve is also shown on Fig. 6 for comparison with the new determination. There is fair agreement between the two series of observations over the range in common, though the earlier curve appears to be displaced by 0·05 to 0·10 km sec^{-1} from the new measures. Such a displacement could arise from errors in the centre wave-lengths which are quite comparable with their estimated uncertainty. From Section 1·2 we have now an estimated uncertainty of 0·04 km sec^{-1} for the centre spectra (since field effects will be the same for all three lines). The 1948 centre measures were for 11 spectra taken on three days and the stated probable errors indicate an uncertainty of apparently the same magnitude as we find now: together these uncertainties might well account for the observed displacement.

Discussion and conclusion.

We can most easily compare our observations with theoretical predictions by considering the extreme limb values which have now been obtained for the first time. According to Freundlich's hypothesis the centre-to-limb shift of a solar line depends upon the path length of the photon in the radiation field of the solar atmosphere. On this theory Freundlich and Forbes (**10**) predict a limb effect $\Lambda(\pi/2)$ of approximately 1·3 km sec^{-1}, which is more than twice the observed value; moreover the form of the $\Lambda(\theta^*)$ curve, which we can now follow to the extreme limb, is quite at variance with the path-length interpretation.

On the radial current theory the red shift of a solar line, (solar wave-length minus vacuum-arc wave-length), arises from the combination of the Relativity shift and shifts due to radial streaming motions in the solar atmosphere (**18**). At the extreme limb any radial motions will be perpendicular to the line of sight and we must therefore observe the exact Relativity shift. From Table IV we see that the solar wave-lengths at the extreme limb already exceed the centre values by an amount equivalent to 0·53 km sec^{-1}, which, from our general knowledge of centre wave-lengths, strongly suggests that the extreme limb red shift is well over the Relativity value. Centre red shifts have not been measured in this investigation, but according to the relation between centre red shift and line strength which we have obtained previously (**2**), we should expect a shift of 0·45 km sec^{-1} or 0·009 A, though admittedly there is considerable scatter in the observational relation. We have more precise information since all three lines appear in the I.A.U. standard solar wave-lengths, and vacuum-arc wave-lengths have been measured for them in the Allegeheny Observatory—Bureau of Standards work (**7**). These wave-

TABLE V

Centre red shifts of measured lines

Wave-length (A)	El.	Row. No.	I.A.U. Solar wave-length	A.O.–B.S. Vac. arc wave-length	Δ_0 (A)
6297·8	Fe	5	·799	·790	0·009
6301·5	Fe	7	·508	·501	0·007
6302·5	Fe	5	·499	·493	0·006

lengths and the resulting centre red shifts Δ_0 are shown in Table V: the mean centre red shift is 0·007 A. We can make some comparison from our own measures with both series of wave-lengths. Using oxygen lines as standards the mean wave-lengths of the three solar lines from our 10 centre spectra average 0·002 A

shorter than the I.A.U. values. Our vacuum-arc lines, measured by the method of circular channels agreed with the A.O.–B.S. values at 6020 A and were 0·002 A shorter at 6500 A, these differences would lead to a mean Δ_0 of 0·006 A. If we take 0·0065 A or 0·31 km sec^{-1} as a likely value for the centre red shift, then with the extreme limb effect of 0·53 km sec^{-1}, the solar red shift at $\theta^* = \pi/2$ is 0·84 km sec^{-1}, which is well over the Relativity value (0·636 km sec^{-1}). This excess is quite inexplicable on the radial current theory.

In conclusion we must point out, that although the discrepancies between observation and theory which we find are marked enough to be decisive, our 'final' limb effect curve is only a small part of the work that is needed to arrive at the correct explanation of solar red shifts and limb effect. The chief use of the present investigation is probably in showing the difficulties in finding the centre to limb change in solar wave-lengths. In the first place the programme must be planned to allow for the existence of velocity fields on the Sun, and also, from the most recent work (**17**), for organised tangential motions on the solar surface. Secondly, allowance must be made for the effect of scattered light, which affects those regions of the disk which are most important theoretically. We find that at the extreme limb errors amounting to 0·2 km sec^{-1} occur at the west equator, under quite fair seeing conditions; at the two poles the estimated error would be 0·1 km sec^{-1}, while it is practically zero at the east equator. With the possible exception of east-limb equatorial disk points, the appropriate corrections must be made in order to find the true limb effect. The limb effect may well be different for different solar latitudes, and vary with element, line strength, excitation potential and other physical properties of the absorbing atoms; all but the most outstanding of such effects are likely to be undetectable unless the real nature of the observational problem is taken into account.

I should like to thank Professor Plaskett for his generous help throughout this investigation, and also Dr A. B. Hart for many helpful discussions on the problems of scattered light.

University Observatory,
Oxford:
1959 *April* 16

References

(1) M. G. Adam, *M.N.*, **108**, 446, 1948; Comm. Univ. Obs., Oxford, No. 26.
(2) M. G. Adam, *M.N.*, **118**, 106, 1958; Comm. Univ. Obs., Oxford, No. 66.
(3) W. S. Adams and J. B. Lasby, *Papers of the Mt. Wilson Observatory*, **1**, Part 1, 1911.
(4) H. D. Babcock, *Ap.J.*, **65**, 147, 1927.
(5) P. ten Bruggencate, H. Gollnow and F. W. Jäger, *Zs.f. Ap.*, **27**, 230, 1950.
(6) K. Burns and W. F. Meggers, *Publ. Alleg. Obs.*, **6**, 105, 1927.
(7) K. Burns and F. M. Walters, *Publ. Alleg. Obs.*, **6**, 159, 1929.
(8) J. Evershed, *M.N.*, **91**, 260, 1931.
(9) E. F. Freundlich, A. v. Brunn and H. Brück, *Zs.f. Ap.*, **1**, 43, 1930.
(10) E. F. Freundlich and E. G. Forbes, *Ann. d'Ap.*, **19**, 183, 1956.
(11) A. B. Hart, *M.N.*, **114**, 17, 1954; Comm. Univ. Obs., Oxford, No. 43.
(12) A. B. Hart, *M.N.*, **116**, 38, 1956; Comm. Univ. Obs., Oxford, No. 54.
(13) W. J. H. Moll, H. C. Burger and J. van der Bilt, *B.A.N.*, **3**, 83, 1925.
(14) H. H. Plaskett, *M.N.*, **112**, 414, 1952; Comm. Univ. Obs., Oxford, No. 34.
(15) H. H. Plaskett, *M.N.*, **114**, 251, 1954; Comm. Univ. Obs., Oxford, No. 44.
(16) H. H. Plaskett, *M.N.*, **115**, 542, 1955; Comm. Univ. Obs., Oxford, No. 52.
(17) H. H. Plaskett, *M.N.*, **119**, 197, 1959; Comm. Univ. Obs., Oxford, No. 70.
(18) E. H. Schröter, *Zs.f. Ap.*, **41**, 141, 1957.

ON THE INTERPRETATION OF SOLAR GRANULATION

Peter Fellgett

(Communicated by the Director of the Cambridge Observatories)

(Received 1959 March 9)

Summary

The technique of interpretation of solar granulation observations is examined with special reference to the stochastic nature of the physical phenomenon, and to the absence in any optical image of sufficient information to allow the intensity distribution in the object to be explicitly inferred. Many of the points made are elementary, and so not essentially novel, but the need for explicit discussion and illustration of each one has been evidenced by the publication in the recent literature of results which do not have the significance attributed to them. Application is made to the simultaneous velocity and brightness observations of Richardson and Schwarzschild and of Plaskett. It is concluded that the evidence for correlation between velocity and brightness is weaker than has been supposed. Harmonically related periodicities in two sets of the Oxford observations may possibly be connected with magneto-hydrodynamic effects, but the suggestion of some authors that there are significant periodicities over large regions of the Sun is not confirmed. The investigation has been planned as a contribution towards bringing techniques of interpretation into line with current advances in the observation of granulation, and the programmes developed for carrying out the required calculations on the EDSAC II computer may form a basis for the rapid analysis of future observations.

1. *Introduction*

It has become increasingly apparent that for many purposes the assumption of plane stratification of the outer layers of the Sun is no longer a sufficiently good approximation. The formation of spectral lines, for example, cannot be treated accurately by a theory which ignores the inhomogeneities which are observed as solar granulation; and other phenomena, such as the structure of the chromosphere, and possibly the supply of energy to the corona, may be essentially dependent on processes of which granulation is the outward and visible sign.

Granulation has accordingly received increasing attention in recent years. The work has three obvious aspects; namely, the observations themselves, the interpretation of the observations, and the incorporation of the information thus gained into theoretical solar models. The present paper is concerned with the second step, the reduction of the raw observational data to a form suitable for theoretical purposes.

The initial difficulty is, of course, that even the largest granular elements are near to the limit of resolution set by ordinary daytime seeing. The problems which this creates are enhanced by the circumstance that conditions on the Sun are so different from those well known to us that we have, to begin with, no model

in terms of which to interpret granulation. A second circumstance which creates special problems is the stochastic nature of the phenomenon.

The first of these circumstances is typical of astronomy generally. In ordinary landscape and portrait photography the existence of previous knowledge normally makes it possible to interpret correctly detail which is near to the limit of the optical resolution. This ability is specially developed in interpreters of air reconnaissance photographs, and it is closely associated with the fact that the observer in everyday living has the opportunity to handle and examine at close quarters the objects represented. This opportunity does not exist in astronomy, and accordingly it is only when all significant details are well resolved that it is safe to assume the reality in the object of the structures which suggest themselves to an observer examining the image. Moreover, it is difficult to establish that this condition is fulfilled, since to trust the visual impression that it is so is to assume just what requires to be investigated. When the structures in the object are not fully resolved, it is obviously misleading to treat measurements made on the image as if they had been made on the object itself, and explicit account has to be taken of the specific way in which the optical system transmits information about the object.

An optical system of given aperture completely suppresses some information about the object, and other information is presented in the image in a metamorphosed form. The most clear and compact way of expressing these relationships is in terms of the two-dimensional Fourier transforms of the object and image distributions (Fellgett and Linfoot 1955, Linfoot 1958). Some spatial frequencies in the object are not reproduced in the image, and others are reproduced with changed amplitude; if aberrations are present, their phase may also be changed. Once the effect of optical imaging on the spatial frequencies has been formulated, its effect on other functions of the image brightness, for example the auto-correlation function, can be obtained by using the ordinary techniques of Fourier theory, and this will be illustrated in what follows.

The difficulties of interpretation are much reduced when it is permissible to assume that the object structures are geometrically simple, or that they can be interpreted in terms of structures known on the Earth. For example, star fields can be taken as effectively consisting of point sources, and the major features of the lunar surface can probably be interpreted in terms of a rocky landscape. In other cases, where no such previously known pattern is applicable, the reservations implied by the theoretical relations correspond very closely to practical difficulties. The surface features of Mars are a well-known example of this, and the effort to interpret granulation in terms of terrestrial experience has traditionally led to comparison with rice grains or willow leaves. A further example may be provided by the comparisons between different surveys of radio sources. The apparatus used in the various surveys is responsive to different ranges of spatial frequencies in the brightness distribution over the sky, and indeed these ranges do not overlap in general. The resultant records have been interpreted in terms of the distribution of point sources which most simply explains each one: it is not obvious that the distributions so found ought to agree with each other, except for the brightest sources which are effectively resolved individually.

The physically stochastic nature of granulation implies that techniques of interpretation appropriate in more deterministic circumstances are not necessarily

well adapted to granulation studies. It may be useful to map a star-field in detail, because the stars remain accessible to subsequent observation, but there is no reason to believe that the presence of a "granule" in the solar disk at a particular place and time ordinarily tells us, in itself, anything of general interest, or allows any prediction to be made that can be checked by subsequent observation. It would in any case be impracticable, even if it were desirable, to record from instant to instant all the changing details of the granular pattern over the Sun. Interest centres in those properties of granulation which may reasonably be supposed to be characteristic of the phenomenon as a whole, and which enable predictions to be made which can later be confronted with further observations. It is accordingly necessary in the reductions to eliminate, as far as possible, those parameters which pertain only to the particular sample observed, and to retain those which are statistical averages in the sense that, as more and more data are included, they may be expected to approach some limit which is independent of the particular set of data used. Of course this separation cannot be made cleanly on the basis of any finite set of observations, and it is necessary to consider the uncertainties which result from the use of a limited sample. An example is discussed in Section 2.4.

Several authors have previously discussed the precautions that need to be taken in the interpretation of observations of granulation. Uberoi (1955) has put forward serious objections to some of the methods that have been used, and indeed there seems little that can be urged against the substance of his criticisms. Wlerick (1957) has presented detailed illustrations of how the method of calculation used can introduce artefacts into the interpretation of the data.

These questions are taken up in Section 2 of the present paper, where several of the more important topics, including some also treated by Uberoi, Wlerick and others, are discussed theoretically and illustrated. Numerical and photographic experiments are presented which show what happens when random data are subjected to processes that have been used in the interpretation of granulation. It is evidently necessary to know this before one can assess the reality of structures which appear to be present in actual granulation data treated in the same way. The implications of this discussion lead to the choice, in Section 3, of methods of calculation aimed at interpreting the brightness and velocity changes observed by Richardson and Schwarzschild (1950) and by Plaskett (1954). The results of these calculations, which constitute the main computational part of the paper, are presented in graphical form in Figs. 7–11 and their significance is briefly discussed in Section 4.

It is not the purpose of the present paper to urge any particular view as to the exact nature of solar granulation, but some comment on this question seems appropriate in order to avoid misunderstanding. The appearance of a discrete granular structure is common when a "random" brightness-distribution is photographed with limited resolution and at high contrast, as has been pointed out by Uberoi and is further illustrated in Section 2.1. It follows that this appearance in images of the solar disk is insufficient in itself to prove that any such structure exists on the Sun, and in particular granulation photographs reproduced at high and unstated contrast are useless as evidence on this point. Uberoi concluded that all the measurements discussed by him were consistent, so far as they went, with a uniform turbulence spectrum. The older observations did not, in fact, establish that granulation was anything else than a random

brightness distribution with statistically uniform spatial power spectrum. From the purely observational point of view, the fact that the patterns seen in images of granulation have suggested discrete convection cells to modern observers is on exactly the same footing as the fact that in the last century they suggested comparison with rice or willows; the latter comparisons are evidently to be taken no more literally than is the appearance of bright rings round stars seen in a small telescope. From a more general point of view, the convection theory acquires special status from the theoretical prediction that the region of the Sun immediately underlying that from which most of the visible light comes will be convectively unstable, and from the independent observational evidence that the formation of spectral lines is affected by turbulence. It does not follow that the convection will be in discrete cells. Ordinary thermal convection at a given spatial wave-number occurs when the lapse rate exceeds the adiabatic rate by an amount which is, roughly speaking, an increasing function of wave-number, so that convection begins at nearly the lowest wave-number which is geometrically possible. For a layer confined between rigid horizontal planes, the circulation accordingly begins in cells having dimensions comparable with the distance between the planes; in an atmosphere the cell size depends on the scale-height. Magnetic or coriolis forces may modify the relative ease of convection at different wave-numbers. If convection is only just initiated, only small velocities develop and the motion is almost entirely in discrete cells corresponding to the most favourable wave-number. The amount of heat that can be transported in this way is small, and this motion prevails only over a narrow range of temperature gradient. It is accordingly hydrodynamically rather unlikely, though possible, that solar granulation represents this sort of convection. If the driving gradient much exceeds the minimum needed to initiate convection, the layer becomes unstable over a wider range of wave-numbers, and the motion at low wave-numbers becomes fast enough to be turbulent, so that energy is fed from lower to higher wave-numbers until dissipated by viscosity. The spectroscopic evidence for microturbulence in the regions where lines are formed suggests that this is indeed what happens on the Sun. Under these conditions it remains true that the bulk of the energy of motion resides in the lower wave-numbers present. When the resolution in an image is sufficient to show only these wave-numbers, the pattern seen, because it lacks higher wave-numbers, resembles the pattern of discrete cellular convection in which higher wave-numbers are absent from the actual motion. One difference which is observable without attaining higher resolution is that in cellular convection the pattern can persist for a long time relative to the time of circulation in a cell, whereas in turbulent convection the large-scale pattern changes more quickly.

Recent observations of granulation appear to show genuine resolution of non-random features. The visual observations of Thiessen (1955) were made with adequate controls to show when real features had been resolved, the only reservations being those inherent in the subjective nature of visual work. An important increase in photographic resolution has been attained in the series of observations made at high altitude by Blackwell, Dewhirst and Dollfus (1957a, b) using a manned balloon of the traditional type, and by Schwarzschild (Rogerson 1958) using an unmanned plastic balloon. Schwarzschild's photographs, in particular, generally confirm Thiessen's conclusions. Valuable additional information has been obtained from ground level by Rösch (1956); and in the

massive and carefully planned photographic observations of Leighton (1957) who has studied the statistical time-changes in the granular pattern.

The structures thus resolved and made available for study accord well with the idea that convection is the underlying cause. The relationship of the observed structures to convection processes in the Sun is necessarily a matter of detailed quantitative study. There are some difficulties in supposing that we see down to the actual convective region, and Whitney (1958), for example, discusses this problem and makes alternative proposals. For the reasons given above, the structures now resolved may be expected to be themselves composed of smaller elements, including those corresponding to the spectroscopic "microturbulence" (Fig. 1 (*c*)). A detailed knowledge of the properties of optical blurring and of the numerical processes used to interpret the data seems likely to be even more essential to the correct interpretation of the more sophisticated observations now becoming available than it has been in the past.

2. *Properties of optical blurring and of data-reduction methods applied to granulation*

2.1. *Granular structures produced from random objects.*—We have already referred to the discrete granular structures often seen when a field of randomly varying brightness is photographed with limited resolution and at high contrast. An effect of this kind is well seen when random noise is viewed on a television monitor screen. The screen appears covered with a closely-packed array of bright spots, changing from instant to instant. If the monitor is de-focused, the number of spots (and their contrast) decreases, while their size increases so that they continue to fill the whole of the scanned area of the screen. This behaviour is closely analogous to the so-called "5 sec-" "2 sec-" and "1 sec-" granulation of the Sun viewed under different seeing conditions.

Skumanick (1955) concluded that the granulation images measured by him showed no significant black–white asymmetry. Since the probability distribution of the brightness variations at each point tends towards a symmetrical Gaussian form in an image where the largest individual object structures are not resolved, there may nevertheless be real asymmetry in images of higher resolution than were used by Skumanick. Dr D. E. Blackwell has very kindly allowed me to examine the original negatives which he obtained from an altitude of 18 000 ft. When the photographic calibrations, which are available for these negatives, are taken into account, it seems quite definite that the images can be interpreted as bright granules separated by relatively narrow dark lanes, but not the other way round. This is of course inherently probable, since if, for example, turbulence on the Sun gave rise to statistically symmetrical temperature fluctuations, then the emission of visible light would have a skew probability distribution.

Another characteristic of granulation images is that they have a reticulated appearance whereby the cells seem to form ordered patterns over a distance of several cell diameters.

I have tried to reproduce these two properties of granulation experimentally, starting from fine photographic grain which can be taken as "random" for present purposes. A skew intensity distribution can readily be obtained by using the non-linear photographic characteristic. The reticulated appearance is associated with a spatial spectrum in which the structural power in the object increases with frequency. When combined with the instrumental cut-off, this may cause the spatial spectrum of the image to be more or less strongly peaked

at some frequency. A rising structural power-spectrum can be obtained photographically by superposing a positive and a negative taken of the same object but with different resolutions. Fig. 1 (*a*) shows the result of repeatedly copying photographic grain using these techniques. If the figure is held at some distance, a marked granular structure appears, whereas close examination shows that this is not in fact the predominant structure present. In Fig. 1 (*b*) the attempt has been made to reproduce a blurred image of Fig. 1 (*a*) showing granular structure. It is not to be expected that with ordinary uncontrolled darkroom techniques it would readily be possible to match quantitatively the appearance of actual solar granulation. It can be said, however, that the original print of Fig. 1 (*b*) shows asymmetry and reticulation in the sense aimed at; and indeed several astronomers to whom it was handed without comment implicitly identified it as a negative of solar granulation. This shows that it is possible, starting from a "random" grain distribution, to reproduce at least some of the characteristics of solar granulation "sans aucune intervention de la main humaine" (Janssen 1896).

It may be mentioned here that the available prints of the excellent granulation picture obtained by Schwarzschild show remarkably *large* granules ($>1''$). The sharpness of the apparent granule-boundaries, and their high contrast, provide immediate evidence that these pictures are of higher resolution than has been attained previously, and the large size of the granules is especially apparent in these parts of the published pictures which are sharpest according to these criteria. This suggests that in some previous pictures the granular structure may be broken up by multiple imaging of the kind often observed in star images under bad seeing conditions. It underlines the incorrectness of judging resolution solely by the size of the finest structures seen.

2.2. *The non-significance of guessed frequencies.*—Experience of the necessary calculations shows that only in the simplest cases can the frequency-components of an observed function or its correlation function be found by inspection. A guessed "quasi-frequency" may mean nothing at all, or it may refer to the cut-off above which frequency components have greatly reduced amplitude. If, as often happens, this cut-off is instrumental, the guess then gives no information about the phenomenon under investigation (see Section 2.5).

As an example of an effect of this kind, the function $\operatorname{sinc} x = \sin(\pi x)/\pi x$ has an "obvious" oscillation with frequency 0·5. But its Fourier transform is in fact

$$\operatorname{rect}(t) = \begin{cases} 1, & |t| < \frac{1}{2} \\ 0, & |t| > \frac{1}{2} \end{cases} :$$

the apparent frequency turns out to be the cut-off. $\operatorname{Sinc}^2 x$ has an "obvious" oscillation at unit frequency; its transform is in fact

$$\operatorname{tri}(t) = \begin{cases} 1 - |t|, & |t| \leqslant 1 \\ 0, & |t| > 1 \end{cases}$$

which has a cut-off but no discontinuity at $t = 1$.

2.3. *Apparent serial correlation caused by blurring.*—If a quantity $f(x,y)$, say the brightness over part of the solar disk, is observed optically, the finite resolution of the observation necessarily introduces correlation between the observed values at neighbouring (x,y). The presence of such correlation does

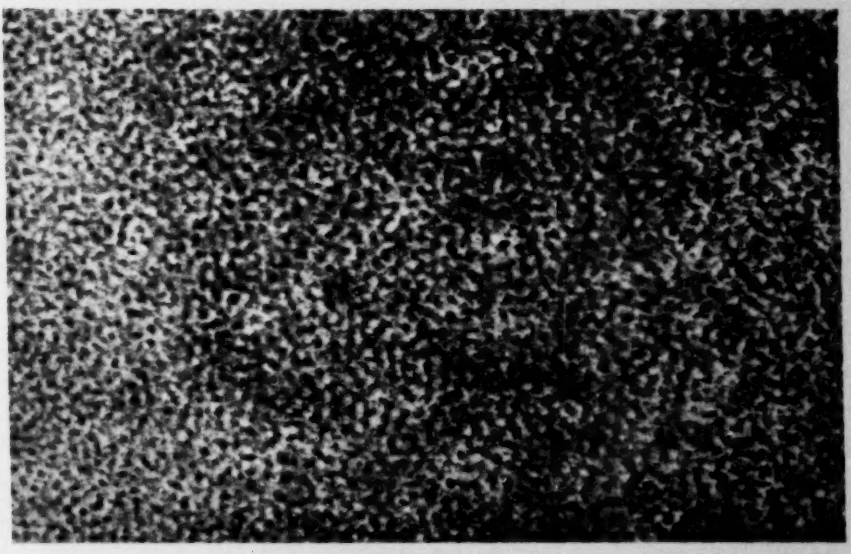

(*a*) *Object made from photographic grain by repeated photographic copying under such conditions (see text) as to give a spatial power spectrum which is an increasing function of frequency over a range of frequencies, and an asymmetric probability distribution of brightness from point to point of the object. It may be regarded as a (negative) model of a possible brightness distribution on the Sun.*

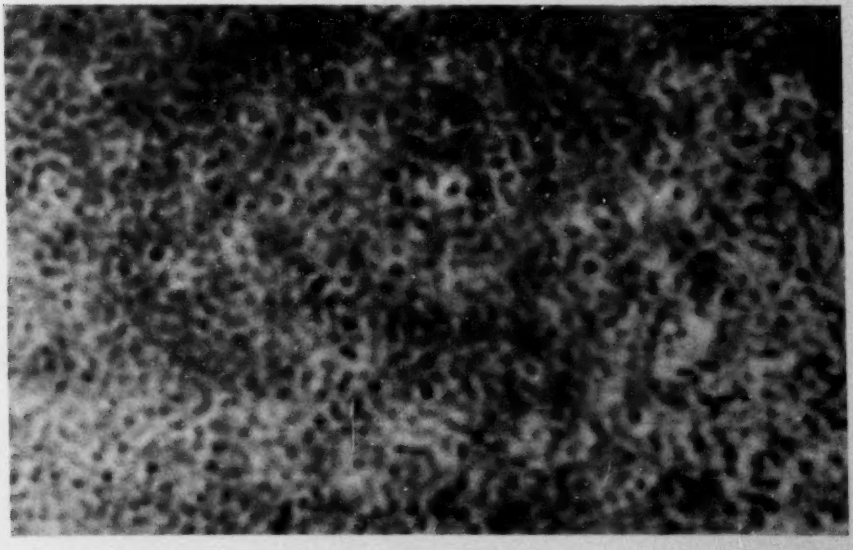

(*b*) *Blurred reproduction of object (a). This reproduction may be regarded as analagous to a (negative) photograph of the solar granulation blurred by seeing. It has a reticulated appearance, and is covered with "granules" which show on the negative as dark spots separated by narrower "intergranular" spaces. This granular structure is not a predominant feature of the object shown in (a), but the two pictures appear more similar when viewed from some distance.*

FIG. 1.—*Resemblances to granulation in photographs derived from random objects (a) and (b), and in cloud formations (c).*

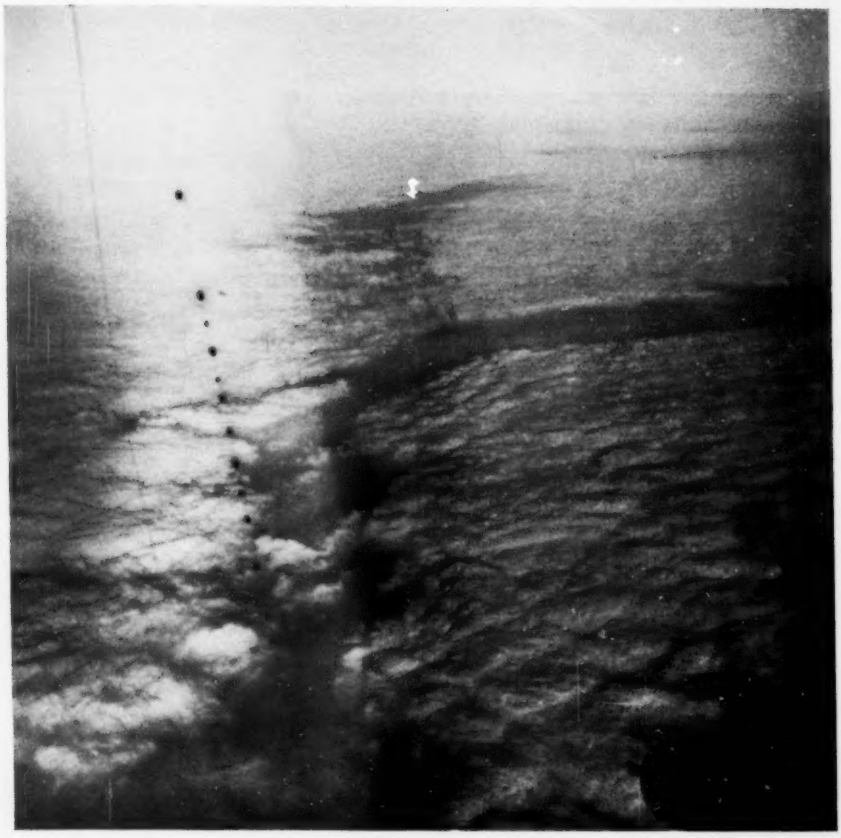

(*c*) *Stratus cloud layer showing small-scale turbulence within larger polygonal structures. If this layer were photographed with limited resolution it could give the appearance of smooth structureless granules. The mechanism of optical contrast is of course quite different here from on the Sun.*

FIG. 1. (*contd.*)—*Resemblances to granulation in photographs derived from random objects* (*a*) *and* (*b*), *and in cloud formations* (*c*).

not therefore of itself indicate that f is similarly correlated. The observed quantity is in fact

$$f*w=\int\int_{-\infty}^{\infty} w(\xi,\eta)f(x-\xi,y-\eta)\,d\xi\,d\eta \qquad (2.31)$$

the convolution of f with the weighting or "apparatus" function w representing the resolution of the observation. From the convolution theorem of Fourier transforms it follows (see Section 2.5) that if f were random, in the sense of being itself serially uncorrelated and therefore having a uniform power spectrum, the observations $f*w$ would have the same auto-correlation function as w. This result is often known as Campbell's theorem.

The situation may be pictured by noting that the observation $f*w(x_1,y_1)$ contains contributions from all the $f(x,y)$ in the neighbourhood of (x_1,y_1), each with weight $w(\xi,\eta)$ depending on the distance (ξ,η) between (x,y) and the point of observation (x_1,y_1). Evidently the weighting of the principal contributions is not much changed if the point of observation is moved to (x_2,y_2) such that $w(x_1-x_2,y_1-y_2)\simeq w(0,0)$. Consequently the observed values $f*w$ at (x_1,y_1) and (x_2,y_2) will be correlated in these circumstances whether or not $f(x,y)$ is itself serially correlated.

An example of this effect may be found in the observations of the variable component of radial velocity across the solar disk reported by Hart (1956). The auto-correlation function of this component falls to one-half for a shift of about $\pm 0^{\circ}\cdot 5$ heliographic longitude, corresponding on average to $\pm 4''\cdot 5$ arc. This correlation-distance agrees with the spread due to seeing, which was estimated as 0–2 on the Oxford scale, corresponding to a tremor disk about $5''$ in radius (Plaskett 1952). That the observed correlation is due to seeing, rather than to any structure on the Sun itself, is the natural inference from Miss Hart's Figs. 1 and 2, which show the variations in velocity plotted against angle, and her Fig. 4 which shows them plotted against distance along the solar surface. The angular plot has the appearance of a statistically stationary series, whereas in the distance plot the fluctuations appear to be much sharper at the end where the solar surface is seen more normally than at the other end where it is seen more foreshortened. Of course this conclusion is not in any way inconsistent with genuine velocity fluctuations having been observed, nor does it call into question Miss Hart's discovery that the larger features of the velocity field persist for longer times than had been previously realized.

2.4. *Peaks in auto-correlation functions caused by the finite size of the available sample.*—Suppose that an observed quantity, such as the deviation of velocity or brightness from its mean value, takes the value $f(x,y)$ at a point (x,y) on the solar disk, and $f(x+\xi,y+\eta)$ at a point distant (ξ,η) from (x,y). Then as (x,y) explores the region covered by the observations, (ξ,η) remaining constant, the product $f(x,y).f(x+\xi,y+\eta)$ takes many values depending on the details of the particular field studied. These variations are of little interest in themselves, and in taking the normalized auto-correlation function for shift (ξ,η) we form the normalized mean of these products. This mean may be written

$$C(\xi,\eta)=\frac{\sum f(x,y)f(x+\xi,y+\eta)}{\sum\{f(x,y)\}^2} \qquad (2.41)$$

where the summations are over all suitable values of $f(x,y)$ available, say N in number. The function $\hat{C}$ defined in this way has useful properties with respect to the values of $f(x,y)$ on which it is based; for example, its Fourier transform is the normalized squared modulus of the Fourier transform of these values (see equation (2.55)). But if another set of values of $f(x,y)$ were taken, the $\hat{C}$ derived from it would generally differ from the previous one, because of failure of the variations in the products $f(x,y).f(x+\xi,y+\eta)$ to "average out" completely. These differences are certainly properties of the sets of data in question but, from the point of view of characterizing granulation, they are accidental and are no more significant than are the variations in the individual products themselves.

For (ξ,η) such that $\hat{C}(\xi,\eta)$ would be practically zero when averaged over a very large set of data, the accidental correlation over a sample containing n independent values has by equation (2.41) a root-mean-square (r.m.s.) expectation $n^{-1/2}$.

Similarly, if N values of $f(x,y)$ are measured, each with independent r.m.s. error ϵ, the error in the derived $\hat{C}$ is uncorrelated from point to point and has r.m.s. value $\epsilon N^{-1/2}(2\bar{f}^2+\epsilon^2)^{1/2}/(\bar{f}^2+\epsilon^2)$. The error of measurement augments $\hat{C}(0,0)$ by $\epsilon^2/(\bar{f}^2+\epsilon^2)$.

In practice, errors such as those made in setting a cross-wire, statistical error due to photographic grain, and rounding errors in calculation, are usually almost independent for each measured value. Measurement is often made at a sufficiently close interval in (x,y) that the values of $f(x,y)$ are fairly strongly correlated over a range of several times the measuring interval; say R times this interval. $\hat{C}(0,0)$ then stands out from the smooth run of $\hat{C}$ by an amount $\epsilon^2\{\epsilon^2+\bar{f}^2\}^{-1}$ and the error of measurement ϵ can be estimated (see Section 3 for an example of this). The scatter of r.m.s. amount $\epsilon N^{-1/2}(2\bar{f}^2+\epsilon^2)^{1/2}/(\bar{f}^2+\epsilon^2)$ in the other values of $\hat{C}$ is not usually important if N is reasonably large.

These results are obvious enough theoretically, but unless they are taken into account the appearance of auto-correlation curves derived from observations may be, at first sight, deceptive. Such curves often have peaks which are much larger than is reasonably consistent with the effect of observational error $\epsilon N^{-1/2}(2\bar{f}^2+\epsilon^2)^{1/2}/(\bar{f}^2+\epsilon^2)$ or with the expected fluctuation $N^{-1/2}$ in the mean of N independent products. Moreover, these peaks are not represented by single isolated points, but are apparently evidenced by the consistent trend of a number of successive points, and so may seem "convincing".

All these putative criteria are in fact incorrect. We have seen that the statistical significance of a feature is properly judged with respect to an r.m.s. expectation $n^{-1/2}$. The r.m.s. amplitude $N^{-1/2}$, which would be expected if all the N observed values were independent, may be considerably smaller than $n^{-1/2}$, since in two dimensions $n \simeq N/R^2$, and in one dimension ($f(x,y)$ replaced by $f(x)$) $n \simeq N/R$ (the definition of R, which was left loose above, can be chosen so as to make these approximations into equalities). The effect of the observational error ϵ is usually smaller still. Moreover, the consistent trend of the points constituting a feature is merely a consequence of the fact that if $f(x,y)$ is smooth then, by equation (2.41), $\hat{C}(\xi,\eta)$ will also be smooth and any feature in it necessarily involves the smooth run of some R neighbouring calculated values.

A good example of these effects has been presented by Zweig (1956), who shows in his Fig. 2 how a secondary peak in the auto-correlation of a sample

of photographic grain disappears as more data are added; this peak would have been taken as significant if the measured values on which it was based had been treated as mutually independent. Wlerick (1957) has demonstrated that peaks, other than the one at the origin, do not generally repeat in auto-correlation curves derived from different samples of actual granulation data.

Fig. 2 of the present paper shows the result of a numerical experiment performed on the EDSAC II computer to illustrate these relationships. A random series of numbers was convoluted (equation (2.31)) in turn with three functions w such that long runs of the convolutions $f*w$ would have the auto-correlation functions displayed in the left-hand column of the figure. The respective auto-correlation functions calculated from a run of $N=100$ values of $f*w$ are shown in the right-hand column. The convoluting functions w used were derived in the manner described in Section 2.5. The random numbers were from a set of some 12000 generated on the EDSAC I computer and available on punched tape in the EDSAC library. They have a Gaussian probability distribution with zero mean and variance 100, and their properties have been subjected to statistical tests. The values of N/R are about 30, 25 and 50 respectively for curves (*b*), (*d*) and (*f*). The r.m.s. amplitudes, in the region away from the peak at the origin are respectively 0·19, 0·26 and 0·16. (These values are based on many more ordinates than it was convenient to plot in the figure.) These auto-correlation curves were created by a numerical process the properties of which can be determined, and so there is no room for doubt that those features of the right-hand set of curves which fail to show up in the left-hand set are an effect of the finite size of sample, and do not represent statistical properties in the usual sense.

The auto-correlation of the brightness distribution in solar granulation given as Fig. 3 by Stuart and Rush (1954) shows similar effects. It fluctuates beyond its first zero with an r.m.s. amplitude of about 0·2. As N is 96 and n is probably about half this value, the expected amplitude is about 0·15, and it is unsafe to attach any significance to the peaks occurring in this region. Similarly Fig. 5 of Miss Hart's (1956) paper shows an auto-correlation of solar velocities which has an r.m.s. amplitude beyond the first zero of 0·06; $N=140$ and n is 30–40. The expected amplitude is therefore about 0·17, so the peaks beyond the first zero are actually fortuitously small.

2.5. *Artificial periodicities caused by smoothing and subtraction of running means.*—In this section we consider for shortness one-dimensional functions, but the results are similar in many dimensions and if desired the variables can be regarded as multi-dimensional vectors. Lower- and upper-case letters will be used to denote functions which are Fourier pairs, and the Fourier operators $\mathbf{F}$ and $\mathbf{F}^*$ will have the meanings implied by

$$\mathbf{F}[v(x)]=V(t)=\int_{-\infty}^{\infty} v(x)\exp\{2\pi ixt\}\,dx, \tag{2.51}$$

$$\mathbf{F}^*[V(t)]=\int_{-\infty}^{\infty} V(t)\exp\{-2\pi ixt\}\,dt \tag{2.52}$$

$$=v(x). \tag{2.53}$$

Equation (2.53) is the Fourier inversion formula (Titchmarsh 1932), which may be expressed by the operator equation $\mathbf{F}\mathbf{F}^*=\mathbf{F}^*\mathbf{F}=\mathbf{1}$. We shall need also the

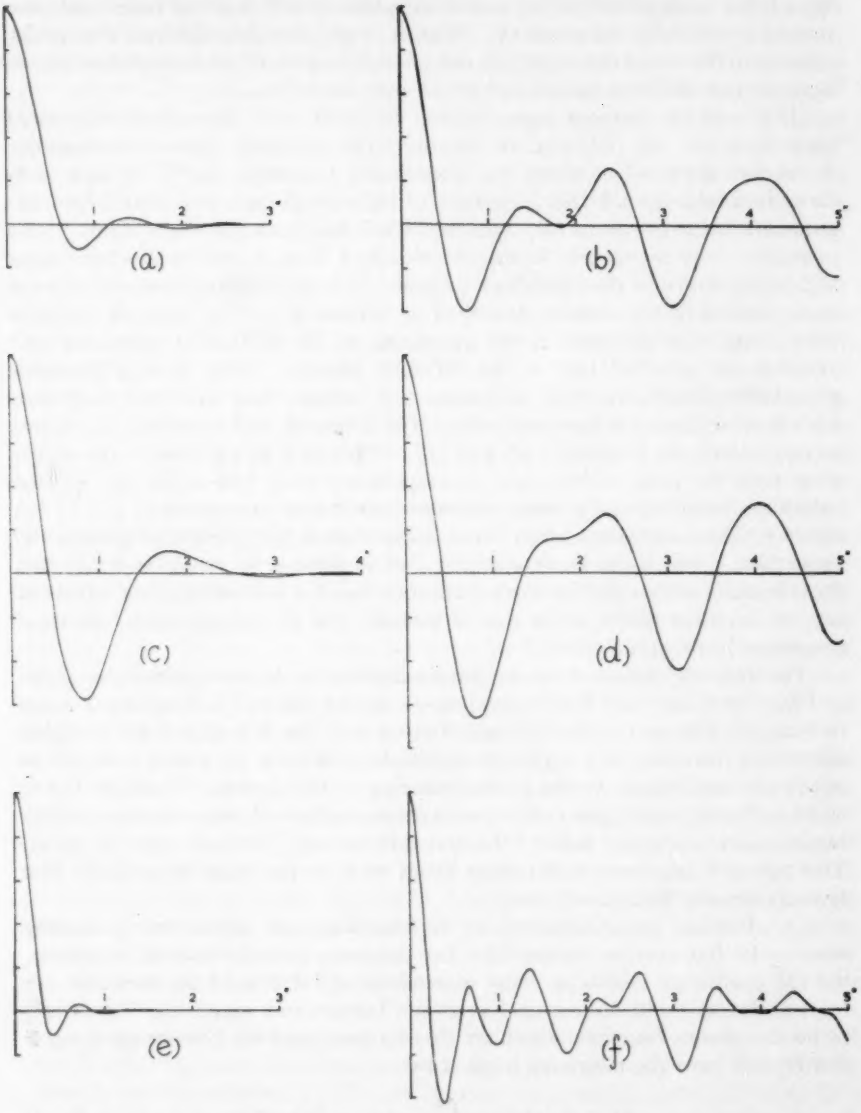

FIG. 2.—*The effect of size sample on secondary peaks of derived auto-correlation functions. (a), (c) and (e). Auto-correlation curves corresponding to very long runs of three statistically stationary series. (b), (d) and (f). The corresponding auto-correlation curves calculated from samples, each comprising 100 values, of the series to which (a), (c) and (e) refer. The right hand set of curves, derived from the limited samples, show secondary peaks which are not present in the left hand set and which therefore have no statistical significance. The heights of these peaks are discussed quantitatively in the text.*

Fourier product theorem (*ibid.*)

$$\mathbf{F}[u^*v] = \mathbf{F}[u] \,.\, \mathbf{F}[v] \tag{2.54}$$

where the asterisk has the meaning given in equation (2.31). In the special case $v(x) = u(-x)$, (2.54) gives

$$\mathbf{F}[\mathbf{C}[u]] = |\mathbf{F}[u]|^2$$
$$\mathbf{C}[u] = \mathbf{F}^*[|U|^2] \tag{2.55}$$

where $\mathbf{C}[u]$ is the (unnormalized) auto-correlation function defined by

$$\mathbf{C}[u] = \int_{-\infty}^{\infty} u(\xi) \,.\, u(\xi - x)\, d\xi \tag{2.56}$$

and $|U|^2$ is called the power-spectrum of u.

Suppose that interest centres in the sharper features of an observed quantity $f(x)$ rather than in its slower variations. The attempt may be made to remove the slow changes by subtracting a running mean; that is to say, replacing $f(x)$ by

$$g(x) = f(x) - \bar{f}(x) \tag{2.57}$$

where

$$\begin{aligned} \bar{f}(x) &= \frac{1}{a} \int_{-\frac{1}{2}a}^{\frac{1}{2}a} f(x-\xi)\, d\xi, \\ &= \frac{1}{a} \int_{-\infty}^{\infty} f(x-\xi)\, \mathrm{rect}\,(\xi/a)\, d\xi, \\ &= \frac{1}{a} f * \mathrm{rect}\,(\xi/a); \end{aligned} \tag{2.58}$$

here "rect" has the same meaning as in Section 2.2. Then by equation (2.54),

$$\begin{aligned} \mathbf{F}[\bar{f}] &= \mathbf{F}[f] \,.\, \mathrm{sinc}\,(at), \\ \mathbf{F}[g] &= \mathbf{F}[f] \,.\, \{1 - \mathrm{sinc}\,(at)\}. \end{aligned} \tag{2.59}$$

These relations are illustrated in Figs. 3–5. Fig. 3 shows (*a*) an assumed real spatial spectrum $\mathbf{F}[f]$; (*b*) the spectrum $\mathrm{sinc}\,(at)$ for a chosen value of a; (*c*) $1 - \mathrm{sinc}\,(at)$; and (*d*) the result of multiplying the original spectrum by $1 - \mathrm{sinc}\,(at)$ in accordance with equation (2.59). It will be seen that the resultant spectrum $\mathbf{F}[g]$ has a fairly pronounced maximum for a certain value of the frequency argument t. This is equivalent to saying that the function g calculated by equation (2.57) has a quasi-periodic structure which is a property of the method of calculation. If f represented (for example) a brightness distribution, and if the modified function g were convoluted with radial velocity observations (say) from which a similar running mean had also been subtracted, then according to equation (2.54) the spectrum of the convolution would be even narrower than that of g and the corresponding velocity function, and the artificial periodicity would be correspondingly enhanced.

The assumed real spectrum $\mathbf{F}[f]$ shown in Fig. 3 (*a*) refers, as it stands, to the observation of a symmetrical and fairly compact solar feature. A more realistic illustration of effects occurring in granulation measurements is obtained when curve (*a*) of Fig. 3 is re-interpreted as the square-root of the mean power spectrum of the observed quantity. Since eqn. (2.59) is true separately for each feature included in the observations, it is true also in the r.m.s. sense. Accordingly the effect of subtracting a running mean from a stochastic function is represented by Fig. 3, and the conclusions drawn above from this figure remain true, in the new interpretation.

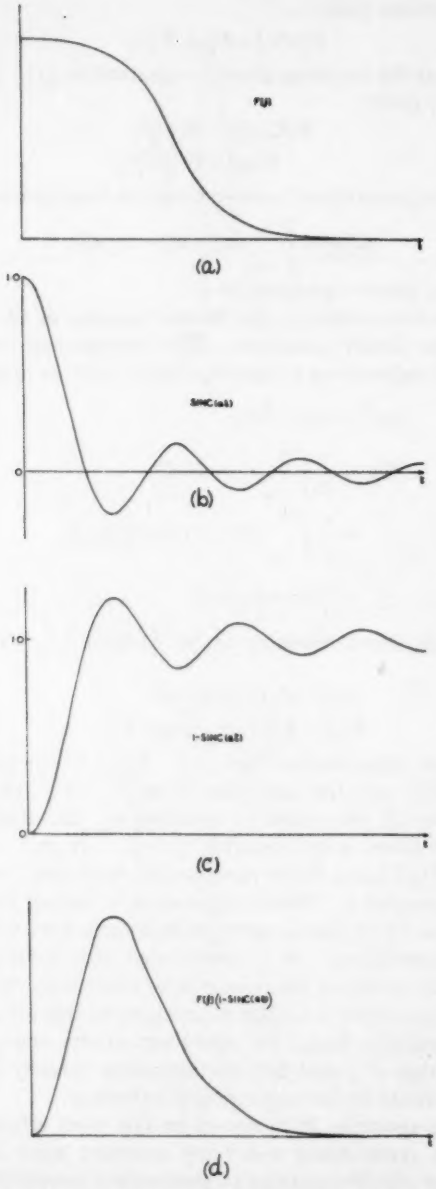

FIG. 3.—*The distortion of frequency-distribution by the subtraction of running means. (a) Assumed amplitude spectrum (Fourier transform) of an observable distribution, such as brightness or velocity along a line of the Sun. (b) Mean spectrum of the running mean of a function having a uniform spectral density (see text). (c) Mean spectrum which results from subtracting a running mean from a function having a uniform spectral density. (d) The spectrum which results from subtracting a running mean from a function having the spectrum shown in (a).*

The subtraction of the running mean has produced a peaked spectrum, and the observed function after subtraction of the running mean will accordingly show apparent periodicities which are artificial.

In a numerical experiment to illustrate these effects, carried out on the EDSAC II computer, a sample out of a set of random numbers (see Section 2.4) was convoluted in turn with three weighting functions w according to the numerical equivalent of eqn. (2.31). Let the sample used be the numerical representation of a function $u(x)$. Then by eqns. (2.54), (2.55) and (2.53)

$$\mathbf{F}[u*w] = U \,.\, W$$

$$\mathbf{F}[\mathbf{C}[u*w]] = |U \,.\, W|^2$$

$$\mathbf{C}[u*w] = \mathbf{F}^*[|U|^2 \,.\, |W|^2]. \qquad (2.591)$$

If the spectrum U is uniform, it follows by a second application of eqn. (2.55) that $\hat{\mathbf{C}}[u*w] = \hat{\mathbf{C}}[w]$ which justifies the statements made earlier to this effect. It also follows (Woodward 1953) that functions which are random (that is, entropy maximized), subject to having mean-squared spectra proportional respectively to the squared ordinates of curves (*a*) and (*d*) of Fig. 3, can be generated by convoluting random numbers with functions w_1 and w_2 given by

$$\mathbf{F}[w_1(x)] = \text{the ordinates of curve } (a) \text{ Fig. 3},$$

$$\mathbf{F}[w_2(x)] = \text{the ordinates of curve } (d) \text{ Fig. 3}.$$

Fig. 4 shows (*a*) the result of this operation with w_1; (*b*) with w_2; and (*c*) with a function $w_3(x) = w_1(2x)$; the scale of seconds of arc in the figure is of course purely notional. The curves displayed on the left-hand side of Fig. 2 are in fact the auto-correlation functions of w_1, w_2, w_3, and the curves on the right-hand side of this figure are the respective auto-correlation functions of curves (*a*)–(*c*) Fig. 4.

The process of generating curve (*a*) Fig. 4 is analogous to the blurring of a random distribution when it is observed with resolution corresponding to a "spread" or "apparatus" function w_1, and it will be seen that some appearance of periodicity has already been produced by this blurring (cf. Section 2.2). The appearance of periodicity is enhanced in curve (*b*), which is of course simply curve (*a*) with a running mean subtracted; this is especially noticeable at the left-hand end. In curve (*b*) the maxima (except those corresponding to fluctuations of less than 1/10 of the general amplitude) always occur at positive values of the function, and the minima correspondingly at negative values; whereas this is not everywhere true of curve (*a*). The effect of convoluting two portions of curve (*b*) is shown in Fig. 5. The periodicity has here become very obvious and, in the analysis of actual observations, this might well be taken as physically significant if it were not realized that its appearance is a simple property of the numerical process used.

The putative periodicity in the velocity-brightness cross-correlation function shown in Fig. 1 of the paper of Stuart and Rush (1954) is apparently due to effects of this kind. These authors are aware of the falsification which occurs when a running mean is subtracted, and seek to avoid it by varying the interval a in accordance with the trend of the observed values; a better method will be described in Section 3. These considerations do not of course invalidate Stuart and Rush's conclusion that the velocity-brightness correlation is greater in the higher spatial frequencies.

We saw in Section 2.4 that the auto-correlation curves shown on the right of Fig. 2 are subject to statistical errors due to the limited size of sample on which

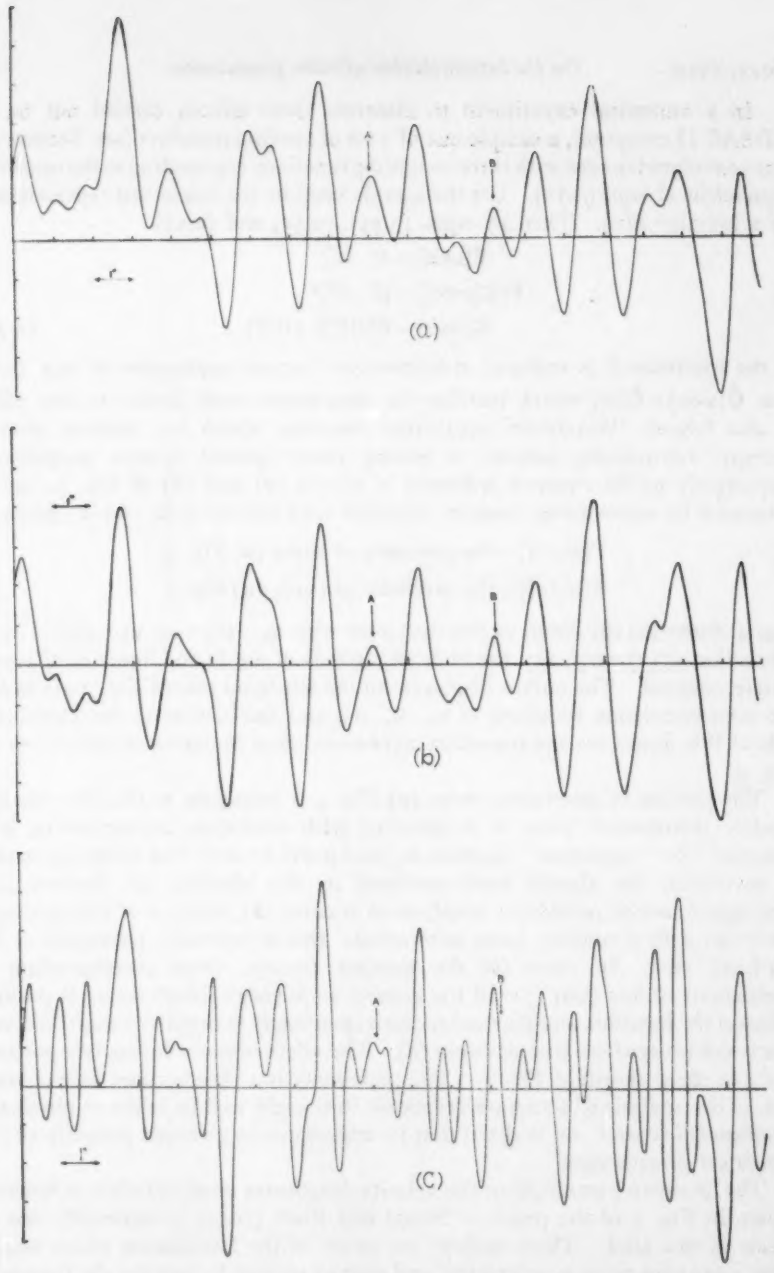

FIG. 4.—*Apparent structures in smoothed random distributions.*

(a) Plot of a sample of random numbers after a smoothing process (convolution) has been applied. (b) Identical to (a) except that the function used in the convolution is such that a running mean is subtracted as part of the smoothing operation. (c) The convoluting function used here has the same shape as that in (a) but only half the width. The curve is accordingly similar to (a) except that it has twice the "resolution".

The smoothing process has caused some appearance of quasi-periodicity in curve (a), and this has been enhanced by the subtraction of running mean in (b). All the curves were made from the same sample of random numbers. The features marked A and B are analogous to features of granulation photographs to which significance has sometimes been attached. The changes in their appearance with variation of resolution and numerical processing is discussed in the text.

they are based, and are significant only in so far as they agree with the corresponding curves on the left of the figure. We now see that the negative peak in curve (*c*) is an artifact caused by the subtraction of running means, and the width of the peak at the origin in each curve is likewise simply a property of the blurring process, as is most obviously demonstrated by curve (*e*) which (from the definition of w_3) corresponds to twice the resolution of the other two. Indeed, these three curves cannot (by the very way they were derived) tell us anything about the random numbers which, in these experiments, played a part analogous to the object-distribution in real observation. The conclusion is that none of the curves of Fig. 2 gives any explicit information about the fact that these numbers had zero mean serial correlation. Analogous curves produced from granulation observations may similarly lack significance. A comparison of curves (*a*) and (*b*) does, of course, give information about the serial correlation of the numbers used in the experiment. This emphasizes the importance of including in granulation observations an accurate determination of the blurring function corresponding to curve (*a*); clearly, this determination must be independent of any assumptions about the phenomenon under investigation.

If the curves in Fig. 4 represented scans across images of granulation, then in a high contrast reproduction of the image corresponding to curve (*a*) it might

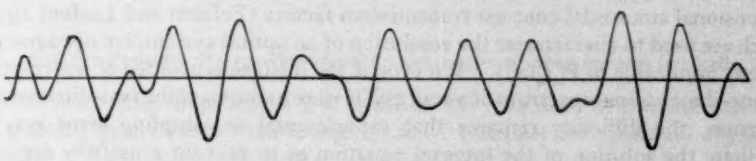

FIG. 5.—*Artificial periodicities created by numerical processes. The curve shows the cross-correlation function between two parts of the function of which Fig. 4 (b) is a sample. It is analogous to cross-correlation functions between solar velocity and brightness observations from both of which running means have been subtracted. The marked quasi-periodic appearance is totally artificial; the curve has been derived from a random set of numbers.*

appear that the feature marked B had a size of 0″·5. Significance has often been attached to the size of the smallest features apparent in granulation images, as indicating either the resolution achieved, or the size of the granulation structure. We see in curve (*b*), which has the same resolution as (*a*) but from which a running mean has been subtracted, that the size of feature B has been reduced to about 0″·3 and A is nearly as small, although it appeared much broader than B in curve (*a*). Curve (*c*), which corresponds to twice the resolution, shows A as a complex structure extending over more than 1″, and B is no longer identifiable. Moreover, both A and B are in fact spurious in the sense that complete resolution would reveal randomness devoid of any coherent structure. Caution is evidently required in interpreting granulation observations in this manner.

2.6. *The indirect equivalence of one- and two-dimensional spatial spectra.*—The observed brightness and velocity fields on the solar disk are two-dimensional manifestations of effects which vary with depth, as well as perpendicular to the line of sight. The relating of these observations to the three-dimensional velocity- and radiation-fields in the Sun would need detailed optical and hydrodynamic treatment, and so lies outside the scope of the present paper.

Our concern here is with the relationship between the two-dimensional variation of a quantity over the solar disk and the information obtained by focusing the Sun on to a spectrograph slit, or from scanning a solar image in a microphotometer.

Some general discussion of scans of two-dimensional distributions has already been given in connection with analysis of photographic grain (Fellgett 1953)*, and the discussion which follows will be mainly concerned with the special case in which the observation can be represented as $f_\eta(x)=f(x,\eta)$, where η is a constant. That is to say, f_η represents the observation secured when an image of the distribution $f(x,y)$ is viewed through a long straight slit of negligible width lying along the line $y=\eta$, or when a microphotometer spot of negligible size scans along $y=\eta$.

Fig. 6 shows a Fourier component of $f(x,y)$ having frequency t, the wavefronts of which make an angle θ with the line of the one-dimensional scan. This component is seen to give rise to a frequency $t_1=t\sin\theta$ in the one-dimensional spectrum of $f_\eta(x)$. As $t_1 \leqslant t$, the total amplitude of the Fourier component of f_η having frequency t_1 is the sum of contributions from all the two-dimensional components of $f(x,y)$ which have frequencies $t \geqslant t_1$. Accordingly, the determination of the two-dimensional spectrum $\mathbf{F}[f(x,y)]$ from the one-dimensional $\mathbf{F}[f_\eta(x)]$ involves the solution of an integral equation, one form of which is given by Uberoi (1955)† as his eqn. (6). Uberoi has emphasized that the two-dimensional sinusoidal contrast transmission factors (Fellgett and Linfoot 1955), which are used to characterize the resolution of an optical system, are of course not directly applicable to $\mathbf{F}[f_\eta(x)]$. But even if the mistake is avoided of interpreting the one-dimensional spectrum of a scan as if it were a section of the two-dimensional spectrum, the difficulty remains that experimental or sampling error may so dominate the solution of the integral equation as to prevent a usefully accurate estimate of $\mathbf{F}[f(x,y)]$ being made from the one-dimensional observations f_η, especially in the lower-frequency range. Dr E. H. Linfoot has pointed out to me that this difficulty is avoided if the small scanning spot, commonly used in this kind of measurement, is replaced by a long slit perpendicular to the direction of scan, as employed in measuring optical spectra. With this method of scanning (which is of course quite different from the case of a *fixed* spectrograph slit masking the image) the observed quantity may be written

$$g(x)=\int dy f(x,y) \tag{2.61}$$

where the integration is over the length of the slit.

In general, when $f(x,y)$ is scanned with a mask having transmission $w(x-a,y-b)$, where (a,b) is at any instant the position of a chosen reference point of the mask, the observed quantity is

$$\phi(a,b)=\int\int_{-\infty}^{\infty} f(x,y)w(x-a,y-b)\,dx\,dy. \tag{2.62}$$

Equation (2.54) then shows how the spectrum of f has been modified by the scanning process, and the effect of any practical shape of slit or other aperture can be determined in this way.

* The Fourier operator in this paper is incorrect by a factor 2π in the exponent.

† In equations 16 to 19 of Uberoi's paper, and in the next unnumbered expression, the factor printed

as $\cos^{-1}\left(\frac{k}{k_0}-\frac{k}{k_0}\right)\left\{1-\left(\frac{k}{k_0}\right)^2\right\}^{1/2}$ should read $\cos^{-1}\left(\frac{k}{k_0}\right)-\frac{k}{k_0}\left\{1-\left(\frac{k}{k_0}\right)^2\right\}^{1/2}$.

The function $f_\eta(x)$ and $g(x)$ have particularly simple properties which it is more convenient to derive by a method which is special to these limiting cases.

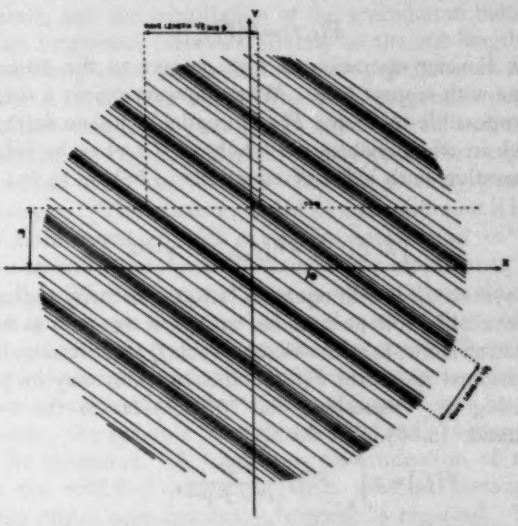

FIG. 6.—*Projection of a two-dimensional Fourier component onto a line scan (see text).*

The effects of the finite length and width of the slits used in practice can then be assessed by reference back to eqn. (2.62). Consider the spectrum of $f(x,y)$, namely

$$\mathsf{F}[f(x,y)] = F(s,t) = \int\int_{-\infty}^{\infty} f(x,y) \exp\{2\pi i(xs+yt)\}\, dx\, dy. \qquad (2.63)$$

Along the s-axis $t=0$,

$$F(s,0) = \int_{-\infty}^{\infty} dx \exp\{2\pi i x s\} \int_{-\infty}^{\infty} dy f(x,y) \qquad (2.64)$$

and, if the scanning slit is so long that infinite limits can be used in equation (2.61),

$$F(s,0) = \mathsf{F}[g(x)]. \qquad (2.65)$$

It follows that $\mathsf{F}[f(x,y)]$ can be simply determined from scans of a long narrow slit across $f(x,y)$ in different directions, without the need to solve an integral equation. If f is symmetric so that $F(s,t)=F(r)$, $r^2=s^2+t^2$, then only a single scan is needed. These favourable properties may be thought of as arising because any localized feature in $f(x,y)$ remains well localized with respect to the set of g taken over all directions, so that "sharpness" is preserved; and because the whole of $f(x,y)$ is covered in each scan.

The whole set of $f_\eta(x)$, for all η, also has these properties of localization and completeness, and $F[f(x,y)]$ can be simply derived from the set. Numerical two-dimensional Fourier transformation is commonly done in this way by using equation (2.63) in the form

$$\mathsf{F}[f(x,y)] = \int d\eta \exp\{2\pi i \eta t\} \int dx f(x,\eta) \exp\{2\pi i x s\} \qquad (2.66)$$

where the integrations are nominally infinite and in practice are taken over the available sample of $f(x, y)$. This equation may be written in the more compact form

$$F(s,t) = \mathbf{F}[\mathbf{F}[f_\eta]] \tag{2.67}$$

where the inner Fourier operation is with respect to the dummy variable x, and the outer one with respect to η. When, however, only a single f_η is known it is evidently impossible to derive $F(s, t)$ explicitly unless further information is available which in effect enables the whole of $f(x, y)$ to be inferred from the sample f_η. Integrating both sides of equations (2.66) or (2.67) yields (after a limiting process)

$$\int dt\, F(s,t) = \mathbf{F}[f_\eta], \qquad \eta = 0. \tag{2.68}$$

This equation is symmetrical with equation (2.64). In many applications where a single scan f_η is available, it is permissible to regard this scan as being along the x-axis. The equation shows that knowledge of this f_η alone fixes only the t-integral of the two-dimensional spectrum $F(s, t)$; this function may be pictured as the result of projecting or "squashing flat" $F(s, t)$ on to the t-axis. If f is symmetrical, equation (2.68) takes the form

$$\mathbf{F}[f_\eta] = 2\int_s^\infty F(r)\frac{r\,dr}{(r^2 - s^2)^{1/2}}, \qquad \eta = 0. \tag{2.69}$$

This is a special case of the conclusion drawn earlier, from Fig. 6, that the value taken by the one-dimensional spectral function $\mathbf{F}[f_\eta]$ at a given frequency is the weighted sum of the values taken by the two-dimensional spectrum $F(s, t)$ at equal and higher frequencies. When (2.69) applies, $F(s, t)$ can be explicitly evaluated from f_η but (as has been mentioned above) often only with low accuracy.

Indeed if f is random, subject to having a statistical mean power-spectrum, the amplitude of a Fourier component of f, or of any scan of it, has a Gaussian probability distribution with zero mean and variance equal to the mean power (Shannon 1948). The squared amplitude is therefore an estimate of this power having variance equal to twice its mean value. It follows that the spectral density of a stochastic phenomenon can be estimated accurately only by considerable averaging, either with respect to frequency or over different scans. This is so even when errors of measurement are negligible; and conversely errors of measurement only a little smaller than the quantities measured need not greatly increase the variance of the estimates of the principal components. For point scans, the relative uncertainty can be so much increased in the transformation from the spectrum of $f_\eta(x)$ to that of $f(x, y)$ (using the inverse of equation (2.69)) that it is not usually worth while to attempt this transformation unless very many scans f_η are measured. It may then be better to arrange them in a raster so that the two-dimensional spectrum can be obtained directly using equation (2.66).

Slit scans, as well as being more convenient (equation (2.65)), avoid this serious loss of accuracy; $g(x)$ is a much better sample of a stochastic function f than is $f_\eta(x)$. Lengthening the slit extends to lower frequencies the frequency-range over which equation (2.65) is a good approximation to equation (2.62). It also has the practical advantage of increasing the total fluctuating signal, asymptotically as the square root of the slit-length. This enables the amplifier gain to be reduced, so that amplifier noise and detector dark-noise have less effect. The signal-to-noise

ratio in the light itself is not increased, however, since noise uncorrelated at the two ends of the slit increases in the same manner as the signal. Photon noise, photographic grain, and the scintillation of the granulation behave in the same way. The mean brightness increases directly as the slit-length, so that if for example the r.m.s. brightness fluctuation were 0·05 of the mean for 1″ slit length, it would be 0·002 for a slit 600″ long. The mean brightness does not affect the amplifier, since zero-frequency response is not required and the detector will normally be coupled to the amplifier through a condenser capable of passing alternating signals of order 10^{-6} V while blocking a steady potential difference some 10^{8} times larger. (The situation would be quite different if it were necessary to *measure the mean brightness* with a relative accuracy of 10^{-3}, which would require the gain-stability and dynamic range of the amplifier to be enhanced by negative feedback.) The low contrast does imply that direct slit-scans of the Sun will be sensitive to changes in the overall brightness of the sunlight, which will presumably be due more to transparency than to seeing effects for a disk 30′ in diameter. If these changes cannot be sufficiently separated in frequency from the desired ones by a suitable choice of rate of scan, it may be necessary to use balanced detectors; for example the difference in the light passed by two halves of a slit may be measured. A brightness discrimination of 10^{-6} has proved practicable in the balanced photocells often used to measure small optical deflections, even where zero-frequency response is required. Photon noise, as modified by the detector, is especially relevant to the measurement of velocity. If the r.m.s. velocity variation were say 0·5 km/sec for a 1″ slit, it would be 0·02 km/sec r.m.s. for a 600″ slit. I am grateful to Mr D. W. Beggs for information that the Cambridge Solar Magnetograph gives an r.m.s. noise equivalent to 0·01 km/sec for a slit only 60″ long, indicating that the 12-inch aperture of this instrument is sufficient for the measurement of Doppler-granulation. The ratio of this r.m.s. noise to the velocity amplitude accords as to order of magnitude with the accuracy of measurement attained in the point-scans discussed in Section 3, as the present discussion leads us to expect.

The disadvantages of the point-scan f_η are somewhat mitigated when the purpose is to determine the two-dimensional power spectrum of a function $f(x,y)$ which is statistically stationary as well as isotropic. In photographic measurements, it has the advantage that the non-linear relation of density to exposure is more easily allowed for than in other methods of scanning. The auto-correlation functions of $f(x,y)$ and $f_\eta(x)$ may be written

$$C(\xi,\eta)_f = \mathbf{C}[f] = \int\int dx\,dy f(x,y).f(x+\xi,y+\eta),$$

$$C(\xi)_f = \mathbf{C}[f_\eta] = \int dx f(x,\eta).f(x+\xi,\eta).$$

The domain of integration is as in equation (2.66). For $\eta = 0$

$$\begin{aligned} C(\xi,0)_f &= \int dy \int dx f(x,y).f(x+\xi,y), \\ &= \int dy\, C(\xi)_f, \\ &= C(\xi)_f \int dy, \end{aligned} \qquad (2.691)$$

where the last step follows from the stationary property. Hence knowledge of f_η is sufficient to fix $C(\xi, 0)$. By isotropy $C(\xi, \eta) = C(\zeta)$, $\xi^2 + \eta^2 = \zeta^2$, and by equation (2.55) the required power spectrum is $|F(s,t)|^2 = \mathbf{F}[C(\xi,\eta)_f]$. In the practical use of this method the heavy work of two-dimensional Fourier transformation is avoided by forming

$$|F(s,0)|^2 = \mathbf{F}\left[\int C(\xi,\eta)_f \, d\eta\right] \tag{2.692}$$

$$= \mathbf{F}\left[2\int_\xi^\infty C(\zeta)\frac{\zeta\, d\zeta}{(\zeta^2-\xi^2)^{1/2}}\right]. \tag{2.693}$$

The proof of these relations follows by comparison with equation (2.64).

3. *The data and calculations*

The foregoing discussion illustrates that a central problem in the interpretation of solar granulation is to determine, in a way which does not introduce artifacts, which frequencies are most strongly present in the observed velocity and brightness fields, and which frequencies contribute most strongly to the correlation between velocity and brightness. It is first necessary to give a definite meaning to these questions in a way which is acceptable to intuitive notions.

Let $v(x)$ and $b(x)$ be respectively the deviations from their mean values of the Doppler velocity, and of the brightness, at a point x of the Sun; as before, x may be regarded as either one- or multi-dimensional, and integrations will be over the available data unless otherwise indicated. The total *power*, or unnormalized variance, of v is defined (since $\bar{v} = 0$) as

$$C_v = \int v^2(x)\, dx; \tag{3.1}$$

the definition for b is of course similar, here and in what follows. The *correlation* between b and v is defined as

$$C_{vb} = \int v(x)\, b(x)\, dx. \tag{3.2}$$

The ordinary *correlation coefficient* is obtained when C_{vb} is normalized by division by $(C_v C_b)^{1/2}$. We have seen that difficulties may arise when the attempt is made to modify the observed quantities $v(x)$ or $b(x)$ by subtracting running means, or in other ways, for the purpose of finding the contribution to C_v or C_b from different frequency ranges. The problem becomes tractable when account is taken of the fact that C_v, C_{vb} are the respective values for $\xi = 0$ of the autocorrelation function

$$\mathbf{C}[v] = C(\xi)_v = \int v(x)\, v(x+\xi)\, dx \tag{3.3}$$

and of the cross-correlation function

$$\mathbf{C}[v,b] = C(\xi)_{v,b} = \int v(x)\, b(x+\xi)\, dx. \tag{3.4}$$

By equations (2.51)–(2.55)

$$\mathbf{F}[C(\xi)_{v,b}] = V(t).B^*(t), \tag{3.5}$$

$$C(\xi)_{v,b} = \mathbf{F}^*[V(t).B^*(t)], \tag{3.6}$$

$$C_{v,b} = C(0)_{v,b} = \int_{-\infty}^{\infty} V(t)B^*(t)\, dt, \tag{3.7}$$

$$= \int_{-\infty}^{t_1} VB^*\, dt + \int_{t_1}^{t_2} VB^*\, dt + \int_{t_2}^{\infty} VB^*\, dt, \tag{3.8}$$

where the asterisk denotes the complex conjugate. Equation (3.8) expresses the correlation C_{vb} as a sum of contributions from different frequency ranges. Each of these contributions is the integral, over the appropriate range of frequency t, of the *cross-correlation spectrum* $\mathsf{F}[C(\xi)_{vb}]$.

Accordingly, we may without inconsistency define

$$\int_{t_1}^{t_2} V(t)B^*(t)\,dt$$

as the *contribution to the correlation C_{vb} from the frequency components of the cross-correlation spectrum lying in the interval t_1 to t_2*. The formal substitution $v(x)=b(x)$ shows that in the same manner

$$\int_{t_1}^{t_2} |V(t)|^2\,dt$$

may be called the *contribution to the power of v from the frequency components of the power-spectrum of v lying in the interval t_1 to t_2*. It will be seen that, in agreement with intuitive ideas, the contribution to C_{vb} from any frequency interval is large and positive if V and B, the frequency-spectra of v and b, both take large values and have the same phase in this interval; it is large and negative if V and B are large but of opposite phase. In a similar way, the contribution to C_v or C_b is large for those frequency intervals in which the power-spectra $|V|^2$ or $|B|^2$ take large values. If C_v, C_b or C_{vb} is real, the contribution from $-t_1$ to $-t_2$ is the complex conjugate of that from t_1 to t_2. The contribution from the interval t_1 to $t_2>t_1$ will then be understood to mean the contribution from the double range $t_1<|t|<t_2$ (a similar convention exists in electrical engineering).

These definitions, by giving a precise form to questions concerning which frequencies contribute most to C_v, C_b or C_{vb}, make it possible to calculate these contributions from the experimental data. It was shown in Section 2 that any "smoothing" or "unsmoothing" process distorts the frequency spectra (equation (2.54)). Therefore the only safe procedure is to calculate the frequency spectra numerically from unmodified raw data, and to pick out explicitly any frequency ranges that show themselves to be of special interest.

The data used are the 340 brightness and velocity measures obtained by Richardson and Schwarzschild (1950) at Mt Wilson and the three sets of 116 measures obtained by Plaskett (1954) at Oxford on 1949 September 11·4306, 1949 September 11·4319, and 1950 May 11·7277. These data will be referred to as Mt Wilson, Oxford September A, Oxford September B and Oxford May respectively. The auto-correlation functions and power spectra of the Mt Wilson data extend slightly the calculations already published and discussed by Frenkiel and Schwarzschild (1952), and by Uberoi (1955). The calculations on the Oxford data, and the calculation of the cross-correlation function and its spectrum for both the Oxford and the Mt Wilson data, are new. The data represent one-dimensional scans; when the one-dimensional correlation and Fourier calculations on them were completed it appeared that little additional information would be gained by deriving spatial spectra of the two-dimensional granulation on the assumption of isotropy (Section 2.6). A much larger sample would be needed before this could be done with useful accuracy.

The auto- and cross-correlations were programmed and run on the EDSAC I computer by Mrs M. Mutch. The Fourier transforms were calculated by Miss C. P. Wilks on Lipson Beevers strips (Lipson and Beevers 1936). This combination of machine and semi-hand methods was very economical in relation to the sources available when the calculations were made. It has been rendered obsolete, however, by the much faster and more convenient computers which have since become available. A programme which I wrote for the EDSAC II computer enables the Fourier transform of 1000-ordinate data to be calculated at a rate of 20 output ordinates per minute, and further economies would be possible by improved programming. When new data on solar granulation are published it should be possible to do the calculations on them with little more time and labour than is needed to convert them to digital form.

The correlations were evaluated in the numerical form

$$c_m = \frac{\sum_{r=M}^{N-M-1} a_r b_{r+m}}{\sum_{r=M}^{N-M-1} a_r b_r}$$

where $a_0(a_r)a_{N-1}$ are the N ordinates of one set of data at equal intervals of the argument, $b_0(b_r)b_{N-1}$ the corresponding ordinates of the other set; m is the value of the shift and is calculated in the range $-M \leqslant m \leqslant M$. If $a_r = b_r$ then c_m is an auto-correlate. This form of c_m was suggested to me by Dr M. V. Wilkes. For use in connection with Fourier methods, it has the advantages that the normalizing factor and the statistical weight are both independent of m. The disadvantage is that the weight is less than it could be for small values of the shift m. The auto-correlation in this form is statistically symmetrical, but not necessarily symmetrical for any particular sample of data.

The results of the computations are presented graphically in Figs. 7–11. The Mt Wilson data are at intervals of $0''{\cdot}45$ arc = 328 km on the Sun, and the correlations are calculated up to a maximum shift of $M = 60$ of these intervals. The Oxford data are at intervals of $1''{\cdot}04$ arc, corresponding to 759 and 756 km on the Sun for 1949 September and 1950 May respectively, and the correlations are for $M \leqslant 30$. The total intervals covered by the Mt Wilson and Oxford data are thus 111 500 km and 88 000 km, and the maximum shifts correspond to $\pm$ 19 700 km and $\pm$ 22 700 km respectively. Only the cosine components of the Fourier transforms are shown; as mentioned above, the sine components are statistically zero.

4. *Discussion*

4.1. *The brightness auto-correlation and power spectra.*—The present brightness auto-correlation curve derived from the Mt Wilson data, the corresponding curve of Frenkiel and Schwarzschild (1952, Fig. 1), and that of Uberoi (1955 a, Fig. 3), differ among themselves by more than might be expected from the differences in numerical techniques.

Each of the four brightness auto-correlation curves shown in Figs. 7–10 has a peak centred on zero shift with width roughly corresponding to the expected instrumental resolution. For the Oxford results, this peak is superposed on a

wider one (particularly marked for September A) which may be of instrumental origin associated with slow changes in sensitivity or black-level.

We saw in Section 2.6 that an ordinate of the unsmoothed power spectrum of a "random" function has an r.m.s. uncertainty equal to $\sqrt{2}$ times the expected value of the ordinate. For the Oxford data, the power spectra have been found by Fourier transformation of correlation functions determined over a total range of 60 units of shift. The total length of the available data is 116 units, and accordingly the power spectra found have a resolution of only about one-half that which corresponds to the whole run of the data. This implicit smoothing gives a ratio of signal to r.m.s. noise of about unity for each ordinate. For the Mt Wilson data, the resolution is about one-third the value corresponding to the length of the data, and the ratio of signal to r.m.s. noise is about 1·2 for each ordinate. The 0th ordinates of the brightness-spectra have no physical significance; they simply reflect the mean level of the brightness compared with the reference level chosen. When these facts are taken into account, the brightness power-spectra appear to be more or less steadily falling functions of frequency and present no very remarkable features. The independent brightness-correlation curves of Uberoi (1955a, Fig. 3) and of Frenkiel and Schwarzschild (1955, Fig. 1) also agree in showing no significant secondary peaks; the latter curve is based on about 2000 independent measures and hence has much greater weight than the brightness data used in the present work.

4.2. *The velocity auto-correlations and power spectra.*—The 0th ordinate of each of the Oxford velocity auto-correlation curves is seen to be larger than would correspond to smooth interpolation between the neighbouring values. This reflects errors of measurement ("noise") uncorrelated from point to point of the velocity data. It causes the mean of the ordinates of the power spectrum at large wave-numbers to be non-zero. The actual value of this mean is about 0·4, corresponding to a ratio (see Section 2.4)

$$\frac{N}{S+N}=0{\cdot}4, \qquad \frac{S}{N}=1{\cdot}5$$

where S = the power of the noise-free data and N = the power of the noise fluctuations. This estimate agrees well with the ratio $S/N=1{\cdot}4$ estimated by Plaskett (1954, p. 256). The Mt Wilson velocity spectrum has a mean value for large wave-numbers of about 0·05, corresponding to $S/N=20$; the value implied by Richardson and Schwarzschild is 25·4.

Apart from the 0th ordinate, the Oxford May velocity auto-correlation appears similar to the Oxford brightness auto-correlations discussed in Section 4.1. The September A and September B correlations, however, have a markedly periodic appearance, which shows up as peakiness in the corresponding power spectra. The likelihood of these curves is quite small on the assumption that the periodicity is accidental. The fact that the periods differ, by a factor of nearly 2 : 1, between the two exposures made within about a minute of time of each other is somewhat opposed to the view that the effect is instrumental. Its reality is also supported by the circumstance that similar periodicities show (though weakly) in the corresponding brightness auto-correlations, and that they are prominent and have consistent sign in the cross-correlation spectra.

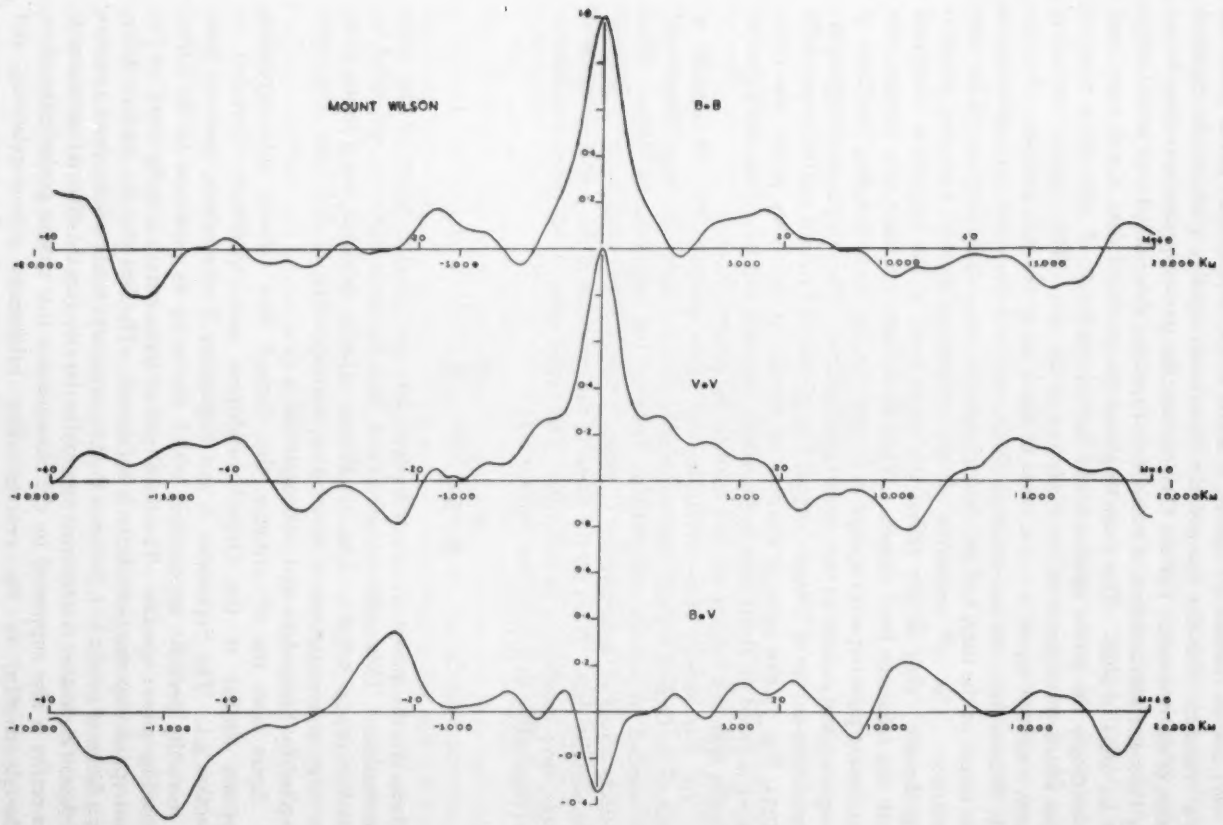

FIG. 7.—*Mt Wilson granulation observations.*
(a) Top, brightness auto-correlation function; centre, velocity auto-correlation; bottom, brightness-velocity cross-correlation.

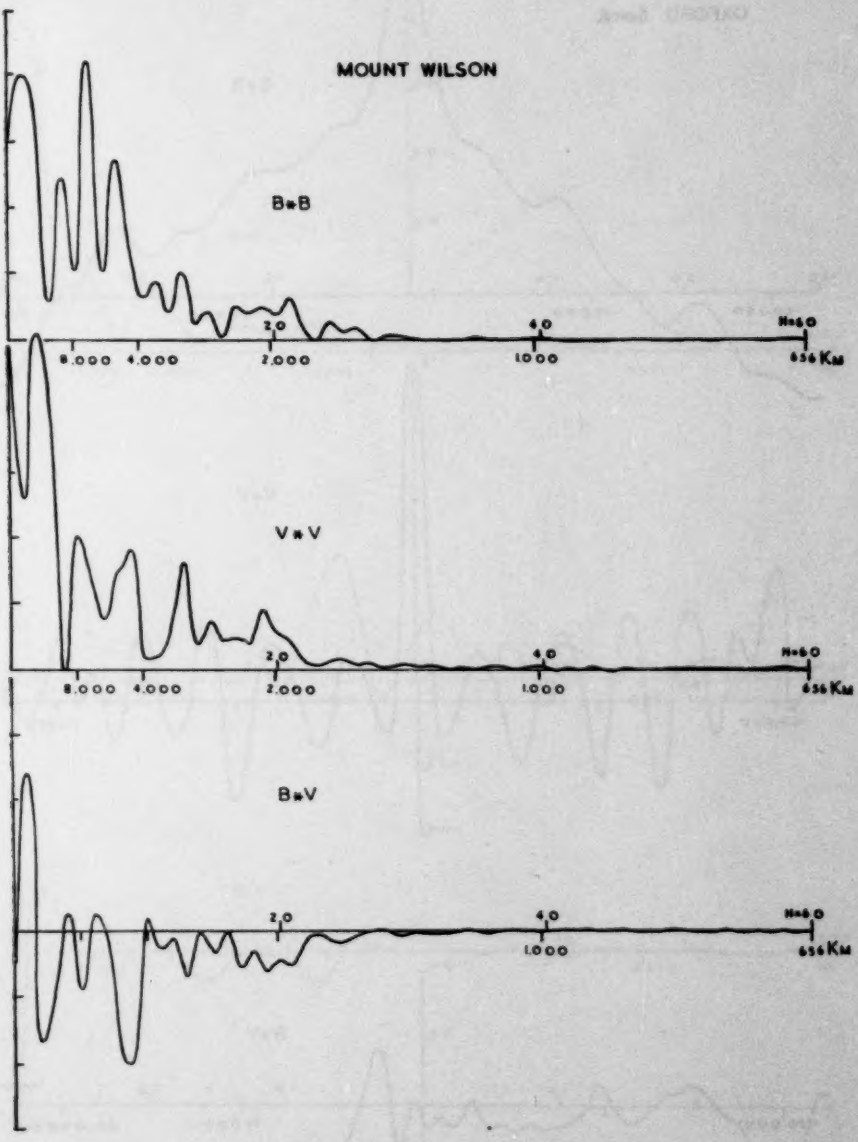

FIG. 7.—*Mt Wilson granulation observations.*

(*b*) *Power spectra and cross-correlation spectra corresponding to the functions displayed in* (*a*) (*see text*).

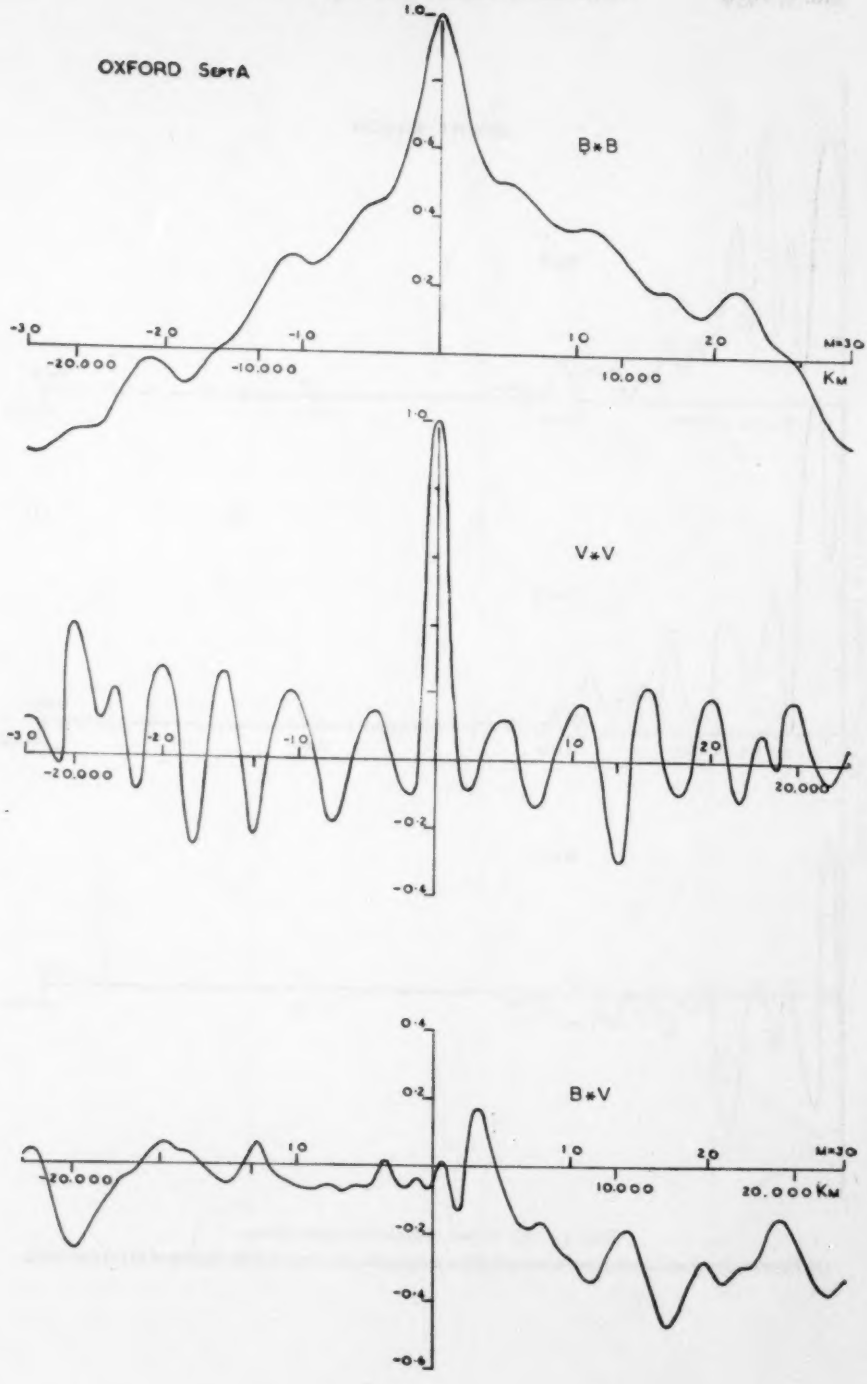

(a)

FIG. 8.—*Oxford September A observations; plotted as in Fig. 7.*

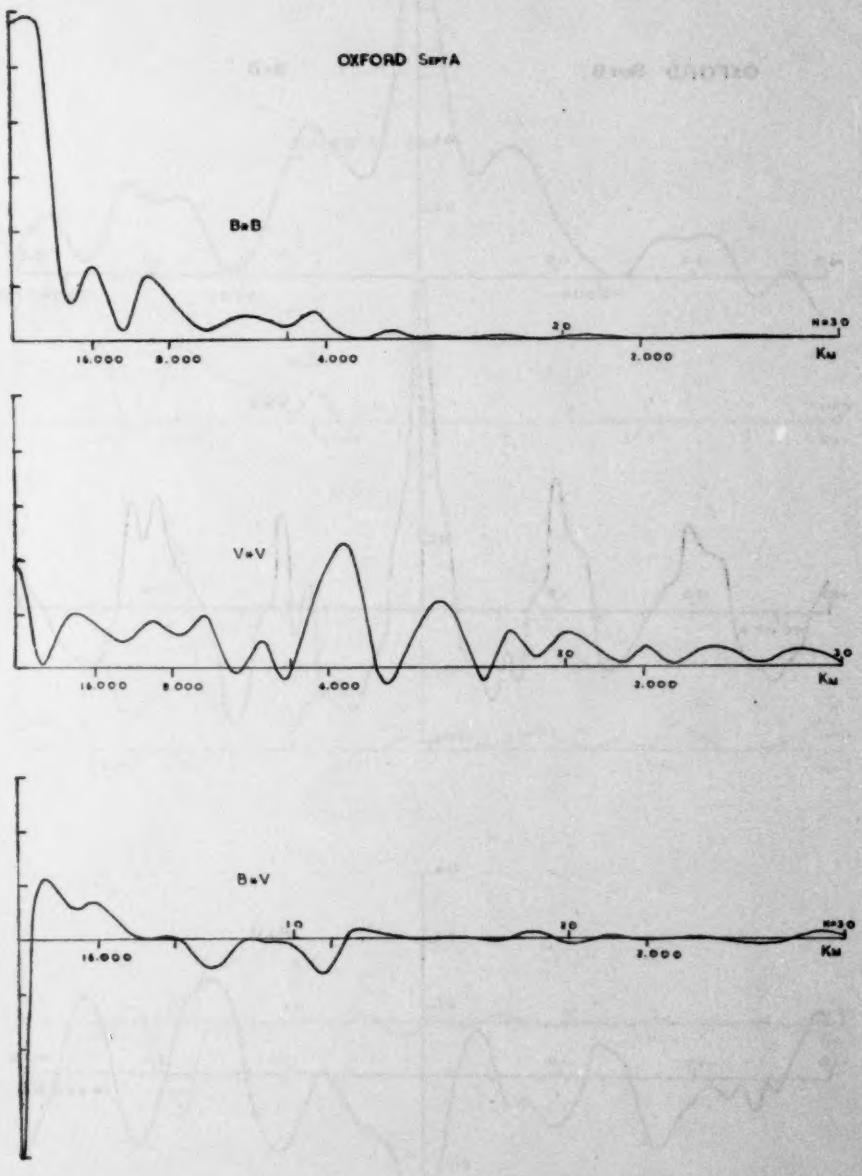

(*b*)

FIG. 8.—*Oxford September A observations; plotted as in Fig. 7.*

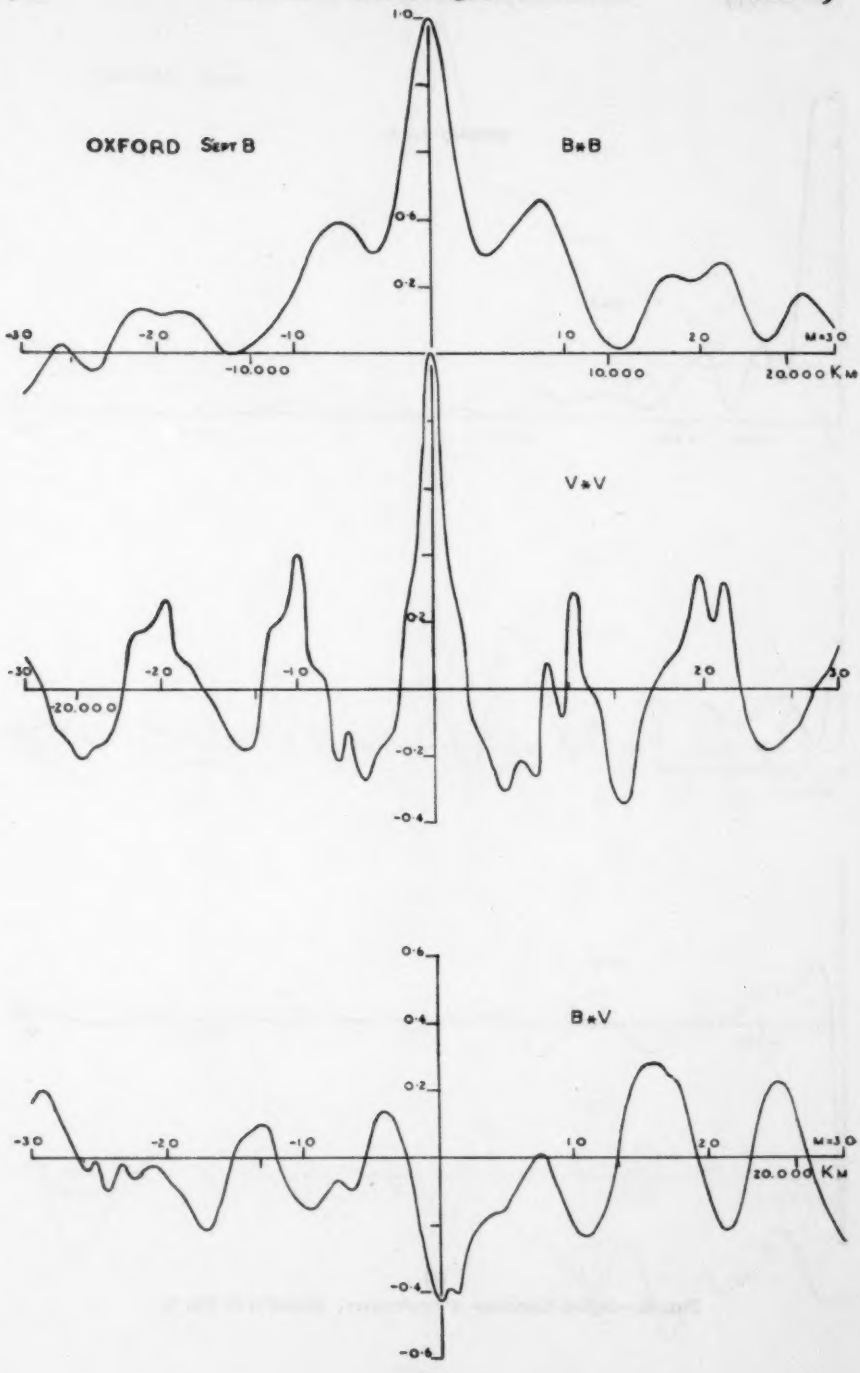

(*a*)

FIG. 9.—*Oxford September B observations; plotted as in Fig. 7.*

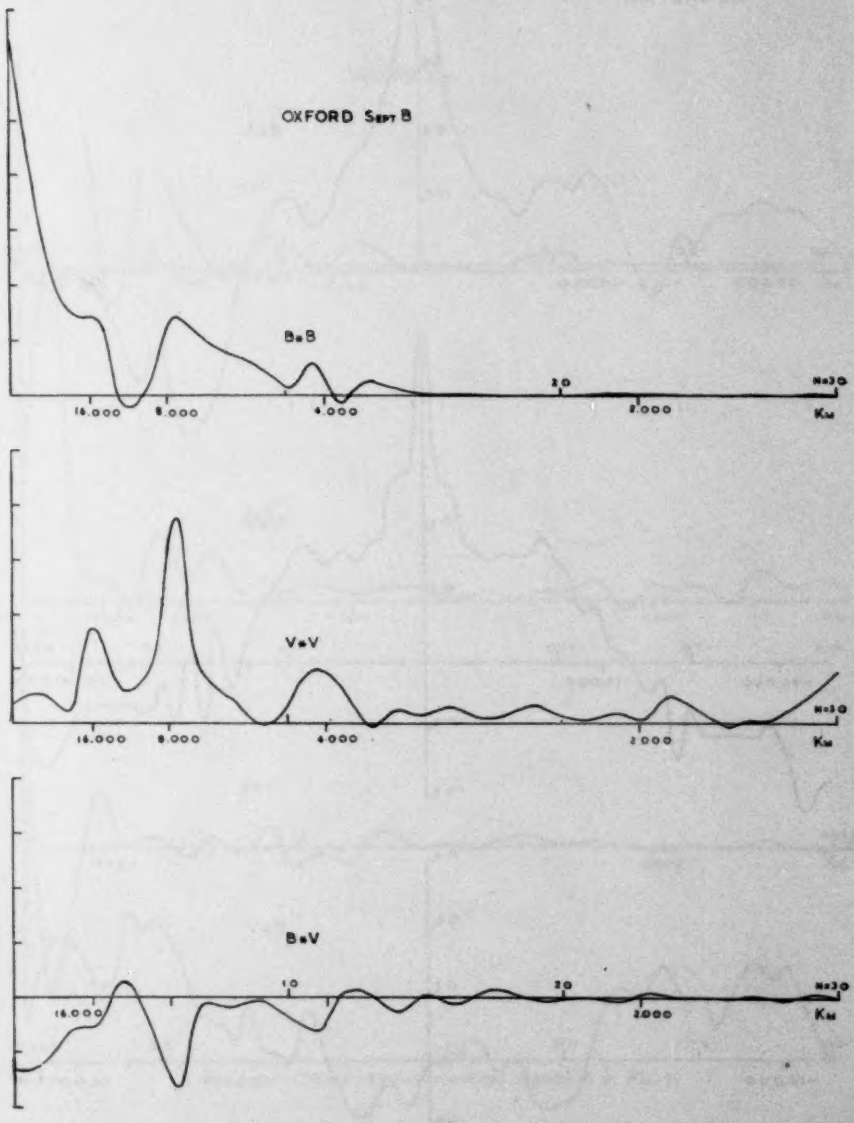

(*b*)

FIG. 9.—*Oxford September B observations; plotted as in Fig. 7.*

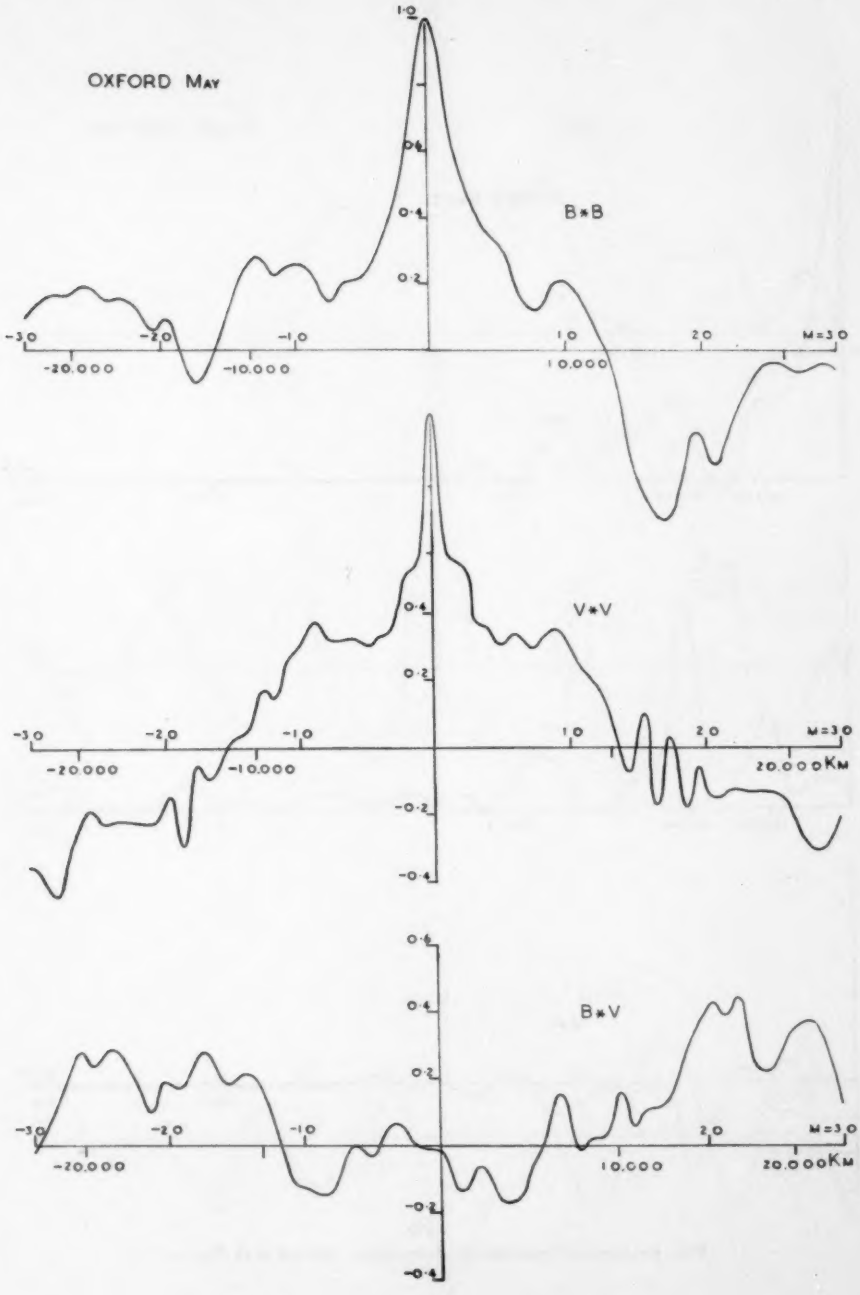

(*a*)

FIG. 10.—*Oxford May observations; plotted as in Fig. 7.*

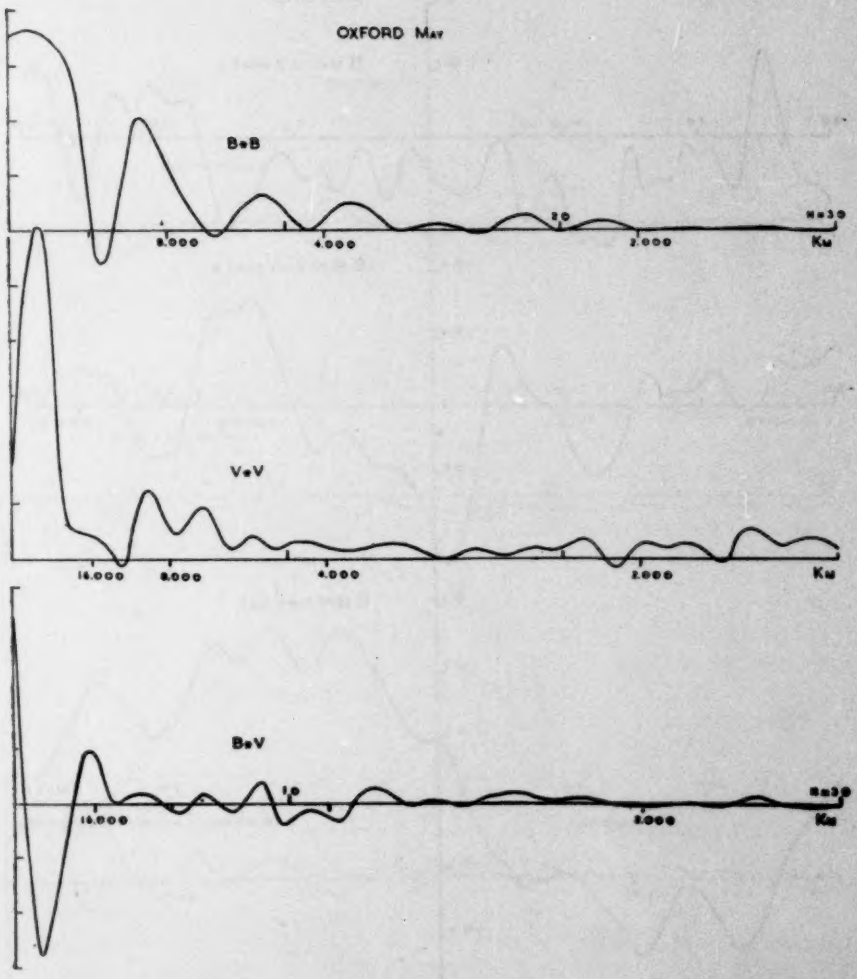

(*b*)

FIG. 10.—*Oxford May observations; plotted as in Fig.* 7.

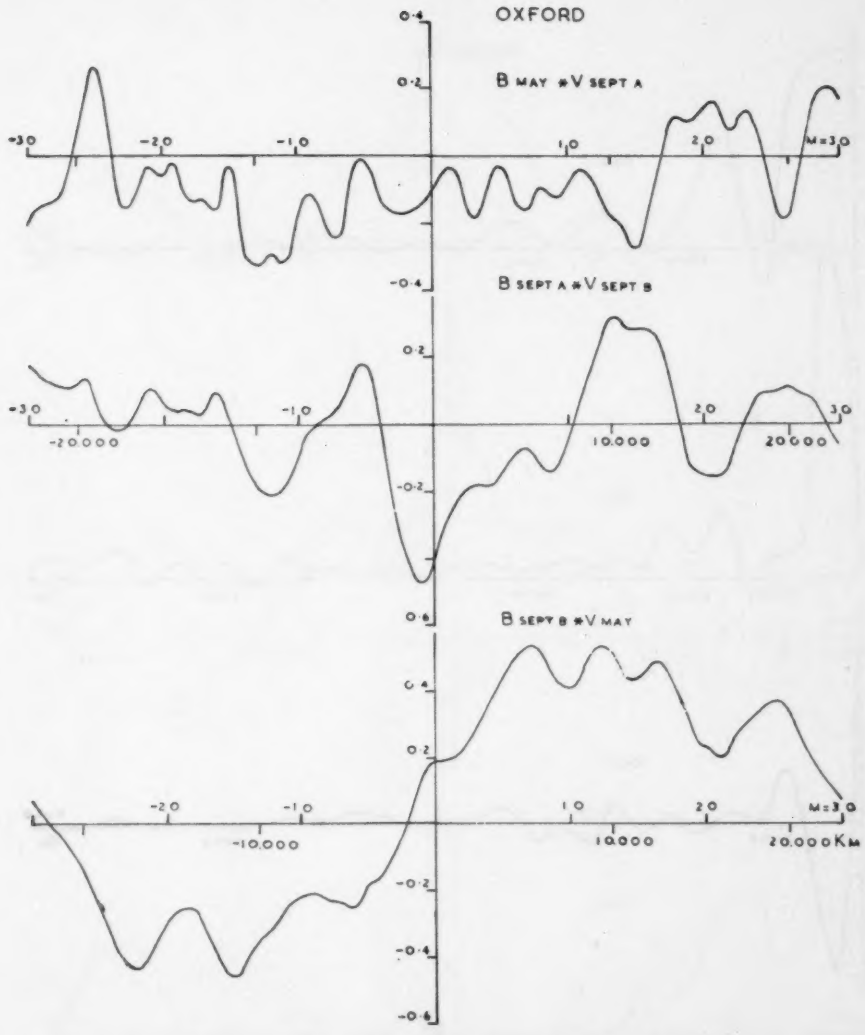

FIG. 11.—*" Incorrect " cross-correlations.*

(a) Cross-correlation between brightness from one Oxford spectrogram and velocity from a different one; top, May brightness—September A velocity; centre, September B brightness—September B velocity; bottom, September B brightness—May velocity.

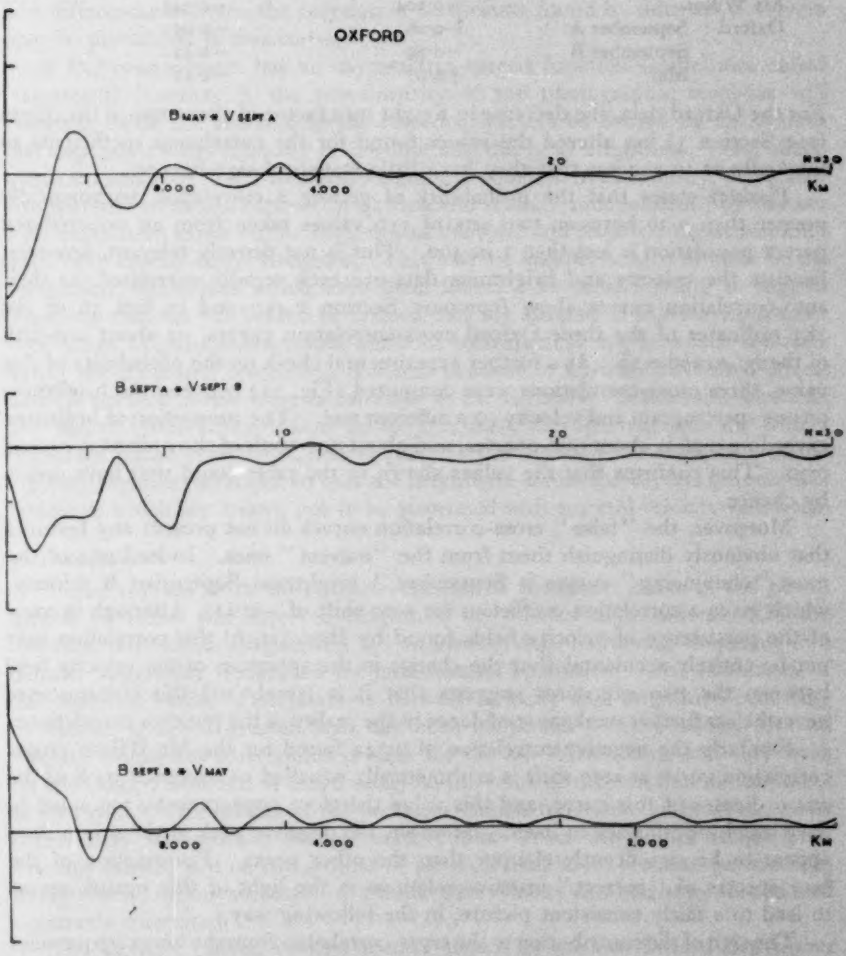

FIG. 11.—*" Incorrect " cross-correlations.*

(b) The cross-correlation spectra corresponding to the functions shown in (a).

4.3. *The brightness–velocity cross-correlations and correlation spectra.*—In the table which follows, the values calculated in the present work of the brightness-velocity cross-correlation coefficient for zero shifts are compared with the values derived by the observers themselves.

	Published value	*Present estimate*
Mt Wilson	−0·304	−0·344
Oxford : September A	−0·26	−0·05
September B	−0·29	−0·42
May	+0·07	−0·18

For the Oxford data, the decrease in weight by a factor of about two at the origin (see Section 3) has altered the values found for the correlation coefficients so markedly as to suggest that they have little statistical significance.

Plaskett states that the probability of getting a correlation arithmetically greater than 0·26 between two sets of 116 values taken from an uncorrelated parent population is less than 1 in 460. This is not directly relevant, however, because the velocity and brightness data are each serially correlated, as their auto-correlation curves show (compare Section 2.4); and in fact 36 of the 183 ordinates of the three Oxford cross-correlation curves, or about one-fifth of them, exceed 0·26. As a further experimental check on the probability of this value, three cross-correlations were computed (Fig. 11) between the brightness on one spectrogram and velocity on a different one. The proportion of ordinates exceeding 0·26 is about one-quarter, and about one-sixth of the ordinates exceed 0·30. This confirms that the values shown in the table could well have arisen by chance.

Moreover, the "false" cross-correlation curves do not present any features that obviously distinguish them from the "correct" ones. Indeed one of the most "convincing" curves is September A brightness–September B velocity, which gives a correlation coefficient for zero shift of −0·41. Although in view of the persistence of velocity fields found by Hart (1956) this correlation may not be entirely accidental (but the change in the spectrum of the velocity field between the two exposures suggests that it is largely so) this circumstance nevertheless further weakens confidence in the reality of the putative correlations.

Similarly the negative correlation of 0·344 found for the Mt Wilson cross-correlation curve at zero shift is arithmetically equalled or exceeded by 8 of the 121 ordinates of this curve, and this value therefore appears to be too small to have much significance in itself. However, the negative peak at the origin does appear to be significantly sharper than the other peaks. Examination of the four spectra of "correct" cross-correlations in the light of this remark seems to lead to a fairly consistent picture, in the following way.

The sign of the contribution to the cross-correlation from the lower frequencies in the correlation-spectra shows no apparent systematic trend, but the higher frequencies make a predominantly negative contribution for the Mt Wilson data, Oxford September A and Oxford September B; their average contribution is small for Oxford May. This is in agreement with the observation of Stuart and Rush (1954) that the negative brightness–velocity correlation for the Mt Wilson data can be approximately doubled by removing the lower frequencies. Moreover, in all the three cases where marked peaks in the velocity spectra for Oxford September A and B coincide with reasonably large values of the brightness spectrum, there is a negative peak at the same frequency in the

corresponding cross-correlation spectrum. The likelihood of these three contributions all being negative by chance is one-eighth. The "false" cross-correlation spectra do not share this systematic property.

The lack of consistent correlation at low frequencies need not be a property of the Sun, since (as was mentioned in Section 4.1) the observations at these frequencies may be strongly affected by slow drifts in instrumental characteristics. The differences between the correlation coefficients found by different observers may be partly due to this cause.

If the spectrograph has an asymmetric spread function (sometimes called "apparatus function"), the non-linearity of the photographic response will evidently cause the centroid of the recorded lines to be shifted by an amount that depends on the intensity of the line and the local brightness. The effect, which is analogous to the so-called magnitude equation in astrometry, may cause an apparent correlation between brightness and velocity, independently of whether such correlation exists on the Sun, unless the solar and telluric comparison lines used have exactly equal strengths. This may be another source of error in the correlation coefficients which have been found. There is nothing to suggest positively that the Mt Wilson or Oxford data are affected in this way, but since even small brightness-correlated shifts of instrumental origin would seriously falsify the measured correlation it seems prudent to envisage that such effects may be present unless there is evidence to the contrary. A desirable check in any future observations would be to illuminate the spectrograph slit with a defocused image of the Sun, and to place in the optical train a screen (such as a grainy negative) arranged so that the brightness across the slit has granule-like variations which are known not to be associated with any real velocity variations.

5. *Conclusions*

There appears to be no reliable evidence of consistent peaks in the power spectra of either the observed brightness or velocity distributions. On the contrary, both kinds of spectrum fall on average with increasing frequency in a manner apparently dominated by instrumental resolution. The likelihood of the observed values of correlations between velocity and brightness occurring by chance is much greater than has been supposed. The evidence for real velocity–brightness correlations is weak for the Mt Wilson data, and very weak for the Oxford data, if it is based solely on the value of the correlation coefficient at zero shift. The spectra of the cross-correlation functions do, however, show consistently non-positive average contributions from the higher frequencies. For this reason, and on the ground of physical likelihood, it seems permissible, though by no means necessary, to assume that velocity and brightness are indeed negatively correlated.

The strongly peaked velocity spectra shown by the two Oxford September exposures are rather surprising, but not inconsistent with the excellent Doppler-granulation pictures secured by McMath *et al.* (1956). Some of these pictures displayed at the I.A.U. Dublin Congress suggest that the velocity variations over limited regions of the Sun may sometimes show strong sinusoidal components. The Oxford September A and B spectrograms were exposed within about a minute of time of each other and on nominally the same region of the Sun. If the effect is real and not merely accidental, one would like to know whether the changes between the two pictures represent time- or space-variations,

and whether the 2:1 frequency ratio represents a progressive change in frequency or a switch from one harmonic to another which might conceivably indicate magneto-hydrodynamic effects.

Apart from this tentative suggestion, there seems no reason to disturb Uberoi's conclusion that all the measures so far made can be satisfactorily described in terms of a uniform turbulence spectrum on the Sun. In order to investigate effectively the non-random features which seem to be present in the latest photographs (see Section 1) it will be necessary to secure statistically more massive data than have been used in the past, and especially to evaluate the distributions over the solar disk in two dimensions so far as is possible. The brightness data discussed in the literature have been obtained by making point-scans across photographs. The evaluation of these in two dimensions would require no new observational procedure; the need is for improved methods of measurement and interpretation (Section 2). The method of two-dimensional auto-correlation by double transmission suggested by Uberoi (1955a) and by myself (1953, p. 278) should reduce the computations to manageable proportions.

The problem of observing two-dimensional velocity fields, and especially simultaneous velocity and brightness fields, with the necessary resolution appears formidable. Possibly the best that can be done is to secure slit-scans, the advantages of which over point-scans have been discussed in Section 2.6. The method would be to scan an image of the Sun across the slit of a spectrometer in which the averages over the slit-length of the brightness and of the Doppler velocity are simultaneously measured by photoelectric means. It seems the more appropriate to call attention to this method of observing because its disadvantages are not quite self-evident.

Acknowledgments

In addition to my debt to those already mentioned in the text, I am much indebted to Dr D. E. Blackwell for discussion and for allowing me to study his high-altitude granulation pictures in advance of detailed publication; to Dr E. H. Linfoot for much valuable help, advice and criticism; to Dr M. V. Wilkes, Director of the Mathematical Laboratory, Cambridge, for allowing me facilities on the EDSAC computers, and to the staff of the Mathematical Laboratory for their generous help; and to Dr R. G. Murgatroyd of the Meteorological Research Flight, R.A.E., for the photograph reproduced as Fig. 1 (*c*).

The Observatories,
Madingley Road,
Cambridge:
1959 *February.*

References

Blackwell, D. E., Dewhirst, D. W., and Dollfus, A., 1957a, *Observatory*, **77**, 20; 1957b, *Nature*, **180**, 211.
Carslaw, H. S., *Theory of Fourier Series and Integrals*. McMillan, London, 1906.
Fellgett, P. B., 1953, *J. Opt. Soc. Amer.*, **43**, 271.
Fellgett, P. B., and Linfoot, E. H., 1955, *Phil. Trans. Roy. Soc.*, **247A**, 369.
Frenkiel, F. N., and Schwarzschild, M., 1952, *Ap. J.*, **116**, 422; 1955, *Ap. J.*, **121**, 216.
Hart, A. B., 1956, *M.N.*, **116**, 38.
Janssen, J., 1896, *Ann. Obs. Paris, Meudon*, **1**, Pl. 10.
Leighton, R. B., 1957, *Pub. Astron. Soc. Pacific*, **69**, 497.
Linfoot, E. H., 1958, *Physica*, **34**, 476.
Lipson, H., and Beevers, C. A., 1936, *Proc. Phys. Soc.*, **48**, 772; *Nature*, **137**, 825.

McMath, R. R., Mohler, O. C., Pierce, A. M., and Goldberg, L., 1956, *Ap. J.*, **124**, 1.
Plaskett, H. H., 1952, *M.N.*, **112**, 414; 1954, *M.N.*, **114**, 297; 1956, *Vistas in Astronomy*, ed. A. Beer, Pergamon Press, London, 1956.
Rogerson, J. B., 1958, *Sky and Telescope*, **17**, 112.
Rösch, J., 1956, *C. R. Acad. Sci., Paris*, **243**, 478.
Richardson, R. S., and Schwarzschild, M., 1950, *Ap. J.*, **111**, 351.
Shannon, C. E., 1948, *Bell Syst. Tech. J.*, **27**, 379, 623.
Skumanick, A., 1955, *Ap. J.*, **121**, 404.
Stuart, F. E., and Rush, J. H., 1954, *Ap. J.*, **120**, 245.
Thiessen, G., 1955, *Z.f. Ap.*, **35**, 237.
Titchmarsh, E. C. *Theory of Functions*, Oxford (1932).
Uberoi, M. A., 1955a, *Ap. J.*, **121**, 400.; 1955b, *Ap. J.*, **122**, 466.
Whitney, C., 1958, *Smithsonian Contr.*, **2**, 365.
Wlerick, W., 1957, *Smithsonian Cont. Astrophys.*, **2**, 25.
Woodward, P. M., 1953, *Probability and Information Theory, with Applications to Radar*, Pergamon Press, London, 1953.
Zweig, H. J., 1956, *J. Opt. Soc. Amer.*, **46**, 805, 812.

ON THE *H*-FUNCTIONS FOR ISOTROPIC SCATTERING

D. W. N. Stibbs and R. E. Weir

(Received 1959 April 10)

Summary

It is shown that the *H*-functions for isotropic scattering in a semi-infinite plane-parallel atmosphere may be readily and accurately obtained by direct quadrature of an integral form. Methods are described which enable the accuracy of the calculations to be maintained in the neighbourhood of singularities in the integrand and its first derivative. The final form has been programmed for the IBM 704 computer, and a total of 160 *H*-functions have been obtained for values of the albedo

$$\varpi = 0\ (0{\cdot}01)\ 0{\cdot}90\ (0{\cdot}005)\ 0{\cdot}95\ (0{\cdot}001)\ 0{\cdot}99\ (0{\cdot}0005)\ 1{\cdot}0.$$

Good agreement has been found in checks involving the zero-order moment and the first and second moments. The *H*-function obtained for the conservative case $\varpi = 1$ agrees to within one unit in the sixth decimal place with that computed by Placzek from a modified form of the Wiener-Hopf integral.

Tables of the *H*-function are presented for $\mu = 0\ (0{\cdot}05)\ 1{\cdot}0$ and selected values of ϖ, the tabular values being rounded to the sixth decimal place. To enable *H*-functions to be obtained for any required value of ϖ, the complete set of computed functions has been approximated for $\mu = 0\ (0{\cdot}05)\ 1{\cdot}0$ by polynomials in ϖ using Chebychev polynomials and the method of least squares, several ranges being used to cover the entire range in ϖ from 0 to 1. The *H*-functions computed from these polynomials are correct to within one unit in the fourth decimal place. The first-order moment has also been obtained in polynomial form.

Introduction.—The *H*-functions were originally introduced by Ambartzumian and later developed extensively by Chandrasekhar. They are solutions of the non-linear integral equations of the form

$$H(\mu) = 1 + \mu H(\mu) \int_0^1 \frac{\Psi(\mu')}{\mu + \mu'} H(\mu')\, d\mu', \qquad (1)$$

where $\Psi(\mu)$ is usually a polynomial of even order in μ satisfying the condition

$$\int_0^1 \Psi(\mu)\, d\mu \leqslant \tfrac{1}{2}.$$

These functions are of considerable importance in the theory of radiative transfer in planetary and stellar atmospheres. The detailed numerical application of the mathematical theory depends, however, upon the availability of the functions in sufficient tabular detail. This requirement has been partly met by the heroic computations of Chandrasekhar and Breen (**1, 2**) for isotropic and anisotropic scattering, supplemented later by similar calculations by Harris (**3**). Valuable though these tabulations have been, there is still a need for more detailed numerical work on the *H*-functions, particularly in a form which would enable the required function to be rapidly and accurately computed for *any value of the particle albedo*.

Accordingly, we have re-examined the question of the computation of the H-functions with the object of providing for current, and we may hope, future requirements for the case of *isotropic scattering*. The work presented in this paper forms part of an extensive investigation on the H-functions for atmospheres with coherent and non-coherent scattering.

1. *Previous methods of solution*

When the scattering is isotropic with particle albedo ϖ, we have

$$\Psi(\mu) = \text{constant} = \tfrac{1}{2}\varpi.$$

The integral equation for the H-function is then

$$H(\mu) = 1 + \tfrac{1}{2}\varpi\mu H(\mu)\int_0^1 \frac{H(\mu')}{\mu+\mu'}\,d\mu'. \tag{2}$$

1.1. *The iterative method.*—The integral equation for the H-function may be written in an alternative form (**2**, Section 38)

$$\frac{1}{H(\mu)} = (1-\varpi)^{1/2} + \tfrac{1}{2}\varpi\int_0^1 \frac{\mu' H(\mu')}{\mu+\mu'}\,d\mu'. \tag{3}$$

Chandrasekhar and Breen solved for $H(\mu)$ by iteration in the integral equation (3), starting with an approximate form for the H-function given by the third or fourth approximation in the method of discrete ordinates. The accuracy of the H-function at any stage in the sequence of iterations was judged by a comparison between the theoretical value of the zero-order moment and the value obtained by quadrature of the computed function.

The same procedure was followed by Harris (**3**) who used a digital computer. Starting with an approximate function $H(\mu) = 1 + 2\mu$ for all ϖ, and using Simpson's rule for the numerical quadratures over μ in the range 0(0·05)1·0, Harris ceased iterating when the difference between the theoretical and computed zero-order moment became less than 0·00005. However, as mentioned by Harris, it is well known that the derivative of $H(\mu)$ at $\mu = 0$ is logarithmically infinite. This singularity should be removed before making the quadratures otherwise it is open to question whether a satisfactory check on the zero-moment is a criterion for the accuracy of the H-function or whether it represents a compensation between errors in the μ-quadrature and errors in the function itself. That there are such errors is indicated by a comparison which Harris made between his results for the conservative case $\varpi = 1$ at $\mu = 0{\cdot}05$ and 0·10 which are in error by +3 in the fourth and +7 in the fifth decimal place respectively when compared with the very accurate values given for this case by Placzek (**4**). Apart from the uncertainties introduced by the presence of the singularity at $\mu = 0$, the H-function for $\varpi = 1$ is almost a pathological case when handled by the iterative method.

1.2. *The Wiener–Hopf integral.*—In the conservative case, that is when $\varpi = 1$, the H-function is given by the well-known Wiener–Hopf integral (**5**)

$$H(\mu) = (1+\mu)\exp\left\{\frac{\mu}{\pi}\int_0^{\pi/2} \frac{\ln[\sin^2\theta/(1-\theta\cot\theta)]}{\cos^2\theta+\mu^2\sin^2\theta}\,d\theta\right\}. \tag{4}$$

Introducing some elegant transformations, Placzek (**4**) reduced the integral to a form which is well suited to accurate numerical quadrature, namely

$$H(\mu) = \frac{1}{(1+\mu)^{1/2}}\exp\left\{\frac{1}{\pi}\int_0^{\pi/2} \frac{\theta\tan^{-1}(\mu\tan\theta)}{1-\theta\cot\theta}\,d\theta\right\}. \tag{5}$$

Placzek calculated the function $\phi(\mu) = \frac{1}{2}H(\mu)$ to 7 decimal places for values of $\mu = 0(0{\cdot}1)1{\cdot}0$, and then obtained $\phi(\mu)$ to 5 decimal places for intermediate values of $\mu = 0(0{\cdot}01)1{\cdot}0$ by interpolation.

The computational simplicity of obtaining this H-function for each value of μ from *only one quadrature* suggests that the use of a suitable integral form for $H(\mu)$ for any ϖ should have some advantages over the method of repeated iteration in the non-linear integral equation.

2. *Integral form for the H-function for non-conservative isotropic scattering*

Chandrasekhar (**2**) has shown that the solution of the integral equation (1) for $H(\mu)$ can be represented as a complex integral in the form

$$\ln H(\mu) = \frac{\mu}{2\pi i}\int_{-i\infty}^{i\infty} \ln T(w)\,\frac{dw}{w^2-\mu^2}, \tag{6}$$

where

$$T(z) = 1 - 2z^2\int_0^1 \frac{\Psi(\mu)\,d\mu}{z^2-\mu^2}.$$

Following Kourganoff and Busbridge (**5,** Section 29.5), the complex integral in equation (6) can be transformed into a real integral by the substitution $w = i\cot\theta$. With $\Psi(\mu) = \frac{1}{2}\varpi$ we obtain

$$T(i\cot\theta) = 1 - \varpi\theta\cot\theta,$$

and

$$\ln H(\mu) = -\frac{\mu}{\pi}\int_0^{\pi/2} \frac{\ln\left[1-\varpi\theta\cot\theta\right]}{\cos^2\theta+\mu^2\sin^2\theta}\,d\theta. \tag{7}$$

When $\varpi = 1$ this is simply the form given by Kourganoff and Busbridge (**5,** equation (29.39)). The corresponding form of equation (7) for a problem in non-coherent isotropic scattering has been given by Busbridge and Stibbs (**6,** Section 4). Apart from the use of an approximation to the integral form in (**6**) to obtain starting values of the H-functions for iteration in the integral equations of the problem, it appears that no detailed application has yet been made of the integral form for non-conservative isotropic scattering.

3. *Analysis of the integral form*

We propose to evaluate the function $H(\mu)$ by means of the integral form

$$H(\mu,\varpi) = \exp\left[I(\mu,\varpi)\right], \tag{8}$$

where

$$I(\mu,\varpi) = -\frac{\mu}{\pi}\int_0^{\pi/2} \frac{\ln\left(1-\varpi\theta\cot\theta\right)}{\cos^2\theta+\mu^2\sin^2\theta}\,d\theta \tag{9}$$

for

$$0 \leqslant \mu \leqslant 1, \qquad 0 \leqslant \varpi \leqslant 1.$$

In general, the integral $I(\mu,\varpi)$ can be computed numerically by means of some suitably accurate quadrature formula. However, the accuracy achieved will not be satisfactory unless any singularities in the behaviour of the integrand are first removed. There are, in fact, two cases which require special consideration. These arise from the fact that both $\partial H/\partial\mu$ and $\partial H/\partial\varpi$ are infinite when $\mu = 0$ and $\varpi = 1$ respectively.

3.1. *The case when μ is small and $\varpi \neq 1$.*—In this case, the integrand in equation (9) increases to a sharp maximum near the end of the range of integration

and falls to zero at $\theta = \pi/2$. In the limit as μ tends to zero, the maximum goes to infinity. This maximum may be eliminated by integration by parts. Since

$$\int \frac{d\theta}{\cos^2\theta + \mu^2 \sin^2\theta} = \frac{1}{\mu} \tan^{-1}(\mu \tan\theta)$$

and the integrated part vanishes, we obtain

$$I(\mu, \varpi) = \frac{1}{\pi} \int_0^{\pi/2} f(\theta)\, d\theta, \tag{10}$$

where

$$f(\theta) = \left\{ \frac{d}{d\theta} \ln(1 - \varpi\theta \cot\theta) \right\} \tan^{-1}(\mu \tan\theta), \tag{11.1}$$

$$= \varpi \frac{\theta \operatorname{cosec}^2\theta - \cot\theta}{1 - \varpi\theta \cot\theta} \tan^{-1}(\mu \tan\theta). \tag{11.2}$$

Although the function $f(\theta)$ is now a monotonic increasing function of θ, the first derivative at $\theta = \pi/2$ is large when μ is small. This is due to the factor $\tan^{-1}(\mu \tan\theta)$ in $f(\theta)$. The remaining factor is zero at $\theta = 0$, and increases monotonically to the value $(\pi/2)\varpi$ at $\theta = \pi/2$. Hence we write

$$g(\theta) = (\pi/2)\varpi \tan^{-1}(\mu \tan\theta), \tag{12}$$

and consider the function

$$I(\mu, \varpi) = \frac{1}{\pi} \int_0^{\pi/2} \{f(\theta) - g(\theta)\}\, d\theta + \frac{1}{\pi} \int_0^{\pi/2} g(\theta)\, d\theta,$$

$$= I_1(\mu, \varpi) + I_2(\mu, \varpi). \tag{13}$$

The function $I_1(\mu, \varpi)$ can now be obtained with satisfactory accuracy by numerical quadrature since the function $f(\theta) - g(\theta)$ vanishes at $\theta = 0$ and $\pi/2$, and is well behaved throughout the entire range. The second function $I_2(\mu, \varpi)$ in equation (13) can be evaluated to any desired accuracy by means of the following formulae* for the integral

$$I_2(\mu, \varpi) = \tfrac{1}{2}\varpi \left\{ \tfrac{1}{2} \ln\mu \ln\frac{1-\mu}{1+\mu} + \sum_{n=0}^{\infty} \frac{\mu^{2n+1}}{(2n+1)^2} \right\}, \quad 0 \leqslant \mu < 1{\cdot}0, \tag{14.1}$$

$$= \tfrac{1}{2}\varpi \left\{ \frac{\pi^2}{8} - \sum_{n=0}^{\infty} \frac{1}{(2n+1)^2} \left(\frac{1-\mu}{1+\mu} \right)^{2n+1} \right\}, \quad 0 < \mu \leqslant 1{\cdot}0. \tag{14.2}$$

The series in equation (14.1) is obviously most convergent near $\mu = 0$ and the series in (14.2) near $\mu = 1{\cdot}0$, the convergence being equal when $\mu = (1-\mu)/(1+\mu)$, that is when $\mu = \sqrt{2} - 1$. Hence equation (14.1) may be used for $\mu \leqslant \sqrt{2} - 1$, and equation (14.2) for $\mu > \sqrt{2} - 1$ if required.

3.2. *The case when ϖ is near unity.*—In this case, the integral $I_1(\mu, \varpi)$ in equation (13) requires further manipulation in order to obtain satisfactory accuracy in the quadrature. The difficulty arises from the behaviour of $f(\theta)$ for small values of θ. Expanding in powers of θ

$$f(\theta) = \tfrac{1}{3}\mu\varpi(\theta^2 - \tfrac{1}{3}\theta^4 - \tfrac{1}{3}\mu^2\theta^4 + \ldots)/[1 - \varpi + \tfrac{1}{3}\varpi\theta^2 + \ldots], \tag{15}$$

so that as $\theta \to 0$, $f(\theta) \to 2\mu$ if $\varpi = 1$ but $f(\theta) \to 0$ if $\varpi \neq 1$.

* The formulae may be obtained by differentiation with respect to μ followed by integration over θ to give $\partial I_2/\partial\mu = -\frac{1}{2}\varpi\,(\ln\mu)/(1-\mu^2)$. Equation (14.1) then follows by straightforward integration over μ. Equation (14.2) is obtained by expanding $\ln\mu$ as a power series in $(1-\mu)/(1+\mu)$ before performing the μ-integration.

When $\varpi = 1$, there is no difficulty in the quadrature for $I_1(\mu, \varpi)$ as the functions $f(\theta)$ and $g(\theta)$ are well-behaved, but the function $f(\theta)$ is discontinuous for small θ when $\varpi \to 1$. This behaviour may be removed by introducing a function $h(\theta)$ which, for small θ, is the difference between $f(\theta)$ when $\varpi \neq 1$ and $\varpi = 1$, namely

$$h(\theta) = -2\mu(1-\varpi)/[1-\varpi+\tfrac{1}{3}\varpi\theta^2]. \tag{16}$$

We now have

$$I_1(\mu, \varpi) = \frac{1}{\pi}\int_0^{\pi/2} \{f(\theta) - g(\theta) - h(\theta)\}\, d\theta + \frac{1}{\pi}\int_0^{\pi/2} h(\theta)\, d\theta,$$

$$= I_3(\mu, \varpi) + I_4(\mu, \varpi). \tag{17}$$

The function $I_3(\mu, \varpi)$ may be obtained with satisfactory accuracy by numerical quadrature for all μ however small, and for all ϖ however close to unity. The function $I_4(\mu, \varpi)$ is an elementary integral which gives

$$I_4(\mu, \varpi) = -\frac{2\mu}{\pi}\sqrt{\left(\frac{3(1-\varpi)}{\varpi}\right)}\tan^{-1}\left\{\frac{\pi}{2}\sqrt{\left(\frac{\varpi}{3(1-\varpi)}\right)}\right\}. \tag{18}$$

To the first order, this function represents the difference between $I(\mu, \varpi)$ and $I(\mu, 1{\cdot}0)$. Hence, from equations (8) and (18) we obtain the following approximation for ϖ near unity,

$$\frac{H(\mu, \varpi)}{H(\mu, 1{\cdot}0)} \simeq \exp\left[\frac{-2\mu}{\pi}\sqrt{\left(\frac{3(1-\varpi)}{\varpi}\right)}\tan^{-1}\left\{\frac{\pi}{2}\sqrt{\left(\frac{\varpi}{3(1-\varpi)}\right)}\right\}\right]. \tag{19}$$

This expression may be reduced to the approximate form quoted by Harris (**3**) by expanding the inverse tangent and exponential functions, and retaining terms to the first order in $(1-\varpi)^{1/2}$. We thus obtain

$$H(\mu, \varpi) \simeq H^*(\mu, \varpi),$$

where

$$\frac{H^*(\mu, \varpi)}{H(\mu, 1{\cdot}0)} = \frac{1}{1+\mu\sqrt{[3(1-\varpi)]}}. \tag{20}$$

To sum up, the required H-function given by equation (8) may be obtained with good accuracy over the range $0 < \mu \leqslant 1$, $0 < \varpi \leqslant 1$ by means of equations (13), (14), (17) and (18), which give the final form

$$I(\mu, \varpi) = \frac{1}{\pi}\int_0^{\pi/2} \{f(\theta) - g(\theta) - h(\theta)\}\, d\theta + I_2(\mu, \varpi) + I_4(\mu, \varpi), \tag{21}$$

the integral being evaluated by numerical quadrature with $f(\theta)$, $g(\theta)$ and $h(\theta)$ given by equations (11), (12) and (16), the functions $I_2(\mu, \varpi)$ and $I_4(\mu, \varpi)$ being given by equations (14) and (18) respectively.

3.3. *Moments of the H-functions.*—The zero-order moment, and the first and second moments with respect to μ of the computed H-functions may be used as an overall check on the accuracy of the computation, using Chandrasekhar's theorems (**2**, Section 38) that if

$$\alpha_n = \int_0^1 H(\mu, \varpi)\mu^n\, d\mu \quad (n \geqslant 0), \tag{22}$$

then

$$\alpha_0 = 2\varpi^{-1}[1-(1-\varpi)^{1/2}] \tag{23}$$

and

$$\tfrac{3}{4}\varpi\alpha_1^2 + 3(1-\varpi)^{1/2}\alpha_2 = 1. \tag{24}$$

In applying these checks, it is necessary that the quadrature over μ should be as accurate as possible. Sufficient accuracy can be achieved by first removing the singular behaviour of $\partial H/\partial\mu$ at $\mu=0$.

It follows from equations (8), (13) and (14.1) that in the limit as μ tends to zero, $H(\mu,\varpi)\sim F(\mu,\varpi)$ where

$$F(\mu,\varpi)=1-\tfrac{1}{2}\mu\varpi\ln\mu. \tag{25}$$

Accordingly, we write equation (24) for the general moment in the form

$$\alpha_n=\int_0^1\{H(\mu,\varpi)-F(\mu,\varpi)\}\,\mu^n\,d\mu+\int_0^1 F(\mu,\varpi)\mu^n\,d\mu, \tag{26}$$

performing the quadrature over the first integral, and using the fact that

$$\int_0^1 F(\mu,\varpi)\mu^n\,d\mu=\frac{1}{n+1}+\frac{\varpi}{2(n+2)^2}. \tag{27}$$

It should be stressed that although the function $F(\mu,\varpi)$ has the same behaviour as $H(\mu,\varpi)$ near $\mu=0$, and is effective in improving the μ-quadrature, it is only a good approximation to the H-function itself for very small values of μ.

4. *Numerical results*

The scheme described in Section 3 for the computation of the H-functions and their moments has been programmed for the IBM 704 computer. The floating point mode has been employed in which the mantissa has 27 binary digits or about 8 decimal digits. Simpson's formula has been used for the quadratures in preference to the formulae of Newton–Cotes or Gauss which were found to be no better for this computation. The time required for the computation of one complete H-function, using 200 divisions in the range of θ and 40 divisions in μ was about 45 seconds. A total number of 160 H-functions* have been computed for $\mu=0(0{\cdot}025)1{\cdot}0$, the values of ϖ being

$$\varpi=0(0{\cdot}01)0{\cdot}09(0{\cdot}005)0{\cdot}95(0{\cdot}001)0{\cdot}99(0{\cdot}0005)1{\cdot}0.$$

4.1. *The H-functions.*—A selection of the H-functions is presented in Table I for the restricted interval in $\mu=0(0{\cdot}05)1{\cdot}0$, the values of $H(\mu,\varpi)$ being rounded to the sixth decimal place. With $\mu=0(0{\cdot}05)1{\cdot}0$, the greatest error in the computed zero-order moment α_0 is found to be 0·0000051 when $\varpi=1{\cdot}0$, the greatest error in the first and second moment check being 0·0000016 also at $\varpi=1{\cdot}0$. However, with $\mu=0(0{\cdot}025)1{\cdot}0$ the error in the computed zero-order moment is reduced to 0·0000001, and in the first and second moment check to 0·0000008. This suggests that most of the inaccuracy revealed by moment checks for $\mu=0(0{\cdot}05)1{\cdot}0$ is due to the interval size in the μ-quadrature. Since there may be some cancellation of errors from the quadratures over θ and μ, the very satisfactory checks involving the moments of the H-functions for the smaller interval size in μ are only taken to indicate, perhaps conservatively, that the tabulations are probably correct to the rounded sixth decimal place. Support for this view is to be found in a comparison with the accurate values computed by Placzek (4) for the case $\varpi=1$ by means of equation (5), the modified Wiener–Hopf integral, which shows a maximum discrepancy at $\mu=1{\cdot}0$ of 1 unit in the sixth decimal place. On the basis that the functions involved in the quadratures for other values of ϖ are better behaved than for the case $\varpi=1$ while the moment checks are equally good, it would appear that we have achieved six-figure accuracy throughout the entire range in μ and ϖ.

* A copy of the complete set of H-functions is available in the Library of the Society.

TABLE I

H-Functions for isotropic scattering

ϖ / μ	0·05	0·10	0·15	0·20	0·25
0	1·000000	1·000000	1·000000	1·000000	1·000000
0·05	1·003854	1·007809	1·011872	1·016053	1·020360
0·10	1·006089	1·012378	1·018881	1·025618	1·032608
0·15	1·007776	1·015841	1·024221	1·032943	1·042039
0·20	1·009135	1·018644	1·028559	1·038917	1·049762
0·25	1·010271	1·020992	1·032204	1·043954	1·056298
0·30	1·011243	1·023005	1·035337	1·048295	1·061945
0·35	1·012087	1·024759	1·038073	1·052094	1·066900
0·40	1·012830	1·026306	1·040491	1·055459	1·071297
0·45	1·013492	1·027684	1·042648	1·058466	1·075236
0·50	1·014085	1·028922	1·044589	1·061176	1·078791
0·55	1·014621	1·030041	1·046346	1·063634	1·082019
0·60	1·015107	1·031060	1·047947	1·065875	1·084968
0·65	1·015552	1·031991	1·049412	1·067929	1·087674
0·70	1·015960	1·032846	1·050759	1·069820	1·090167
0·75	1·016336	1·033634	1·052003	1·071567	1·092474
0·80	1·016683	1·034364	1·053155	1·073186	1·094615
0·85	1·017006	1·035042	1·054226	1·074693	1·096607
0·90	1·017306	1·035673	1·055223	1·076098	1·098468
0·95	1·017586	1·036263	1·056156	1·077412	1·100209
1·00	1·017848	1·036815	1·057029	1·078644	1·101843
First moment	0·507588	0·515610	0·524114	0·533154	0·542797

ϖ / μ	0·30	0·35	0·40	0·45	0·50
0	1·000000	1·000000	1·000000	1·000000	1·000000
0·05	1·024805	1·029401	1·034163	1·039110	1·044265
0·10	1·039875	1·047448	1·055359	1·063650	1·072369
0·15	1·051546	1·061509	1·071980	1·083021	1·094710
0·20	1·061146	1·073129	1·085781	1·099189	1·113461
0·25	1·069298	1·083033	1·097592	1·113087	1·129653
0·30	1·076365	1·091646	1·107899	1·125258	1·143889
0·35	1·082580	1·099243	1·117017	1·136060	1·156568
0·40	1·088109	1·106017	1·125169	1·145745	1·167972
0·45	1·093072	1·112111	1·132519	1·154500	1·178307
0·50	1·097559	1·117631	1·139192	1·162466	1·187735
0·55	1·101641	1·122662	1·145285	1·169755	1·196381
0·60	1·105374	1·127272	1·150876	1·176456	1·204347
0·65	1·108805	1·131513	1·156030	1·182644	1·211717
0·70	1·111971	1·135432	1·160799	1·188379	1·218559
0·75	1·114902	1·139066	1·165227	1·193712	1·224932
0·80	1·117626	1·142446	1·169351	1·198686	1·230885
0·85	1·120164	1·145599	1·173203	1·203337	1·236460
0·90	1·122536	1·148549	1·176810	1·207698	1·241693
0·95	1·124758	1·151314	1·180196	1·211796	1·246617
1·00	1·126844	1·153913	1·183380	1·215654	1·251259
First moment	0·553121	0·564221	0·576212	0·589240	0·603484

TABLE I—*continued*

ϖ	0·55	0·60	0·65	0·70	0·75
μ					
0	1·000000	1·000000	1·000000	1·000000	1·000000
0·05	1·049655	1·055317	1·061295	1·067655	1·074483
0·10	1·081576	1·091348	1·101788	1·113032	1·125274
0·15	1·107143	1·120442	1·134770	1·150344	1·167476
0·20	1·128729	1·145164	1·162991	1·182516	1·204176
0·25	1·147462	1·166733	1·187758	1·210934	1·236832
0·30	1·164003	1·185868	1·209842	1·236419	1·266306
0·35	1·178790	1·203044	1·229757	1·259517	1·293174
0·40	1·192133	1·218600	1·247867	1·280619	1·317848
0·45	1·204263	1·232789	1·264447	1·300018	1·340641
0·50	1·215359	1·245807	1·279709	1·317945	1·361796
0·55	1·225560	1·257808	1·293824	1·334581	1·381510
0·60	1·234980	1·268920	1·306929	1·350079	1·399943
0·65	1·243713	1·279245	1·319139	1·364562	1·417230
0·70	1·251837	1·288870	1·330550	1·378135	1·433485
0·75	1·259418	1·297870	1·341244	1·390889	1·448806
0·80	1·266510	1·306307	1·351291	1·402900	1·463278
0·85	1·273163	1·314235	1·360750	1·414236	1·476973
0·90	1·279418	1·321701	1·369675	1·424956	1·489958
0·95	1·285311	1·328746	1·378112	1·435110	1·502288
1·00	1·290874	1·335406	1·386102	1·444745	1·514015
First moment	0·619179	0·636632	0·656264	0·678667	0·704720

ϖ	0·80	0·85	0·90	0·925	0·950
μ					
0	1·000000	1·000000	1·000000	1·000000	1·000000
0·05	1·081914	1·090171	1·099678	1·105175	1·111508
0·10	1·138808	1·154170	1·172143	1·182774	1·195232
0·15	1·186640	1·208619	1·234918	1·250664	1·269354
0·20	1·228639	1·257012	1·291434	1·312301	1·337337
0·25	1·266322	1·300863	1·343271	1·369262	1·400740
0·30	1·300588	1·341089	1·391350	1·422458	1·460454
0·35	1·332034	1·378302	1·436280	1·472486	1·517056
0·40	1·361089	1·412941	1·478496	1·519773	1·570954
0·45	1·388080	1·445338	1·518327	1·564638	1·622452
0·50	1·413262	1·475756	1·556033	1·607335	1·671788
0·55	1·436842	1·504409	1·591826	1·648067	1·719155
0·60	1·458989	1·531471	1·625880	1·687006	1·764711
0·65	1·479848	1·557092	1·658344	1·724296	1·808593
0·70	1·499539	1·581400	1·689347	1·760061	1·850917
0·75	1·518169	1·604504	1·719000	1·794411	1·891784
0·80	1·535827	1·626502	1·747401	1·827441	1·931286
0·85	1·552595	1·647478	1·774637	1·859238	1·969501
0·90	1·568542	1·667507	1·800787	1·889877	2·006503
0·95	1·583731	1·686658	1·825919	1·919428	2·042357
1·00	1·598219	1·704991	1·850098	1·947955	2·077123
First moment	0·735815	0·774376	0·825315	0·858767	0·901875

TABLE I—*continued*

ϖ	0·960	0·970	0·975	0·980	0·985
μ					
0	1·000000	1·000000	1·000000	1·000000	1·000000
0·05	1·114406	1·117633	1·119418	1·121367	1·123542
0·10	1·201015	1·207516	1·211146	1·215132	1·219616
0·15	1·278122	1·288052	1·293631	1·299786	1·306750
0·20	1·349185	1·362688	1·370314	1·378763	1·388366
0·25	1·415753	1·432958	1·442720	1·453574	1·465962
0·30	1·478704	1·499723	1·511700	1·525062	1·540368
0·35	1·538604	1·563535	1·577797	1·593757	1·612105
0·40	1·595848	1·624776	1·641386	1·660026	1·681526
0·45	1·650732	1·683729	1·702742	1·724137	1·748892
0·50	1·703485	1·740613	1·762077	1·786293	1·814396
0·55	1·754293	1·795603	1·819560	1·846656	1·878193
0·60	1·803307	1·848842	1·875329	1·905360	1·940408
0·65	1·850657	1·900451	1·929501	1·962513	2·001144
0·70	1·896454	1·950536	1·982176	2·018211	2·060488
0·75	1·940796	1·999186	2·033439	2·072534	2·118516
0·80	1·983767	2·046481	2·083366	2·125554	2·175294
0·85	2·025446	2·092492	2·132026	2·177335	2·230881
0·90	2·065900	2·137284	2·179480	2·227934	2·285329
0·95	2·105192	2·180915	2·225782	2·277402	2·338686
1·00	2·143380	2·223439	2·270984	2·325788	2·390993
First moment	0·923547	0·949349	0·964480	0·981748	1·002057

ϖ	0·9900	0·9925	0·9950	0·9975	1·0000
μ					
0	1·000000	1·000000	1·000000	1·000000	1·000000
0·05	1·126071	1·127550	1·129278	1·131483	1·136575
0·10	1·224875	1·227978	1·231624	1·236318	1·247350
0·15	1·314972	1·319851	1·325613	1·333076	1·350834
0·20	1·399767	1·406565	1·414626	1·425121	1·450351
0·25	1·480742	1·489593	1·500126	1·513902	1·547326
0·30	1·558713	1·569741	1·582909	1·600205	1·642522
0·35	1·634185	1·647509	1·663467	1·684510	1·736403
0·40	1·707503	1·723233	1·742128	1·767136	1·829275
0·45	1·778913	1·797153	1·819124	1·848307	1·921349
0·50	1·848601	1·869448	1·894628	1·928189	2·012778
0·55	1·916709	1·940257	1·968772	2·006905	2·103677
0·60	1·983355	2·009690	2·041661	2·084554	2·194133
0·65	2·048633	2·077838	2·113379	2·161213	2·284214
0·70	2·112624	2·144775	2·183995	2·236945	2·373974
0·75	2·175394	2·210565	2·253569	2·311804	2·463459
0·80	2·237003	2·275263	2·322151	2·385832	2·552704
0·85	2·297503	2·338918	2·389784	2·459069	2·641738
0·90	2·356941	2·401571	2·456505	2·531546	2·730587
0·95	2·415358	2·463260	2·522349	2·603291	2·819271
1·00	2·472792	2·524021	2·587346	2·674331	2·907809
First moment	1·027181	1·042721	1·061730	1·087487	1·154700

4.2. *Polynomial approximations.*—The H-functions are frequently required for values of ϖ other than those tabulated. To facilitate the computation of the functions for intermediate values of ϖ, polynomials of the form

$$H(\mu,\varpi)=A_0+A_1(\varpi-\varpi_0)+A_2(\varpi-\varpi_0)^2+\ldots, \qquad (28)$$

have been obtained for each value of μ by the method of least squares using Chebychev polynomials. For convenience, ϖ_0 was taken to be the mid-point of the range of ϖ for which $H(\mu,\varpi)$ was being approximated. The degree of the polynomial was determined by specifying a tolerance on the maximum permissible magnitude of the residual at any tabulated point, the polynomial of lowest degree within the specified tolerance being adopted. A tolerance of 0·000025 was chosen in order to ensure that the polynomial approximation would give H-functions accurately to four decimal places. It is, of course, impossible to fit a polynomial over the whole range of ϖ due to the increasing curvature of the H-function with increasing ϖ, culminating in the singular behaviour of $\partial H/\partial\varpi$ at $\varpi=1{\cdot}0$. Accordingly, the range was subdivided into the ranges $\varpi=0$ to 0·4, 0·4 to 0·6, 0·6 to 0·8, and 0·8 to 0·9 before fitting the polynomials by means of equation (28). With this subdivision, the tolerance was satisfied by quartics when $\mu=1{\cdot}0$ and by polynomials of lower degree for smaller values of μ.

In order to obtain a sufficiently accurate polynomial representation in the range $\varpi=0{\cdot}90$ to 1·0, it is necessary to remove the singular behaviour of $\partial H/\partial\varpi$ before approximation. The form

$$H(\mu,\varpi)-H^*(\mu,\varpi)=B_0+B_1(1-\varpi)+B_2(1-\varpi)^2+\ldots, \qquad (29)$$

where the function $H^*(\mu,\varpi)$ is given by equation (20), was found to be satisfactory and was applied with the tolerance 0·000025 in the separate ranges $\varpi=0{\cdot}90$ to 0·95, 0·95 to 0·99, and 0·99 to 1·0.

The coefficients for the polynomial approximations (28) and (29) are given in Tables II and III. These polynomials reproduce the tabular values of the H-functions with an accuracy better than 0·000025. It has been verified by some additional computations of the H-functions from the integral form that the errors at intermediate points do not exceed the required tolerance. This indicates that the polynomials are satisfactory functional forms in the chosen ranges, and that the H-functions calculated from them are only in error by round-off in the fourth decimal place.

The first-order moment $\alpha_1(\varpi)$ of the H-functions has also been approximated by polynomials for the same subdivision of the range in ϖ and the same tolerance, the coefficients being given in Tables II and III. The singular behaviour of $\partial\alpha_1/\partial\varpi$ at $\varpi=1$ has been removed by means of a function $\alpha_1^*(\varpi)$ which is an approximation to the first-order moment of the function $H^*(\mu,\varpi)$. Using

$$\begin{aligned}\alpha_1^*(\varpi)&=\int_0^1(1-\mu\sqrt{[3(1-\varpi)]})H(\mu,1{\cdot}0)\mu\,d\mu\\&=\alpha_1(1{\cdot}0)-\alpha_2(1{\cdot}0)\sqrt{[3(1-\varpi)]}\end{aligned} \qquad (30)$$

with $\alpha_1(1{\cdot}0)=1{\cdot}154700$ and $\alpha_2(1{\cdot}0)=0{\cdot}820352$, the first-order moment has been approximated in the ranges $\varpi=0{\cdot}90$ to 0·95, 0·95 to 0·99, and 0·99 to 1·0 by the polynomial

$$\alpha_1-\alpha_1^*=B_0+B_1(1-\varpi)+B_2(1-\varpi)^2+\ldots. \qquad (31)$$

Only the first-order moment α_1 has been obtained in this way since the second-order moment α_2 may be obtained from α_1 by means of equation (24),

TABLE II

Polynomial approximations to the H-functions and their first moments

$$\left.\begin{matrix} H(\mu, \varpi) \\ \alpha_1(\varpi) \end{matrix}\right\} = A_0 + A_1(\varpi - \varpi_0) + A_2(\varpi - \varpi_0)^2 + \ldots$$

$0 \leqslant \varpi \leqslant 0{\cdot}4, \quad \varpi_0 = 0{\cdot}2$

μ	A_0	A_1	A_2	A_3	A_4
0·05	1·01605	0·08484	0·0257	0·014	...
0·10	1·02561	0·13718	0·0514	0·030	...
0·15	1·03294	0·17805	0·0760	0·047	...
0·20	1·03891	0·21186	0·0991	0·065	...
0·25	1·04394	0·24071	0·1208	0·081	...
0·30	1·04830	0·26581	0·1382	0·098	0·079
0·35	1·05209	0·28796	0·1566	0·114	0·094
0·40	1·05546	0·30771	0·1738	0·130	0·108
0·45	1·05847	0·32548	0·1899	0·145	0·123
0·50	1·06118	0·34158	0·2050	0·159	0·137
0·55	1·06363	0·35626	0·2192	0·173	0·150
0·60	1·06588	0·36970	0·2325	0·187	0·163
0·65	1·06793	0·38207	0·2451	0·200	0·176
0·70	1·06982	0·39350	0·2569	0·212	0·189
0·75	1·07157	0·40409	0·2681	0·224	0·201
0·80	1·07319	0·41395	0·2787	0·235	0·213
0·85	1·07469	0·42314	0·2887	0·246	0·224
0·90	1·07610	0·43174	0·2982	0·256	0·235
0·95	1·07741	0·43980	0·3073	0·266	0·246
1·00	1·07864	0·44737	0·3158	0·276	0·256
α_1	0·53315	0·18656	0·1203	0·099	0·088

$0{\cdot}4 \leqslant \varpi \leqslant 0{\cdot}6, \quad \varpi_0 = 0{\cdot}5$

μ	A_0	A_1	A_2	A_3	A_4
0·05	1·04426	0·1056	0·047	...	...
0·10	1·07237	0·1790	0·098	0·09	...
0·15	1·09471	0·2409	0·150	0·15	...
0·20	1·11346	0·2949	0·201	0·20	...
0·25	1·12965	0·3431	0·251	0·26	...
0·30	1·14389	0·3866	0·299	0·32	...
0·35	1·15656	0·4263	0·346	0·38	...
0·40	1·16797	0·4628	0·391	0·44	...
0·45	1·17830	0·4964	0·434	0·49	...
0·50	1·18773	0·5275	0·476	0·55	...
0·55	1·19637	0·5565	0·516	0·61	...
0·60	1·20434	0·5836	0·554	0·66	...
0·65	1·21171	0·6089	0·591	0·72	...
0·70	1·21855	0·6327	0·627	0·77	...
0·75	1·22492	0·6550	0·661	0·82	...
0·80	1·23087	0·6761	0·694	0·87	...
0·85	1·23645	0·6960	0·725	0·92	...
0·90	1·24168	0·7148	0·755	0·97	...
0·95	1·24662	0·7326	0·771	1·01	1·4
1·00	1·25126	0·7495	0·798	1·06	1·5
α_1	0·60348	0·2985	0·294	0·36	...

TABLE II—*continued*

$0{\cdot}6 \leqslant \varpi \leqslant 0{\cdot}8$, $\varpi_0 = 0{\cdot}7$

μ	A_0	A_1	A_2	A_3	A_4
0·05	1·06765	0·1315	0·096	0·15	...
0·10	1·11302	0·2340	0·204	0·32	...
0·15	1·15033	0·3258	0·319	0·52	...
0·20	1·18252	0·4100	0·423	0·73	1·5
0·25	1·21093	0·4883	0·539	0·96	2·0
0·30	1·23642	0·5616	0·655	1·19	2·5
0·35	1·25952	0·6306	0·771	1·43	3·1
0·40	1·28062	0·6956	0·886	1·68	3·7
0·45	1·30002	0·7571	0·999	1·93	4·2
0·50	1·31795	0·8154	1·110	2·18	4·8
0·55	1·33458	0·8707	1·220	2·44	5·4
0·60	1·35008	0·9233	1·327	2·69	6·1
0·65	1·36456	0·9735	1·431	2·94	6·7
0·70	1·37814	1·0213	1·534	3·19	7·3
0·75	1·39089	1·0669	1·634	3·44	7·9
0·80	1·40290	1·1106	1·731	3·69	8·5
0·85	1·41424	1·1523	1·826	3·93	9·2
0·90	1·42496	1·1923	1·918	4·17	9·8
0·95	1·43511	1·2306	2·008	4·41	10·4
1·00	1·44475	1·2674	2·096	4·65	11·0
α_1	0·67867	0·4808	0·721	1·51	3·5

$0{\cdot}8 \leqslant \varpi \leqslant 0{\cdot}9$, $\varpi_0 = 0{\cdot}85$

μ	A_0	A_1	A_2	A_3	A_4
0·05	1·09017	0·1756	0·250	0·80	...
0·10	1·15411	0·3290	0·542	1·76	...
0·15	1·20861	0·4757	0·864	2·84	...
0·20	1·25700	0·6178	1·209	4·04	...
0·25	1·30085	0·7561	1·573	5·33	...
0·30	1·34107	0·8908	1·952	6·71	...
0·35	1·37830	1·0220	2·254	8·17	35·0
0·40	1·41294	1·1498	2·636	9·69	41·7
0·45	1·44534	1·2742	3·024	11·27	48·8
0·50	1·47576	1·3954	3·416	12·90	56·2
0·55	1·50441	1·5133	3·810	14·58	63·8
0·60	1·53147	1·6281	4·206	16·29	71·7
0·65	1·55709	1·7398	4·602	18·03	79·8
0·70	1·58140	1·8485	4·997	19·79	88·1
0·75	1·60451	1·9542	5·390	21·58	96·5
0·80	1·62650	2·0572	5·781	23·38	105·1
0·85	1·64748	2·1573	6·170	25·20	113·9
0·90	1·66751	2·2547	6·555	27·02	122·7
0·95	1·68666	2·3496	6·937	28·85	131·6
1·00	1·70499	2·4419	7·314	30·69	140·8
α_1	0·77438	0·8713	2·369	9·48	42·4

TABLE III

Polynomial approximations when ϖ is near unity

$$\left.\begin{matrix} H(\mu,\varpi)-H^*(\mu,\varpi) \\ \alpha_1(\varpi)-\alpha_1{}^*(\varpi) \end{matrix}\right\} = B_0+B_1(1-\varpi)+B_2(1-\varpi)^2+\ldots$$

$0{\cdot}90 \leqslant \varpi \leqslant 0{\cdot}95$

μ	B_0	B_1	B_2
0·05	−0·00037	−0·0625	...
0·10	−0·00026	−0·1124	0·107
0·15	−0·00043	−0·1460	0·168
0·20	−0·00063	−0·1738	0·229
0·25	−0·00085	−0·1974	0·290
0·30	−0·00109	−0·2176	0·348
0·35	−0·00134	−0·2349	0·404
0·40	−0·00160	−0·2500	0·457
0·45	−0·00187	−0·2630	0·507
0·50	−0·00214	−0·2742	0·554
0·55	−0·00242	−0·2838	0·598
0·60	−0·00270	−0·2921	0·638
0·65	−0·00298	−0·2991	0·675
0·70	−0·00326	−0·3051	0·709
0·75	−0·00354	−0·3100	0·741
0·80	−0·00382	−0·3141	0·769
0·85	−0·00409	−0·3174	0·796
0·90	−0·00437	−0·3201	0·819
0·95	−0·00464	−0·3220	0·840
1·00	−0·00490	−0·3235	0·860
$\alpha_1-\alpha_1{}^*$	0·00371	1·2862	−1·241

$0{\cdot}95 \leqslant \varpi \leqslant 0{\cdot}99$

μ	B_0	B_1	B_2	B_3
0·05	−0·00009	−0·0681	...	...
0·10	−0·00005	−0·1209	0·20	...
0·15	−0·00009	−0·1603	0·32	...
0·20	−0·00014	−0·1946	0·45	...
0·25	−0·00019	−0·2254	0·59	...
0·30	−0·00024	−0·2532	0·73	...
0·35	−0·00015	−0·2976	1·57	−7·8
0·40	−0·00018	−0·3248	1·86	−9·3
0·45	−0·00022	−0·3504	2·15	−11·0
0·50	−0·00025	−0·3745	2·44	−12·7
0·55	−0·00029	−0·3971	2·74	−14·4
0·60	−0·00033	−0·4186	3·04	−16·2
0·65	−0·00038	−0·4388	3·33	−18·0
0·70	−0·00042	−0·4579	3·63	−19·9
0·75	−0·00047	−0·4761	3·92	−21·8
0·80	−0·00052	−0·4931	4·21	−23·6
0·85	−0·00057	−0·5093	4·50	−25·4
0·90	−0·00062	−0·5246	4·78	−27·3
0·95	−0·00067	−0·5393	5·06	−29·2
1·00	−0·00072	−0·5528	5·33	−31·0
$\alpha_1-\alpha_1{}^*$	0·00041	1·459	−4·46	−21·4

TABLE III—*continued*

$0{\cdot}99 \leqslant \varpi \leqslant 1{\cdot}00$

μ	B_0	B_1	B_2	B_3
0·05	−0·00000	−0·074	...	...
0·10	−0·00001	−0·124	...	...
0·15	−0·00002	−0·165	...	...
0·20	−0·00000	−0·216	1·4	...
0·25	−0·00001	−0·255	1·9	...
0·30	−0·00001	−0·291	2·5	...
0·35	−0·00001	−0·326	3·0	...
0·40	−0·00001	−0·360	3·7	...
0·45	−0·00001	−0·392	4·3	...
0·50	−0·00002	−0·423	5·0	...
0·55	−0·00002	−0·453	5·7	...
0·60	−0·00002	−0·483	6·4	...
0·65	−0·00001	−0·536	13·4	−415
0·70	−0·00001	−0·566	14·9	−466
0·75	−0·00001	−0·597	16·5	−521
0·80	−0·00001	−0·626	18·1	−575
0·85	−0·00001	−0·656	19·8	−633
0·90	−0·00001	−0·684	21·5	−693
0·95	−0·00001	−0·713	23·3	−755
1·00	−0·00002	−0·740	25·1	−819
$\alpha_1 - \alpha_1^*$	0·00001	1·564	−15·2	−444

and the zero-order moment α_0 is given explicitly in terms of ϖ by equation (23). The value in having α_0, α_1 and α_2 readily calculable for any ϖ lies in the fact that the flux of radiation can often be written down in terms of these moments.

Conclusion.—The scope of this paper has been limited to a discussion of the *H*-functions which arise in the case of the coherent isotropic scattering of radiation in a semi-infinite plane-parallel atmosphere, and to the presentation of the results of calculations in a form suited to the need for rapid computation of the *H*-functions and their moments for any value of the particle albedo. The methods described in the paper may, however, be extended with further elaboration to the scattering functions (6) which arise in the theory of the formation of multiplet lines by non-coherent isotropic scattering.

Theoretical Physics Division,
United Kingdom Atomic Energy Authority,
A.W.R.E., Aldermaston, Berkshire:
1959 *April.*

References

(1) S. Chandrasekhar and F. H. Breen, *Ap. J.*, **106**, 143, 1947.
(2) S. Chandrasekhar, *Radiative Transfer* (Oxford: Clarendon Press, 1950).
(3) D. L. Harris, *Ap. J.*, **126**, 408, 1957.
(4) G. Placzek, *Phys. Rev.*, **72**, 556, 1947.
(5) V. Kourganoff and I. W. Busbridge, *Basic Methods in Transfer Problems* (Oxford: Clarendon Press, 1952).
(6) I. W. Busbridge and D. W. N. Stibbs, *M.N.*, **114**, 2, 1954; Comm. Univ. Obs., Oxford, No. 42, 1954.

THE DWARF BINARY HD 16157: AN INTERIM REPORT

David S. Evans

(Communicated by H.M. Astronomer at the Cape)

(Received 1959 April 11)

Summary

Spectroscopic observations of this remarkable star have been carried on since 1951 using the equipment of the Radcliffe Observatory, Pretoria. It now seems tolerably certain that it is a spectroscopic binary, of which the primary component is a late K-type dwarf, having an orbital period of 1·56145 days, and a mass function with the very low value of 0·00871 solar masses. On a few plates evidence of the spectrum of the secondary component is thought to have been found. The parallax has been measured as 0″·083. The spectra resemble those of YY Geminorum in showing Balmer lines and Calcium lines in emission. The star also resembles YY Geminorum in the fact that it is also a light variable showing changes in the light curve from season to season which are even more pronounced than those shown by the latter. It seems difficult to account for these in terms of the ordinary eclipsing binary model, and the data which have been obtained so far are presented with the object of encouraging independent observations elsewhere.

The star HD 16157 (=CZC 1209), R.A. $2^h\,32^m{\cdot}5$, Dec. $-44^\circ\,01'$ (1950), was included in the Cape radial velocity programme with the Radcliffe reflector because of its high parallax. This amounts to 0″·083, and is the mean of two determinations (**1**), the relative parallax being given as 0″·084. In the Henry Draper Catalogue, the spectral type is given as K5, but a re-determination from the Cape radial velocity plates gives K7 V, or possibly even a shade later, but not as late as Mo V. In addition to the typical absorption spectrum, the following emission lines are found: Balmer series, alpha to zeta; Ca II, H and K. Both the radial velocity and the magnitude of the star are variable.

With a few exceptions, the spectra show only single lines, the derived velocities ranging from +5 to +80 km/s. The velocity determined from the absorption lines is always essentially identical with that derived from either group of emission lines, and deviations are confined to cases where the absorption spectrum is underexposed and the velocity derived from it inaccurate. The results of the radial velocity measures are shown in Table I. Here the Julian dates have been corrected for light-time to the Sun. The measured velocity from the absorption lines is accompanied by its probable error and the number of lines measured. The number of Balmer emission lines measured is also indicated. The adopted velocity for each spectrum is, usually, the absorption line velocity corrected to the system of the *Mount Wilson General Catalogue of Radial Velocities* in the way described in a previous publication (**2**). Exceptionally, when the absorption spectrum is weak, the emission lines have been taken into the adopted velocity to give greater weight. These cases are indicated by a colon, and the resulting velocity assigned half the normal weight for a good observation. All the spectra were obtained using the c-camera (49 A/mm) with exposures ranging up to 3 hours in extreme cases, the normal exposure being about 60–90 minutes.

TABLE I

Results of radial velocity measures

Julian date 2430000+	Phase	Measured velocities: Absorption lines	Measured velocities: H & K	Measured velocities: Balmer lines	Adopted velocity *M.W.C.* System	Wt.
4250·596	0·2095	+ 3·0 ± 4·8(7)	+18	+41(2)	+11:	1
4261·547	·2224	+37·7 2·8(4)	+25	+29(3)	+31:	1
4297·472	·2301	+23·0 1·3(12)	+21	+32(3)	+21·8	2
5444·327	·7101	+73·8 1·1(14)	+68	+67(4)	+72·9	2
5704·580	·3842	+50·2 1·6(12)	+54	+52(4)	+48·3	2
5708·573	·9412	+17·7 1·8(13)	+19	+21(5)	+15·8	2
5711·471	·7976	+47·7 2·5(12)	+50	+49(4)	+45·8	2
5855·301	·9105	+25·9 2·1(13)	+29	+32(5)	+24·0	2
5858·298	·8295	+46·3 3·0(12)	+50	+57(3)	+46·7	2
6084·615	·7702	+54 5 (13)	+58	+56(4)	+52·9:	1
6087·603	·6836	+73·1 2·2(13)	+76	+74(5)	+71·2	2
6090·580	·5902	+80·4 4·5(12)	+82	+84(4)	+79·5	1
6158·446	·0533	−14 (3)	0	+15(3)	− 2:	1
6172·299	·9254	+19·6 1·3(13)	+26	+24(4)	+17·7	2
6181·266	·6682	+83·0 1·5(14)	+84	+84(5)	+81·1	2
6202·271	·1205	+ 6·4 1·7(13)	0	+ 5(4)	+ 4·5	2
6204·309	·4257	+72 (3)	+59	+58(2)	+62:	1
6212·324	·5586	+81·5 1·5(13)	+80	+84(4)	+79·6	2
6444·639	·3400	+43·3 1·4(13)	+41	+46(5)	+41·4	2
6446·561	·5711	+82·8 2·1(12)	+83	+84(4)	+80·9	2
6470·537	·9261	+25·0 1·6(14)	+21	+18(4)	+23·1	2
6479·486	·6572	+78·7 2·2(14)	+77	+81(4)	+76·8	2
		Secondary	−27K		−29 S	
6486·437	·1090	+ 7·9 1·8(11)	+ 6	+ 7(3)	+ 6·0	2
6515·412	·6651	+82·1 ± 1·1(13)	+80	+81(4)	+80·2	2
		Secondary	−23	−24(1)	−25·4 S	
Check observations :						
6612·291	·7095	+71·8 ± 3·1(5)	...	+56(2)	+65:	
6614·253	·9660	+14·9 2·6(13)	+12	+ 4(3)	+13·0	
		Secondary	?+95K		+93 S?	

Trial and error have yielded a period of 1·56145 days from the spectroscopic data, ($P^{-1} = 0{\cdot}64043$) and phases have been reckoned, using this period, from J.D. 2430000·0. The last two observations in the table were not included in the solution for the orbital elements, being obtained subsequently when it became necessary to make as certain as possible that the correct elements had been obtained. For the derivation of the orbital elements the following normal points were used, the period being taken as known:—

TABLE II

Velocity	Phase	Weight	Computed V	O–C
+ 3·80	0·1025	5	+ 5·54	−1·74
+21·40	·2230	4	+18·69	+2·71
+48·28	·3748	5	+49·77	−1·49
+80·10	·5699	5	+79·79	+0·31
+79·37	·6635	6	+77·06	+2·31
+72·05	·6969	4	+72·84	−0·79
+47·58	·8049	5	+49·15	−1·57
+20·15	·9258	8	+20·03	+0·12

The last column represents the residuals of the observed normal points from the velocities computed on the basis of the derived elements. These were found in the usual way by computation of corrections to preliminary elements, the results being:—

$P = 1{\cdot}56145$ days, $\gamma = +41{\cdot}94$ km/s, $K = 37{\cdot}77$ km/s
$e = 0{\cdot}0461$, $\omega = 63°{\cdot}83$, $\phi_0 = 0{\cdot}7635$

where ϕ_0 is the phase corresponding to passage through periastron. The two check observations fit these elements well, the residual, O–C, having the values, respectively, -5 km/s and $+2$ km/s. The adequacy with which the data are represented can be judged from Fig. 1.

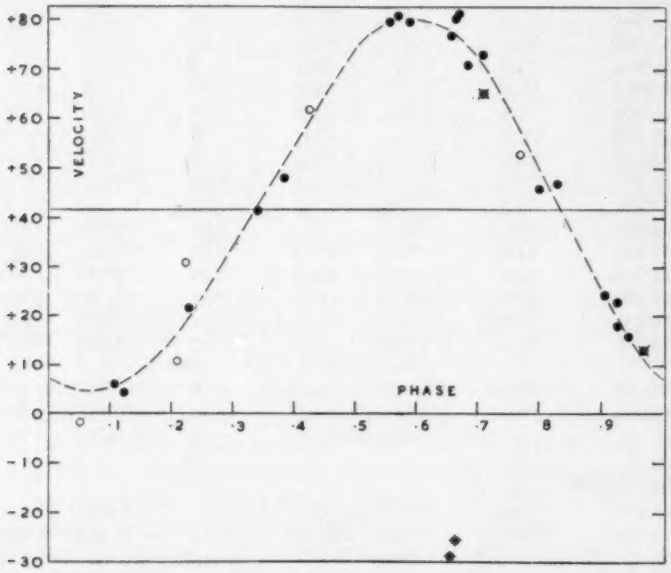

FIG. 1.—*Radial velocity observations of HD 16157. Filled circles: absorption line measures of primary. Vertical crosses: emission lines attributed to secondary. Open circles: halfweight observations of primary (see text). Diagonal crosses: check observations.*

Table I contains three entries marked "Secondary". These refer to plates on which one or more of the emission lines have faint secondary components. In the best case three such components can be detected. Careful examination of the absorption spectra has led to suspicions that, in certain cases, duplicity of some lines, notably the neutral calcium line at 4226 A, can be detected, but there is nothing which inspires a feeling of certainty. In view of this, it is best to adopt an attitude of reserve towards these faint components, and not to assume too readily that they belong to the secondary component of the binary.

We can begin by computing from the derived orbital elements the mass-function of the system, which can be expressed in terms of the unknown masses and inclination:

$$\frac{m'^3 \sin^3 i}{(m+m')^2} = 0{\cdot}00871 \text{ solar masses}$$

where m and m' are the masses of the primary and secondary respectively.

If, for the moment, we assume the secondary to be both considerably fainter and less massive than the primary, we can temporarily ignore its existence. Then, if we take from the photometric data (dealt with in detail below) an apparent visual magnitude of the order of $V = 8{\cdot}76$, and a value of $B - V = 1{\cdot}39$, we find from the calibration by Evans, Menzies and Stoy (2), a type of about K9 V, and $M_v = 8{\cdot}47$, leading to a photometric parallax of $0''{\cdot}087$ (compare the trigonometrical value $0''{\cdot}083$ quoted above and the estimated type of K7 V). This system of values is quite self-consistent and will suffer no serious change if we assume, as we legitimately can from the experience with the spectra, that the secondary is at least two magnitudes fainter than the primary.

From the discussion of the mass-luminosity relation for late-type dwarfs given by Eggen (3), we can infer a mass for the primary of about 0·47 solar units. Introducing this value for m into the mass function we find, for different values of $\sin i$, the following corresponding quantities:

$\sin i$	m'
1·000	0·150
·900	·170
·800	·196
·700	·230
·600	·285
·500	·365

One can hardly assume that the fainter component is the more massive and one is, therefore, driven to the conclusion that $\sin i$ is, probably, greater than about 0·5 and that the mass ratio is greater than unity and less than about three. This is a range into which the data will fall if we decide to take the faint emission components as belonging to the second star of the system. If we do this we easily find $K' = 73{\cdot}3$ km/s, giving a mass-ratio of 1·94, and we have

$$a \sin i = 810{,}000 \text{ km} \qquad a' \sin i = 1{,}571{,}000 \text{ km}$$

$$m \sin^3 i = 0{\cdot}1462 \qquad m' \sin^3 i = 0{\cdot}0753$$

Moreover the measured value of the faint emission component on the last check plate is +93 km/s while the computed value is +98 km/s. The evidence is not strong but is, at least, not discouraging.

The assumption of $m = 0{\cdot}47$ then gives $m' = 0{\cdot}24$, $\sin i = 0{\cdot}678$, $i = 42°{\cdot}7$, $a = 1\,200\,000$ km and $a' = 2\,310\,000$ km. This set of figures creates difficulties for us. We shall, presently, have to consider whether this can be an eclipsing binary system, and, if this is to be possible, either the stars must be large enough to be almost in contact, or the inclination of the orbit must be near 90°. It seems impossible to secure these conditions. According to Allen (4) a dwarf with $M_v = 8{\cdot}5$, should have a radius of about 63 per cent of that of the Sun, that is, about 440 000 km, which, unless the secondary has a radius grossly inflated in comparison with what might be expected, is totally inadequate to bridge the gap of about 3 million km between the star centres. Even if we took the bull by the horns and postulated that $i = 90°$ we should still have about the same distance between the star centres. This follows because the expression for $a \sin i$, depending, as it does, only on constants derived from the orbit of the primary, remains unchanged and our assumption thus gives $a = 810\,000$ km. We must also accept the consequences of the assumption, that is, a mass ratio of 3·1 and

hence a value of $a' = 2\,540\,000$ km. Thus, if we throw out the evidence from the secondary, we can force the system into being an eclipsing binary but, if the star radii are normal, any eclipses there can be will occupy only a very small fraction of the period.

The point of the foregoing discussion will become clear as we turn to a discussion of the photometric data. These are set out in Table III.

TABLE III

Photoelectric observations of HD 16157 made with the McClean refractor

$(B-V)$ = constant = 1·39.
$(U-B)_C$ = refractor *UV* colour = constant = 2·19.

Julian date 2430000 +	Phase	*V*	Julian date 2430000 +	Phase	*V*
5759·457	0·5290	8·92	5815·390	0·3502	8·92
5773·395	·4554	8·93	5815·433	·3778	8·95
5776·404	·3824	8·91	5815·481	·4085	8·94
5777·409	·0260	8·77	5818·333	·2347	8·87
5779·359	·2749	8·86	5819·348	·8846	8·76
5779·476	·3498	8·88	5820·403	·5602	8·88
5780·387	·9332	8·76	5821·319	·1467	8·79
5783·337	·8225	8·75	5821·359	·1724	8·80
5783·407	·8673	8·76	5821·430	·2178	8·87
5785·312	·0874	8·76	5828·319	·6290	8·83
5785·357	·1162	8·79	5828·357	·6534	8·81
5786·405	·7874	8·78	5829·326	·2739	8·85
5788·352	·0343	8·77	5829·383	·3104	8·89
5789·332	·6619	8·81	5837·354	·4144	8·94
5791·342	·9492	8·76	5837·413	·4522	8·91
5792·406	·6306	8·84	5841·358	·9783	8·75
5793·341	·2294	8·83	5841·441	·0315	8·73
5793·433	·2883	8·88	5842·344	·6097	8·82
5796·294	·1206	8·74	5842·394	·6417	8·78
5797·371	·8103	8·77	5843·347	·2519	8·89
5798·388	·4616	8·93	5847·343	·8107	8·76
5799·348	·0764	8·77	5848·345	·4523	8·92
5800·378	·7361	8·76			
5801·290	·3202	8·90			
5801·319	·3387	8·92	6105·477	·1016	8·80
5801·345	·3554	8·94	6142·379	·7311	8·87
5801·367	·3695	8·95	6161·388	·9031	8·81
5801·388	·3829	8·93	6162·400	·5511	8·94
5801·406	·3944	8·94	6168·409	·3989	8·93
5804·289	·2408	8·86	6169·426	·0501	8·80
5804·366	·2901	8·90			
5807·291	·1634	8·84			
5807·357	·2056	8·84	6486·541	·1413	8·83
5811·370	·7757	8·75	6497·501	·1264	8·80
5812·298	·3700	8·94	6532·470	·5181	8·74
5812·397	·4334	8·95	6546·446	·4673	8·75
5812·459	·4731	8·91	6553·391	·9144	8·98
5813·358	·0489	8·76	6570·345	·7706	8·98
5814·299	·6515	8·83	6583·324	·0814	8·86
5814·331	·6720	8·81	6584·335	·7288	8·91
5814·372	·6983	8·78	6589·306	·9119	9·03
5814·447	·7463	8·76	6595·305	·7532	8·96
5814·493	·7758	8·76	6598·307	·7538	×·91
5814·532	·8007	8·76	6599·308	·3948	8·70
5815·335	0·3150	8·92	6604·303	0·5938	8·80

In this Table the Julian dates have been corrected to the Sun. The phases have been computed as were the phases of the radial velocity observations. The magnitudes were usually determined by comparison with the nearby star CZC1204, but the observations have also been reduced independently by comparison with standard E-region stars, and it is clear that the comparison star is not itself a variable. It has been found convenient to group the observations according to the season (1956–7, 1957–8, 1958–9) in which they were made.

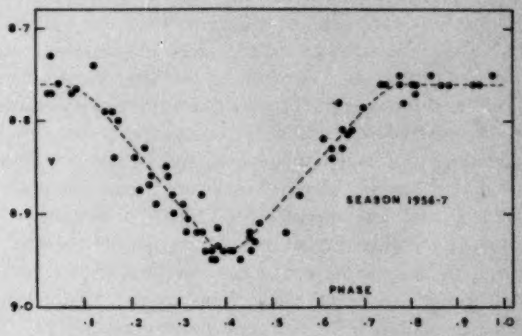

FIG. 2.—*Visual magnitudes of HD 16157.*

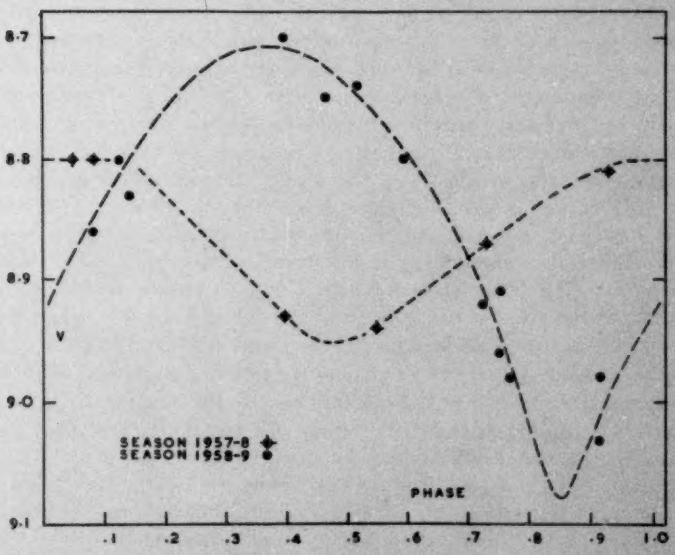

FIG. 3.—*Visual magnitudes of HD 16157.*

These results are plotted graphically in Figs. 2 and 3. The observations for the season 1956–57 are not too intractable; we see a single very broad depression in the curve, which might be attributable to an eclipse. The depth of the minimum is about 0·18 magnitudes, and is pointed, not flat, at the minimum phase. The position of the minimum does not coincide precisely with the phase of passage of the velocity curve through its mean value. However, the phase

difference, approximately 0·07, is not so large that it might not, conceivably, be explained away by some special hypothesis. The real difficulty presented by this light curve is the breadth of the depression, which lasts for something like 0·7 of the period, and the absence of any secondary eclipse. These difficulties may not be insuperable. We can imagine that the radius of the primary star has its normal value and that the absorption spectrum is produced in its outer layers. We can further imagine that it has, in addition, a very extended tenuous atmosphere, which is the source of the emission spectrum, and that it is the radius of the latter which counts so far as the production of the eclipse phenomena is concerned. Finally, if there is such an extended atmosphere surrounding a star of small mass, the gravitational field controlling its outer parts will be weak so that we could imagine that this atmosphere would not be entirely stable. If it suffers, possibly erratic, changes of size and form the eclipses will sometimes be early, sometimes late, leading to a broadening of the light curve averaged over a season of observation. All this is speculative but, even at this stage, we are faced with phenomena which do not lend themselves to easy explanation in conventional terms. It is not worth while to try to make a detailed analysis of this light curve, but, if we assume that the eclipse curve has been broadened by some such effect as that suggested above, and that the eclipse is only just total, possible parameters are $L=85$ per cent, $L'=15$ per cent, $r/r'=5$ and $i=48°$, the orbits being assumed circular. This keeps the depth of the secondary eclipse below the range where it would have been certainly detected observationally.

However, although these parameters may well describe the state of the system as it was during that season, the photometric observations obtained during the next two seasons show that it has certainly not exhausted its capacity to surprise us. These photometric observations are plotted in Fig. 3. Those obtained in the season 1957–58 are rather few in number, largely because of the mistaken idea then entertained that all that would be necessary would be to define the curve more precisely. Instead, in that season the indications are that the uneclipsed brightness has dropped from $V=8·76$ to $V=8·80$, that the range of variation has been reduced, and that there is a phase-shift of the minimum. These are relatively minor changes, however, in comparison with those which have taken place by the next season (1958–59). The uneclipsed brightness is now $V=8·71$: the star has been observed as faint as $V=9·03$, and, if the rather speculative light-curve can be trusted, the minimum may go as faint as 9·08. There is no constant phase anywhere, and the phase of minimum is now such as to correspond to an eclipse of the primary star by the secondary.

What are we to make of all this? First, can we be sure that the period used in discussing the radial velocity observations is the correct one? The check observations, which post-date the latest photometric observation, were secured in order to verify this and, as far as can be judged, they rule out the possibility of such an error. Clearly more observations of all kinds are desirable. So far it seems that the light curve changes rather slowly and that from one season to the next it is relatively stable, but it can only be coincidence that we have found it so. Sooner or later we may hope to catch the system in the act of changing from one kind of light curve to another.

Any conclusions must be of the most tentative kind, but it does seem that the most probable explanation must be sought in the hypothesis of an extended unstable atmosphere which partakes to a greater or less extent in the motion of the

component stars. The system would then not be a true eclipsing binary system at all, for the actual star disks would not eclipse each other. The possibility of the existence of such an atmosphere might be of importance in considering the evolution of late-type dwarfs, but it will still be necessary to discover whether such a phenomenon is a characteristic only of binaries, or whether it can occur in the case of single stars. One would naturally feel more certainty if a precedent for behaviour of this type could be found. The closest analogy seems to be that of YY Geminorum, where Kron (5) has found evidence of erratic changes in the light curve, far less pronounced, it is true, than in the present case. His explanation was based on the hypothesis of the occurrence of "starspots" analogous to sunspots, but this explanation does not seem a possible one for this system, if only because we have to explain the extraordinary duration of the eclipse phenomena.

I am much indebted to colleagues working at the Cape and Radcliffe Observatories for valuable assistance. Dr P. A. Wayman has, at my request, obtained some of the spectra at crucial phases. Dr A. J. Wesselink has re-examined all the data to ensure that another value of the period could not be found. Professor R. H. Stoy has critically examined all the photometric data and re-reduced them to ensure that some less bizarre account of the system was not possible.

The Royal Observatory,
Cape of Good Hope:
1959 *April.*

References

(1) Seventeenth list of Parallaxes determined at the Cape Observatory, *M.N.*, **110**, 405, 1950.
(2) Evans, Menzies and Stoy, *M.N.*, **117**, 534, 1957.
(3) O. J. Eggen, *A.J.*, **61**, 361, 1956.
(4) C. W. Allen, *Astrophysical Quantities*, London, 1955.
(5) G. Kron, *Ap. J.*, **115**, 301, 1952.

VISUAL AND FAR-RED GRADIENTS AND COLOUR TEMPERATURES OF γ CASSIOPEIAE, II

D. R. Barber

(Received 1959 April 29)

Summary

A further series of spectrophotometric gradients of γ Cass at mean wavelengths 5120 A and 7090 A, and corresponding colour temperatures, are listed for the period 1951 April to 1958 December. Probable errors of ϕ are $\pm 0{\cdot}03$ (visual), and $\pm 0{\cdot}11$ (far-red) respectively.

Although during the six-year interval, 1952–57, ϕ_{5120} fluctuated between extreme values of $0{\cdot}56$ and $1{\cdot}23$, the mean level showed no significant change ($\Delta\phi = +0{\cdot}03$) when compared with its average value for the preceding six-year period.

By contrast, the mean value of ϕ_{7090} for the same period, 1952–57, decreased by as much as $0{\cdot}38$; and there commenced towards the end of 1951 a cyclic fluctuation of the far-red gradient whose amplitude was $\sim 0{\cdot}75$. When plotted, these gradient values fit a curve yielding periods of $\sim 1{\cdot}0$ yr. in 1951–52, and $\sim 1{\cdot}8$ yr. in 1956–57. These changes, undoubtedly real, appear to be connected with short-period variations of infra-red intensity in the spectrum of γ Cass associated with a variable continuum to the red of the Paschen series limit.

Since 1938 routine colour temperature observations of γ Cass have been made at Sidmouth using the 12-inch McClean prismatic camera; and results for the years, 1938–41, and 1945–50 have already been published (**1**, **2**).

The observations reported here cover the period 1951 April to 1958 December, and the gradient values are based on 26 spectrograms of γ Cass and the Greenwich standard, δ Cass, photographed in blue, and red regions (mean wavelength, 5120 A) on Kodak I-E plates; and 16 spectrograms of the same two stars in red, and infra-red regions (mean wavelength, 7090 A) on Kodak I.R.E.R. plates. The 12-inch McClean prismatic camera was again used for both series.

Photometric calibration, and reduction of the spectrograms followed the same procedure as that described in Paper I(**2**). The probable error of a single determination of gradient remains the same as that found previously, namely, $\pm 0{\cdot}03$ at 5120 A, and $\pm 0{\cdot}11$ at 7090 A*.

In Table I the observed visual and far-red gradients, together with equivalent colour temperatures, are listed in chronological order (with Julian date). Those entries marked with a colon indicate a lower weight due to uncertain correction for atmospheric extinction, difficulty in setting the true continuum level on the microphotometer tracing, or imperfections of the photographic plate.

* These values are derived from direct inter-comparison of Greenwich standard stars. Twenty-five stars were used in the visual series; and thirteen stars brighter than $3^{m}{\cdot}1$, including the adopted primary standard star, δ Cass, formed the far-red series. The P.E. of a single visual gradient was found from a discussion of the residuals by the method of least squares. Because of the smaller number of far-red gradients a least squares solution was not applied. Instead, the P.E. was obtained directly, using mean residuals from repeated gradient comparisons of each Greenwich standard star with δ Cass.

TABLE I

Gradients and colour temperatures of γ Cassiopeiae

Date	J.D.	ϕ		T(deg.)	
		5120	7090	5120	7090
1951	2433				
Apr. 14	751	1·08	...	16 000	...
Oct. 22	942	1·08	0·87	16 000	47 000
1952	2434				
Jan. 3	015	1·08	...	16 000	...
18	030	0·97	...	19 100	...
31	043	...	0·54	...	> 50 000
Mar. 22	094	0·62	0·69	> 50 000	> 50 000
May 17	150	1·06	...	16 400	...
Aug. 25	250	0·82	1·13	27 200	19 800
Oct. 10	296	...	0·87	...	47 000
15	301	0·86	...	24 400	...
Dec. 13	360	0·80		29 000	...
1953					
Jan. 18	396	0·56	...	> 50 000	...
Mar. 3	440	...	0·37	...	> 50 000
Apr. 7	475	1·23	...	13 300	...
Sep. 6	627	1·14	0·44	14 000	> 50 000
8	629	1·32	...	12 200	...
Oct. 7	658	1·00	0·71	17 900	50 000
10	661	0·86	...	24 400	...
Nov. 4	686	0·76	...	33 000	...
1954					
Jan. 7	750	1·13	1·21	15 200	16 700
Apr. 4	837	...	0·52:	...	> 50 000:
	2435				
Sep. 21	007	0·67	...	50 000	...
Oct. 30	046	0·73:	...	37 200:	...
Nov. 14	061	0·82	...	27 200	...
1955					
Jan. 18	126	1·14	0·54	14 900	> 50 000
Oct. 6	387	0·98	...	18 700	...
10	391	0·91	1·34	21 800	13 900
Nov. 16	428	1·13	0·37	15 200	> 50 000
1956					
Jan. 12	485	0·93	0·62	20 600	> 50 000
Oct. 31	778	0·90	...	22 400	...
1957	2436				
Aug. 21	072	0·63	...	> 50 000	...
Oct. 16	128	0·98	0·87	18 700	47 000
Nov. 22	165	0·93	0·54	20 600	> 50 000
1958					
Jan. 13	217	1·47	...	10 500	...
Feb. 12	247	0·85	...	25 000	...
18	253	0·56:	...	> 50 000:	...
Apr. 14	308	0·78	...	31 000	...
Jul. 16	401	0·77	...	32 000	...
Oct. 16	493	0·81	...	28 200	...
Nov. 3	511	0·93	...	20 600	...
Dec. 3	541	0·78	...	31 000	...

The tabulated results show clearly that for both visual and infra-red regions the dispersion in the gradient is always well above the experimental error. Comparison of the gradient data for the two wavelengths reveals also important differences in the nature of the variation in each spectral region; for, whereas the visual gradient showed quite irregular changes of amplitude $\pm 0{\cdot}45$ with no significant alteration in the mean gradient over the whole period of eight years, the far-red gradient exhibited a remarkably persistent sequence of quasi-periodic fluctuations of amplitude about seven times the probable error, and average period equal to 1·4 yr. Maximum and minimum values of ϕ_{7090} were 1·34, and 0·37 respectively. The latter corresponds to an equivalent colour temperature approaching infinity that is obviously not a measure of the true stellar temperature. This is confirmed by a direct comparison of the monochromatic intensities in visual and far-red spectral ranges which suggests that the very low gradient values measured at 7090 A are due almost entirely to a decreased infra-red flux at 7846 A, thus indicating a strong continuous absorption below the Paschen series limit.

If the above explanation is correct, it may be inferred also that the short-period variation in ϕ_{7090} is due to transitions from strong absorption to intense emission, and vice-versa, in the region of the Paschen continuum. Some confirmation of this is given by the independent observations of Fellgett (3) and Mlle. Lunel (4) using Pb–S cells. They report abnormally strong infra-red radiation between 0·7 and 2·7 μ present in the spectrum of γ Cass in 1950 March, and 1953 September respectively. Sidmouth spectrograms taken on close dates also show some continuous emission, superimposed on the water-vapour bands beyond 7846 A, and associated with a rising far-red gradient.

In addition to the changes in the infra-red region just described, there appeared also towards the end of 1951 a very marked discontinuity in the average value of ϕ_{7090}; and this is shown most clearly when the mean values of far-red gradient for the consecutive six-year intervals, 1946–51, and 1952–57, are directly compared. Table II facilitates this comparison by listing gradients and colour temperatures for the two periods. In the last column of the Table is entered the gradient difference, $\Delta\phi_{7090}$, denoting the departure of the observed gradient value from that computed by extrapolation of the visual gradient, ϕ_{5120}, for the same epoch assuming a grey-body energy distribution in the spectrum of γ Cass.

TABLE II

Comparison of long-term average values of gradient, and colour temperature for the years 1946–51 and 1952–57

6-year Period	ϕ_{5120}	ϕ_{7090}	T_{5120} (in 10^3 deg.)	T_{7090}	$\Delta\phi_{7090}$ (O—C)
1946–51	0·89 (33)	1·10 (18)	23·0	21·4	+0·03
1952–57	0·92 (26)	0·72 (15)	21·4	>50·0	−0·38

(The numbers in parentheses indicate the total observations in each group)

The observed decrease of $\sim 0{\cdot}40$ in the far-red gradient for the second six-year period appears in striking contrast to the constancy (within the error of measurement) shown by the visual gradient over the same period of time.

As already stated, this feature can be accounted for by a large, though probably temporary, decrease of spectral intensity at 7846 A associated with a

varying Paschen continuum. It does not appear likely that Fellgett's suggested modification of the infra-red intensity in the spectrum of γ Cass by surrounding nebulosity (3) can contribute significantly in this instance.

Acknowledgment.—I am greatly indebted to Professor H. H. Plaskett for his most helpful comments on the MS. of this paper. My thanks are due also to Mr S. Archer for his valued assistance in the preparation and reduction of the microphotometer tracings from which the results presented here were obtained.

Norman Lockyer Observatory,
University of Exeter,
Sidmouth, Devon:
1959 *April* 28.

References

(1) Edwards, D. L., *M.N.*, **103**, 222, 1943.
(2) Barber, D. R., *M.N.*, **110**, 275, 1950 (Paper I).
(3) Fellgett, P. B., *M.N.*, **111**, 537, 1951.
(4) Lunel, M., *Ann. d'Astrophys.*, **17**, 153, 1954.

GLOBULAR CLUSTERS, II. THE SPECTRAL TYPES OF INDIVIDUAL STARS AND OF THE INTEGRATED LIGHT

T. D. Kinman

(Communicated by the Radcliffe Observer)

(Received 1959 March 4)

Summary

The problem of classifying the spectra of individual stars and spectra taken in integrated cluster light is discussed. Types are given to the spectra of both kinds previously discussed in Paper I and a comparison is made with Mayall's and also Morgan's classification for spectra of lower dispersion. Mayall's types show small systematic differences from both the Radcliffe and Morgan types: a correction is therefore applied to Mayall's types to give integrated types for 63 clusters on a uniform system.

The effect of the metal/hydrogen ratio on the metal line strengths in the spectra of the cluster giants is discussed and an attempt is made to calculate this ratio for different clusters from the present spectra. It is concluded that the metal/hydrogen ratio ranges from greater than 1/10 to less than 1/100 the solar value for different clusters. For a cluster such as NGC 5272, it is shown that if this ratio has ~1/10 solar value then the cluster giants should have nearly normal spectra for their colour and luminosity as is observed but that the metal lines in the spectra of the subgiants should be weakened. An attempt is made to predict integrated spectral types for NGC 5272 and (with less accuracy) for five other clusters. Differences in the integrated spectra are largely due to the differences in the metal/hydrogen ratio and to the different relative populations of the horizontal branch. The predicted types agree with the observed types within the expected accuracy in support of the present analysis.

A correlation is found between the integrated spectral type of a cluster and its concentration to the galactic plane. Clusters of the earliest spectral type whose stars have a very low metal abundance form an extended spherical distribution with little concentration to the plane, while those of latest type whose stars have the highest metal abundance show a strong concentration to the plane: clusters of intermediate type, which are the most numerous, show an intermediate distribution. The less definite correlation between spectral type and the properties of the RR Lyrae stars is also discussed.

Introduction.—In the first paper of this series (**16**) details were given of the spectra of thirty globular clusters and of the radial velocities derived from them. These spectra are classified and compared with previous observations in the first section of this paper. The second section deals with the derivation of metal abundances from the spectra of the cluster giants and the third section is an analysis of the integrated spectra. The correlation of the cluster spectra with galactic distribution and with the properties of the RR Lyrae stars in the clusters is discussed in a final section.

1.1. *Spectral types for individual stars.*—Spectral types taken from the present spectra will be uncertain for the following reasons:

(1) The stars are faint so that with a dispersion of 86 A/mm at Hγ the spectra are narrow: for about one half of the stars the spectrum width is 0·25 mm while for the faintest stars the width is 0·10 mm. In some cases the spectrum does not extend to the blue beyond λ4226.

(2) The stars are intrinsically red and often further reddened by absorption. Prismatic spectra of such objects have a steep density gradient with wave-length; in most cases the range suitable for obtaining types does not exceed 250 A (usually λλ4400–4150) and is sometimes less. Grating spectra would be preferable for this purpose.

(3) The spectra are peculiar and do not in general match the spectra of MK stars (taken with the same slit width, dispersion and emulsion) which were used as standards. Comparison with spectra of other high velocity galactic stars proved unsatisfactory, partly because too few of such spectra were available and partly because the luminosity classes were not in general comparable.

The luminosity class may be found for a few spectra by observing the ratio λ4077/λ4045. In the majority of cases however, the ratio λ4290/λ4325 (cf. Popper (**23**)) was used and also the appearance of the red side of the G band. In all cases stars were found to be luminosity class II–Ib in agreement with the absolute magnitudes given by colour magnitude diagrams (e.g. (**2**)). For this luminosity class the CN band at λ4215 was in general found to be weak.

In these spectra the usual criteria involving hydrogen to metal line ratios (e.g. Hγ/λ4325) give an approximate type denoted by (H/m) which is earlier than the type (m_1/m_2) derived from the ratios of different metal lines. This difference has been interpreted as being due to a metal deficiency in the cluster stars compared to nearby stars. Attempts have been made to find the type (m_1/m_2) from the ratio Cr I λ4254/Fe I λ4250 (cf. Deutsch (**6**)) but the lines are poorly resolved in these spectra; the ratio (λ4226/λ4325) has proved helpful if the luminosity class is taken into account. A Hartmann spectrocomparator, kindly loaned by the Royal Observatory, Cape, was used for comparing the spectra.

Following Deutsch (**5**), it is found that the clusters may be assigned into three groups: A, B and C. This classification is one of convenience, however, and does not necessarily signify that a continuous range of properties does not occur in cluster stars. One cluster in each group is common to both Deutsch (38 A/mm) and the present observations and these clusters have served to some extent as prototypes. The following properties have been found for each group from the Radcliffe spectra.

Group A: Type $(m_1/m_2) \sim$ K2 – K4 ~ Type (H/m); Spectra roughly match MK standards although metal lines may be slightly weaker. (Prototype NGC 6121.)

Group B: Type $(m_1/m_2) \sim$ G8; Type (H/m) definitely earlier (~G5). (Prototype NGC 6656.)

Group C: Type $(m_1/m_2) \sim$ G5; Type (H/m) much earlier (~F8). (Prototype NGC 7078.)

Different stars in the same cluster are all found to belong to the same group, and the classification into these groups is given in Table I*a*.

1.2. *Spectral types for integrated spectra.*—Although the width (0·50–0·25 mm) and the available wave-length range (λλ4400–4100) of these spectra make them more suitable than the stellar spectra for estimating types, their composite nature

TABLE I*a*

Classification of spectra of globular cluster giants

Group A		Group B		Group C	
	NGC		NGC		NGC
Radcliffe	104	Radcliffe	3201	Radcliffe	4833
	288		4372		6397
	6362		5139		
	6121		6752		7078
			6809	Deutsch	5053
Deutsch	5272		6656		5466
	5904	Deutsch	4147		5897
	6093		5024		6341
	6205		6254		
	6218		6779		
			7089		

makes this estimation difficult. For the sake of uniformity, Morgan's (**21**) method of classifying McDonald globular cluster spectra (150 A/mm Hβ–Hϵ) has been followed and three types have been given to each cluster by comparison with MK standards. (CH/Hγ) is a fundamental type obtained by comparing the G band with Hγ; (H) is a hydrogen type from the absolute strength of Hγ while (Fe) is a metallic line type from the absolute strength of the Fe I lines in the region $\lambda\lambda$ 4250–4400. These types are given for sixteen clusters in Table I*b* and types corresponding to (CH/Hγ) types are given for five clusters from Newtonian spectra in Table I*c*. Different Radcliffe spectra of the same cluster match well and suggest that the cluster light was adequately integrated on all occasions. Mayall's (**19**) types for Crossley spectra agree best with the fundamental type (CH/Hγ) for both Radcliffe and McDonald spectra with an r.m.s. difference of $\pm$0·2 to 0·3 class for a cluster (Fig. 1). There is some evidence for systematic differences between the low dispersion (430 A/mm) Crossley

TABLE I*b*

Spectral types for integrated Cassegrain spectra of 16 globular clusters

NGC	(CH/Hγ)	(H)	(Fe)	NGC	(CH/Hγ)	(H)	(Fe)
104	G3	G3	G3	6397	F5	F5	F4
362	F8	Go	F7	6541	F6	Go	F4
1851	F7	F8	F7	6715	F7	F7	F7
1904	F6	F8	F4	6752	F6	F7	F5
2808	F8	F7	F7	6864	F8	Go	F6
5286	F8	Go	F6	7078	F3	F6	<Fo
6266	F8	Go	F7	7089	F3	F8	Fo
6388	G3	G3	G3	7099	F3	F7	Fo

TABLE I*c*

Spectral type for the integrated Newtonian spectra of 5 globular clusters

NGC	(CH/Hγ)
1261	F8
5139	F7
5927	G2
6139	F8
6584	F7

types and the more recent types on higher dispersion. In particular the latter show a smaller range largely because the Crossley types are systematically too early with respect to the latter for the earliest types. Morgan and Mayall's estimates from the same Crossley spectra also show differences of the order of 0·2 to 0·3 of a class for a cluster. Mayall's 36″ refractor spectra (130 A/mm at Hγ) agree best with the mean of the (CH/Hγ) and (Fe) types with an r.m.s. difference of ±0·3 class for a cluster. For NGC 6715 however the Lick type differs from the Radcliffe type (3 spectra) by 0·9 class. Only one cluster (NGC 7078) was observed in common with Morgan who obtained F3 : F6 : [0], compared with the Radcliffe F3 : F6 : < Fo for the (CH/Hγ), (H) and (Fe) types respectively. From these small samples it is judged that the Radcliffe and McDonald (CH/Hγ) types form a consistent system to within 0·2–0·3 class and that the Crossley spectra may be converted to this system using the curve in Fig. 1. Table V gives a list of the (CH/Hγ) type for 63 clusters from either the Radcliffe, McDonald or corrected Crossley type.

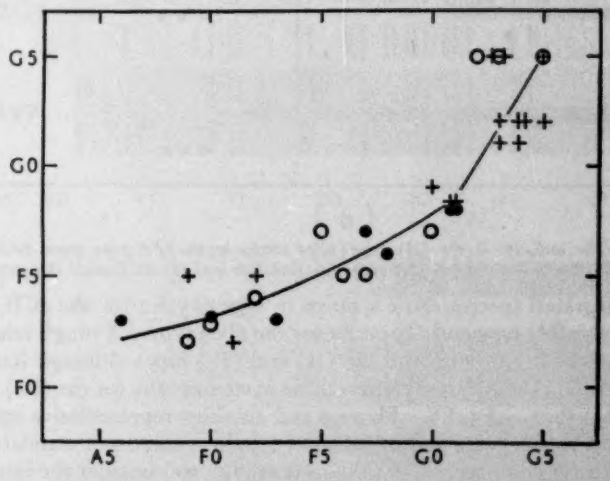

FIG. 1.—*A comparison of spectral types. The ordinate is the Radcliffe (filled circle) or McDonald (open circle) (CH/Hγ) type or Morgan's type for the Crossley spectrum (cross); the abscissa is Mayall's type for the Crossley spectrum of the same cluster.*

Figures 2a and 2b show the variation of the (H) type (filled circles) and the (Fe) type (open circles) with the (CH/Hγ) type (abscissa) for the Radcliffe and McDonald spectra respectively. The general trend of both sets of observations agree although they have only one cluster in common. The (H) type is somewhat later, and the (Fe) type earlier, than the (CH/Hγ) type. These differences are greatest for the earliest (CH/Hγ) and progressively decrease as we move to later (CH/Hγ) types until for (CH/Hγ) ~ G3–5 all three types are roughly equal. The only difference between the Radcliffe and McDonald types is for the (Fe) type for clusters with a (CH/Hγ) type F5–8, where the McDonald types are systematically 0·4 class earlier than the Radcliffe type: this is somewhat larger than the likely error noted above.

To summarize: the spectra of the cluster giants may be divided into three groups: Group A, for which the spectra are practically normal when compared with normal K type giants (9 clusters); Group B, for which the lines are definitely weakened (11 clusters); and Group C, in which the lines are very much weakened (7 clusters). It must be emphasized that this classification is only one of convenience and does not *necessarily* signify grouping as distinct from a continuous range of parameters.

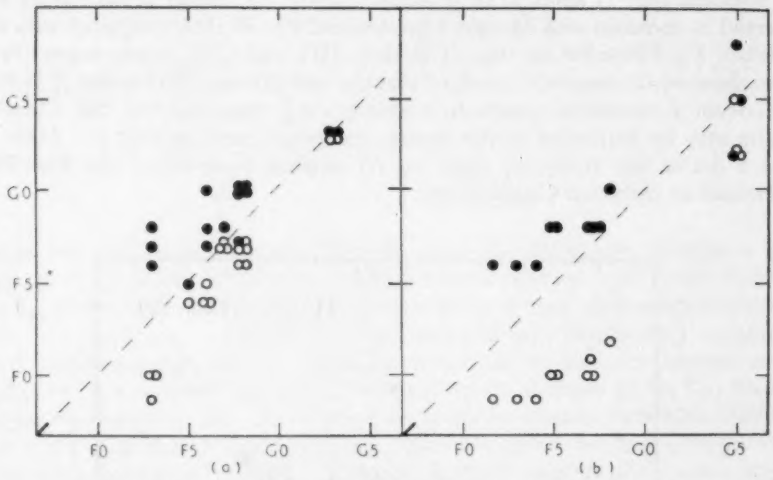

FIG. 2.—*The ordinate is the (H) type (filled circle) or the (Fe) type (open circle). The abscissa is the fundamental type (CH/Hγ): (a) Radcliffe and (b) McDonald integrated spectra.*

The integrated spectra show a range in type G5–F2 for the (CH/Hγ) type, G5–F5 for the (H) type and G5–< Fo for the (Fe) type. A rough relation holds between the (CH/Hγ) types and the (H) and (Fe) types although Radcliffe and McDonald spectra of *different clusters* differ systematically for the (Fe) type when the (CH/Hγ) type ~F5–F8. Plates 9 and 10 show representative spectra both of individual cluster stars and in integrated light; spectra of standard stars are also included for comparison. In the next section we consider the interpretation of the cluster giant spectra and in the third section the interpretation of the integrated spectra.

2. *The interpretation of the spectra of cluster giants*

2.1. *The colours and magnitudes of cluster giants.*—No colours are at present available for the stars from which the present spectra of cluster giants were taken. Since however these stars were amongst the brightest visually in each cluster, we may assume that they belong to the brightest stars of the red giant sequence. Fig. 3 is a composite colour magnitude diagram derived from Arp's data (**2**) of the bright end of this giant sequence for six clusters. These clusters have been combined into three groups of two clusters according to the classification of their giant star spectra. The clusters are NGC 5904 and 6205 of Group A, NGC 6524 and 7089 of Group B and NGC 6341 and 7078 of Group C. These mean curves give absolute visual magnitude (M_V) assuming (with Arp) that for all clusters the RR Lyrae stars have $M_V = -0{\cdot}10$; the vertical lines give the r.m.s. scatter of individual stars about the mean curve.

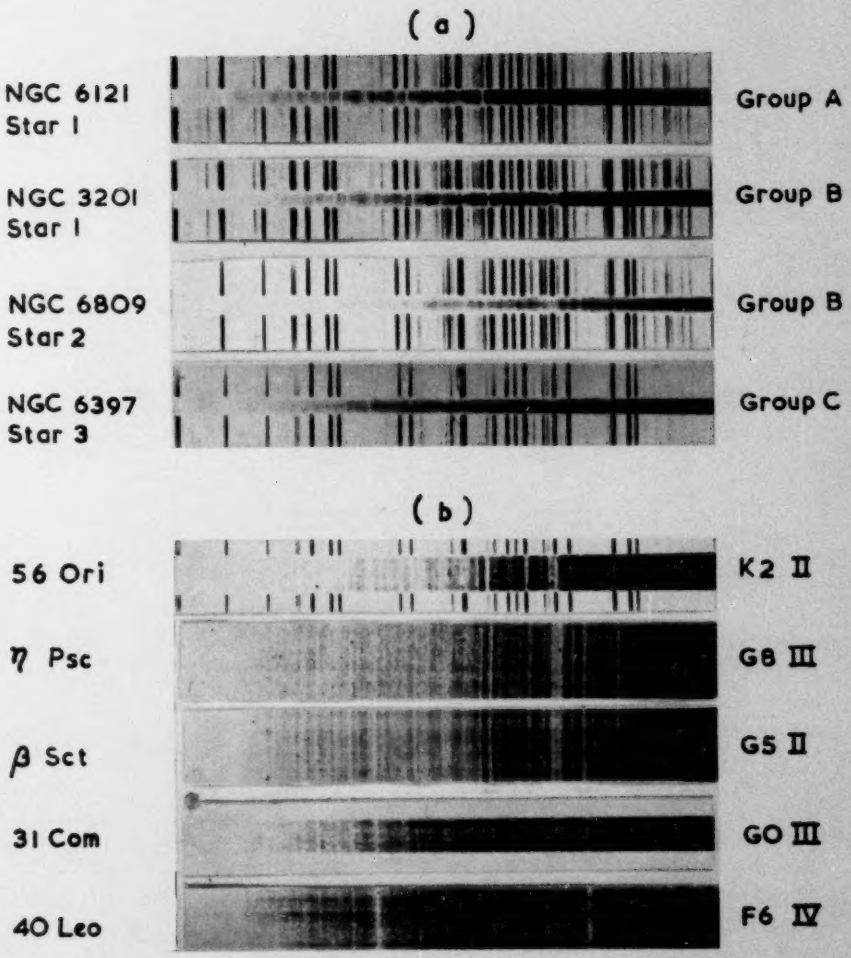

Representative spectra of individual cluster giants (a) and MK standards (b).

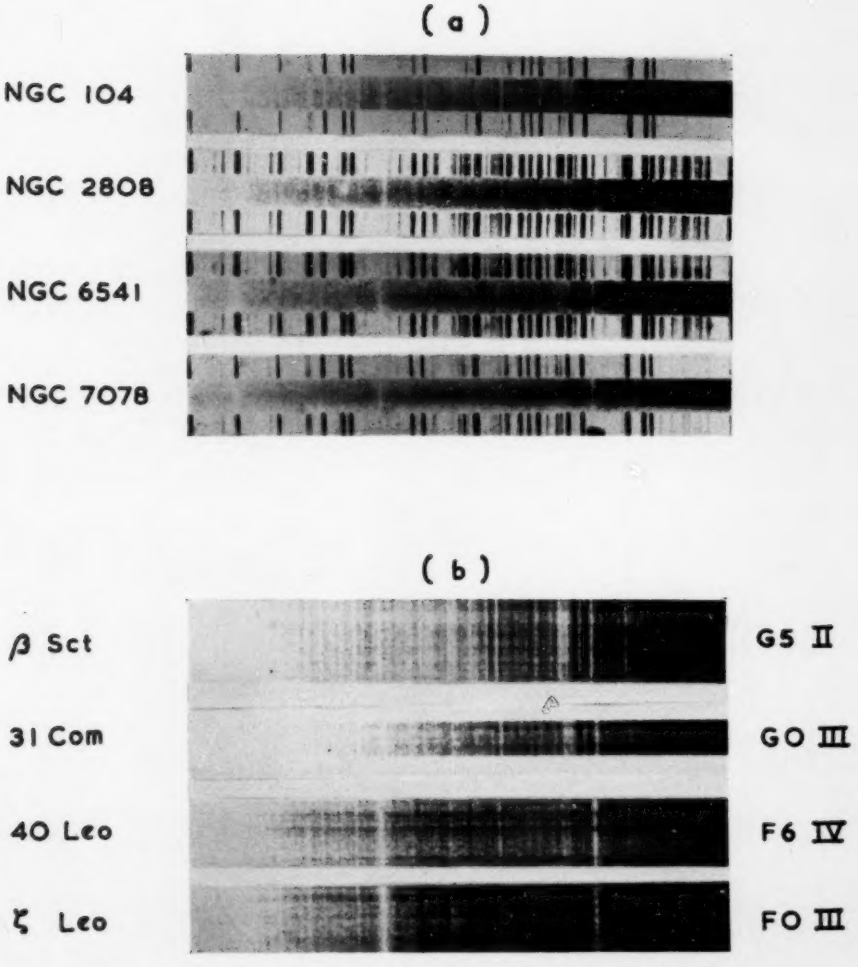

Representative integrated cluster spectra (a) and MK standards (b).

Arp (*loc. cit.*) suggested that the position of the giant sequence in a colour-magnitude diagram depended upon whether the cluster stars had nearly "normal" spectra or spectra in which the metal lines were appreciably weakened; this effect is clearly shown in Fig. 3. The different extensions of the mean curves of the three groups may have significance but could be due in part to the smaller number of stars observed in clusters of Groups B and C compared with Group A. Considering all stars with C.I. $> +1{\cdot}20$, Group C is $0^{m}{\cdot}21 \pm 0^{m}{\cdot}25$ visually brighter than Group B which is not significant. For the same range of colour, however, Groups B and C together are $0^{m}{\cdot}39 \pm 0^{m}{\cdot}06$ visually brighter than Group A which on a Student's *t*-test is highly significant. At C.I. $= +1{\cdot}3$, the absolute visual magnitudes of the stars of Groups B and C are $\sim 0^{m}{\cdot}5$ brighter than those of Group A, if the RR Lyrae stars in all groups have the same absolute magnitudes.

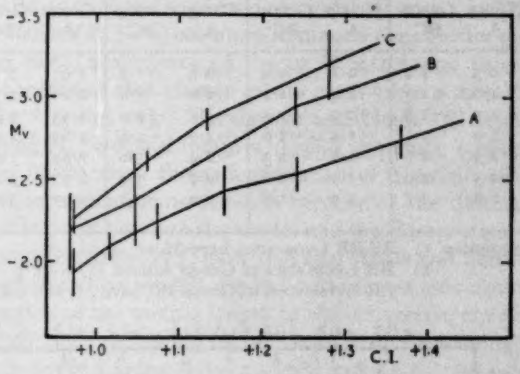

FIG. 3.—*Composite colour magnitude diagrams from Arp's data.*
Group A (NGC 5904 and 6205);
Group B (NGC 6524 and 7089);
Group C (NGC 6341 and 7078).

Arp (*loc. cit.*) also suggested that the mean period of the RR Lyrae stars of type ab in a cluster was correlated with the spectra of the giant stars; those clusters whose giants have nearly "normal" spectra (Group A) having the shortest period RR Lyrae stars. Some support for this suggestion is given in Section 4.2. On the pulsation hypothesis (**15**) (**25**), this has been interpreted as being due to the RR Lyrae stars of Groups B and C being $\sim 0^{m}{\cdot}3$ visually brighter than those of Group A. If this be so, then the M_V for Groups B and C giants is $\sim 0^{m}{\cdot}8$ brighter than those of Group A at C.I. $= +1{\cdot}30$. The absolute magnitude of field RR Lyrae stars determined by Alania (**1**) from Pavlovskaya's proper motions is $M_V = +0{\cdot}2 \pm 0{\cdot}2$. Eggen,* however, from a study of the common motions of groups containing these variables, gives the provisional value $M_V = +0{\cdot}5$ for RR Lyrae stars of the period associated with clusters of Group A.

The calculation of the luminosities and effective temperatures of cluster giants from their magnitudes and colours is set out in Table II. Col. 1 gives the colour index (C.I. scale) and col. 2 gives log T_{eff} interpolated for these colours from the data given by Morgan and Keenan (**20**) and Johnson and Morgan (**13**) for luminosity class II stars. These temperatures can only be regarded as approximate because only meagre data are available for such stars. Cols. 3 and 4

*I am grateful to Dr O. J. Eggen for giving me this information in advance of publication.

give the corresponding M_V from Arp's data for clusters representing Group A and Groups B and C respectively. Cols. 5 and 6 give the same M_V corrected for the assumption that the RR Lyrae stars of clusters of Groups B and C have $M_V = +0.2$ and those of Group A have $M_V = +0.5$. Kuiper's bolometric corrections (**18**) are applied to these magnitudes to obtain the bolometric magnitudes

TABLE II

Assumed magnitudes, colours, temperatures and luminosities for cluster giants

		M_V				M_{bol}		log $L/L_\odot$		Normal spectral type for colour
Assumption		1		2		2		2		
C.I.	log T_e	Group A	Group BC	Group A	Group BC	Group A	Group BC	Group A	Group BC	
+0·7	3·694	−0·5	−1·2	+0·1	−0·9	−0·2	−1·2	1·97	2·37	G2
+0·8	3·674	−1·0	−1·5	−0·4	−1·2	−0·8	−1·6	2·21	2·53	G3
+0·9	3·655	−1·5	−1·8	−0·9	−1·5	−1·4	−2·0	2·45	2·69	G4
+1·0	3·638	−2·0	−2·3	−1·4	−2·0	−2·0	−2·6	2·69	2·93	G6
+1·1	3·622	−2·3	−2·6	−1·7	−2·3	−2·4	−3·0	2·85	3·09	G8
+1·2	3·600	−2·5	−2·9	−1·9	−2·6	−2·7	−3·4	2·97	3·25	K0
+1·3	3·580	−2·6	−3·1	−2·0	−2·8	−2·9	−3·8	3·05	3·41	K1–2

Assumption 1: All RR Lyrae stars have $M_V = -0.10$
„ 2: RR Lyrae stars of Group A have $M_V = +0.5$
RR Lyrae stars of Group BC have $M_V = +0.2$

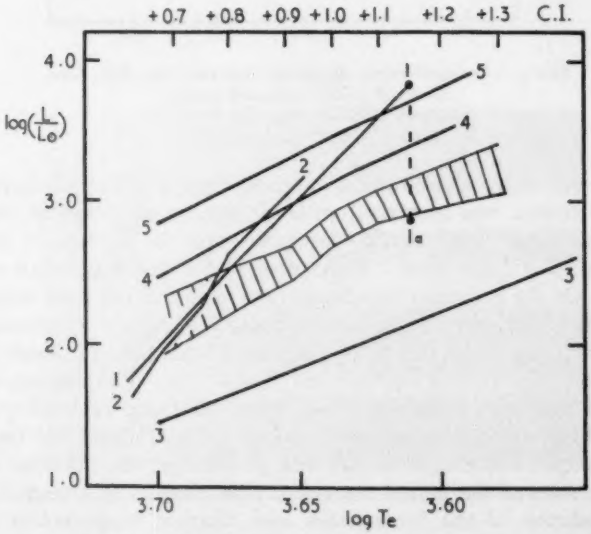

FIG. 4.—*Comparison of models of globular cluster giants. Upper line of hatched area: cluster giants of spectral Groups B and C; lower line of hatched area: cluster giants of spectral Group A.*

Curve 1: Hoyle and Schwarzschild ($A^{-1}=0$); *Point 1a: last model of 1 with* $A^{-1}=7{\cdot}5\times10^{-6}$.
Curve 2: Haselgrove and Hoyle ($A^{-1}=0$).
Curve 3: Kippenhahn, Temesváry and Biermann ($A^{-1}=7{\cdot}5\times10^{-6}$, $\alpha=1$).
Curve 4: Kippenhahn, Temesváry and Biermann ($A^{-1}=7{\cdot}5\times10^{-6}$, $\alpha=2$).
Curve 5: Kippenhahn, Temesváry and Biermann ($A^{-1}=5\times10^{-7}$, $\alpha=1$).

in cols. 7 and 8, and cols. 9 and 10 give the corresponding relative luminosities expressed as log $(L/L_\odot)$ (assuming $M_{\odot\,\mathrm{bol}} = 4{\cdot}73$). The final column gives the normal spectral type for the colour for a star of luminosity class II. The main errors present are due to uncertainties in the RR Lyrae absolute magnitudes and also in the bolometric corrections. Log $(L/L_\odot)$ may be uncertain by perhaps $\pm 0{\cdot}2$ and in addition errors are undoubtedly present in the effective temperatures. Fig. 4 is a plot of log $(L/L_\odot)$ against log T_{eff} or C.I.; the upper limit of the hatched area corresponds to the clusters of Groups B and C and the lower limit to those of Group A.

2.2. *Stellar models of cluster giants.*—Stellar models have been calculated for cluster giants on the assumption that they have about 1·2 solar masses and an isothermal helium core which is unmixed with the outer hydrogen envelope. Hoyle and Schwarzschild (**11**) give a sequence of models (curve 1 in Fig. 4) which for zero metal abundance ($A^{-1}=0$) are more luminous than cluster giants but which for normal solar metal abundance ($A^{-1}\sim 10^{-4}$) correspond to normal late type giants. They concluded that cluster giants must have a metal/hydrogen ratio of $A^{-1}=7{\cdot}5\times 10^{-6}$ (point 1a). Hazelgrove and Hoyle (**8**) repeated these calculations assuming $A^{-1}=0$ and found a similar sequence (curve 2) but terminating at a lower luminosity: their identification of this limit with the observed end of the giant sequence seems dubious because of the difference in effective temperature at this point between the model and the cluster stars. Kippenhahn, St. Temesváry and Biermann (**17**) have repeated Hoyle and Schwarzschild's calculations and find that their models depend critically on assumptions made about α which is a function of the mixing length in the convective envelope of the star: Curves 3 and 4 are their sequences for $A^{-1}=7{\cdot}5\times 10^{-6}$ assuming $\alpha=1$ and $\alpha=2$ respectively while curve 5 is for $A^{-1}=5\times 10^{-7}$ and $\alpha=1$. All models agree that a lower metal abundance produces a higher luminosity at the same effective temperature, which is in qualitative agreement with the observation that Group B and C cluster giants are brighter than those of Group A of the same colour. It does not seem possible to draw further conclusions at present, however, because of the uncertainties in both models and the observed colours and luminosities.

2.3. *The metal line strengths in globular cluster giants.*—The present spectra of cluster giants are not suitable for spectrophotometric analysis. We note, however, that the normal spectral type for a luminosity class II star of C.I. $\sim +1{\cdot}3$ is about K1–K2 and this is about the same type as we found for the giants of Group A. The giants of Group C, on the other hand, have metal lines whose absolute strengths correspond to about F8. Using the equivalent widths of strong Fe I lines in G and K giants found by Pannekoek (**22**) and Wright (**31**) and also the photometric atlas of Hiltner and Williams (**10**), it is estimated that the weakening of the observed metal lines in Group C giants corresponds to a change in equivalent width W given by $\Delta \log W = -0{\cdot}5$. For the giants of Group A, we put $\Delta \log W \leqslant -0{\cdot}15$ which corresponds to the error of our estimation.

The metal lines observed in low dispersion spectra of late type stars are strong lines for which log $(W/\lambda)\sim -3$ and may thus be expected to be formed on the damping part of the curve of growth. For such lines

$$W \propto \sqrt{\frac{Nf\delta}{\kappa_\lambda}} \qquad (1)$$

where N is the number of absorbing atoms per gram of stellar atmosphere, f is

the oscillator strength which is constant for a given line and κ_λ is the continuous mass absorption coefficient at the wave-length of the line. The damping in a strong line will be caused mainly by collisions with neutral hydrogen atoms and so the damping constant δ will be proportional to the gas density ρ (cf. Unsöld's (**29**) discussion on the metal line strengths in subdwarfs). At constant temperature, the equivalent width of the line is thus given by:

$$\log W = \tfrac{1}{2}(\log \rho + \log N - \log \kappa_\lambda + \text{constant}). \tag{2}$$

For stars of colour index C.I. $\sim +1{\cdot}3$, the effective temperature will be taken as 3800°. Wright's investigation of late type giants suggests that the excitation temperature (T_i) for neutral iron lines of low excitation potential should be at least 350° cooler than this giving $T_i \leqslant 3450°$. In order to find the degree of ionization of the metals from the Saha equation, let us consider magnesium as representative of an abundant metal with an ionization potential typical of the iron group. For $T_i \leqslant 3450°$, the fraction $\bar{\phi}$ of Mg atoms which are ionized is given by:

$$\log\left(\frac{\bar{\phi}}{1-\bar{\phi}}\right) \leqslant -2{\cdot}2 - \log p_e \tag{3}$$

where p_e is the electron pressure. Wright (*loc. cit.*) gives $p_e = 0{\cdot}01$ dynes/sq. cm for early K giants whilst Miss van Dijke (**30**) gives 0·003 dynes/sq. cm. It may be noted that Ueno (**28**) gives a much higher value (0·1 dynes/sq. cm) in a theoretical model. The metals must contribute most of the electrons and if (as we suspect) there is a metal deficiency in the globular cluster giants, this and the low surface gravity should mean that the electron pressure is lower in these stars than normal giants so that the metals should be largely ionized. As there is some doubt in this matter we shall consider two models: one with the metals largely neutral and one in which they are largely ionized.

Let it be assumed that the continuous opacity is caused by negative hydrogen absorption. For $\theta_e = 5040/T_e > 0{\cdot}9$, the mean mass absorption coefficient given by Chandrasekhar and Münch (**4**) may be represented by

$$\log \bar{\kappa} = -2{\cdot}83 + 1{\cdot}58\theta_e + \log p_e. \tag{4}$$

In an isothermal atmosphere (cf. (**27**, equation 14)) the density ρ is given by:

$$\log \rho = \log g - \log T_e - \log \bar{\kappa} + \text{constant}. \tag{5}$$

Let $\bar{\phi}$ and y be the ionized fractions of the metal and hydrogen respectively, then:

$$\log p_e = \log (y + \bar{\phi}/A) + \log \rho + \log T_e + \text{constant} \tag{6}$$

and for small y:

$$\log y = -13{\cdot}54\theta_i + \tfrac{5}{2}\log T_i - \log p_e - 0{\cdot}48. \tag{7}$$

At constant temperature, equations (4), (5), (6) and (7) yield the following relations for the density, electron pressure and continuous opacity:—

$$\rho \propto g^{1/2}\left(y + \frac{\bar{\phi}}{A}\right)^{-1/2} \text{ and } \kappa_\lambda \propto \bar{\kappa} \propto p_e \propto \left(y + \frac{\bar{\phi}}{A}\right)^{1/2} g^{1/2}. \tag{8}$$

Case I: *Metals largely neutral.*—In this case $(1-\bar{\phi}) \sim 1$ and $\bar{\phi} \propto p_e^{-1}$. Since $\bar{\phi}$ is small we may put $\bar{\phi} = \zeta y$ where $\log \zeta = (\chi_H - \chi_m)\theta_i$. (9)

Here χ_H and χ_m are the respective ionization potentials of hydrogen and a metal such as magnesium representative of the iron group. We then have:

$$\kappa_\lambda \propto \bar{\kappa} \propto p_e \propto g^{1/3}\left(1+\frac{\zeta}{A}\right)^{1/3} \text{ and } \rho \propto g^{2/3}\left(1+\frac{\zeta}{A}\right)^{-1/3}. \qquad (10)$$

It may be noted that equation (10) and also (16) reduce to those obtained in a similar analysis by Schwarzschild, Spitzer and Wildt (**27**, eqn. 16) if the hydrogen ionization is ignored. Putting the values from equation (10) into equation (2) we have:

$$\log W = -\tfrac{1}{6}\log\left(A(A+\zeta)^2\right) + \text{constant} \qquad (11)$$

for the equivalent width of a line in the atmosphere of a star at constant g and T. If the hydrogen/metal ratio changes from the solar value $A_\odot$ to that for a globular cluster giant $A_\oplus$, then the decrease in equivalent width of a strong metal line will be:

$$\Delta \log W = \tfrac{1}{6}\log\left\{\frac{A_\oplus(A_\oplus+\zeta)^2}{A_\odot(A_\odot+\zeta)^2}\right\}. \qquad (12)$$

The theoretical models discussed in Section 2.2 suggest that an increase in A produces an increase in $L/L_\odot$ and since

$$\log\left(\frac{g}{g_\odot}\right) = \log\left(\frac{\mathfrak{M}}{\mathfrak{M}_\odot}\right) + 4\log\left(\frac{T_e}{T_{\odot e}}\right) - \log\left(\frac{L}{L_\odot}\right) \qquad (13)$$

it will lead to a decrease in g. Our comparison is therefore between two stars having the same temperature and surface gravity; one is the globular cluster giant having mass $1{\cdot}2M_\odot$ and a hydrogen/metal ratio $A_\oplus$ and the other is a more massive giant of luminosity class II with solar metal abundance $A_\odot$. The observed differences between the equivalent widths of cluster stars and standard stars of the same effective temperature and luminosity are given at the beginning of this section; from this data and equations (9) and (12) we find that the hydrogen ionization is negligible and that for

$$\text{clusters of Group A, } \frac{\text{metals}}{H} \geqslant \frac{1}{8} \text{ solar abundance}$$

$$\text{clusters of Group C, } \frac{\text{metals}}{H} \sim \frac{1}{1000} \text{ solar abundance.}$$

These low metal abundances indicate that the electron pressures must be lower than in normal giants; consequently by equation (3), the metals are likely to be ionized and the initial assumption of case I is wrong. Furthermore it is likely that weak atomic metal lines contribute to the continuous opacity in these stars. We may determine the consequences of this by considering the continuous opacity to be wholly due to this cause, in which case:

$$\log \bar{\kappa} = \log N + \text{constant} \qquad (14)$$

and then from (1), (5) and (14)

$$\log W = -\tfrac{1}{2}\log N + \text{constant} = \tfrac{1}{2}\log A + \text{constant}. \qquad (15)$$

In this case the strong metal lines actually increase in strength as the metal abundance falls—an effect which has been considered by Deutsch and others (**6**). The effect will be greatest for the clusters of Group A in which the metal content is relatively high, so it is likely that the metal abundances found for this group are overestimated. We shall therefore consider the metals to be largely ionized in both groups.

Case II: *Metals largely ionized.*—In this case $\bar{\phi} \sim 1$ and $(1-\bar{\phi}) \propto p_e$ and hence:

$$\kappa_\lambda \propto \bar{\kappa} \propto p_e \propto (y+A^{-1})^{1/2} g^{1/2} \text{ and } \rho \propto g^{1/2}(y+A^{-1})^{-1/2}. \tag{16}$$

We also have in this case:

$$\log N = \log(1-\bar{\phi}) - \log A \tag{17}$$

and hence

$$\log W = -\tfrac{1}{4}\log(A^2(y+A^{-1})) + \text{constant} \tag{18}$$

for a star of given g and T. The decrease in equivalent width in changing the abundance from $A_\odot$ to $A_\oplus$ will be:

$$\Delta \log W = \tfrac{1}{4}\log\left\{\frac{A_\oplus{}^2(y_\oplus + A^{-1}{}_\oplus)}{A^2{}_\odot(y_\odot + A^{-1}{}_\odot)}\right\}. \tag{19}$$

The hydrogen ionization y may be found from equations (4), (5), (6) and (7) to be:

$$\log[y^2(y+A^{-1})] = -27{\cdot}08\theta_i + 5\log T_i + 1{\cdot}58\theta_e - 3{\cdot}79 - \log g. \tag{20}$$

Since $\log g$ is known from (13), (19) and (20) may be solved for $A_\oplus$ using the observed values of $\Delta \log W$. Assuming $A_\odot = 10^4$, the hydrogen ionization is found to be negligible and we have for

$$\text{clusters of Group A, } \frac{\text{metals}}{H} \geqslant \frac{1}{4} \text{ solar abundance}$$

$$\text{clusters of Group C, } \frac{\text{metals}}{H} \sim \frac{1}{100} \text{ solar abundance.}$$

The second abundance has an uncertainty of at least a factor 4 because of the uncertainties in $\Delta \log W$ alone. As remarked above, these metal abundances are likely to be too high (A too small) because of the neglect of the contributions of the metal lines to the continuous opacity. These values may be compared with those found by Helfer, Wallerstein and Greenstein (9) for the giant stars in NGC 6341 (our Group C) and NGC 6205 (our Group A) using the curve of growth method. I am indebted to them for providing this information before publication.

$$\text{(Group A) NGC 6205 } \frac{\text{metals}}{H} \text{ have } \frac{1}{20} \text{ solar abundance.}$$

$$\text{(Group C) NGC 6341 } \frac{\text{metals}}{H} \text{ have } \frac{1}{200} \text{ solar abundance.}$$

They remark that these values could easily be in error by a factor of 4 either way but are unlikely to be in error by a factor as great as 10. Considering this, and the approximate nature of the present analysis, the agreement is as satisfactory as could be expected. We conclude that the metal/hydrogen ratio is likely to lie in the range 0·01–0·001 the solar value for clusters of Group C while for Group A clusters it is relatively indeterminate but is likely to be of the order 0·1 of the solar value. The two chief difficulties in this analysis are finding the source of the continuous opacity and fixing the excitation temperature.

We have hitherto considered strong lines. A weak line formed on the Doppler part of the curve of growth will have an equivalent width

$$W \propto \frac{Nf}{\kappa_\lambda}. \tag{21}$$

In this case, for no contribution to the electron pressure from hydrogen and with the metals largely ionized, the line weakening is given by:

$$\Delta \log W = \log\left(\frac{A_\oplus}{A_\odot}\right) \tag{22}$$

and a much larger change in line strength occurs for a given abundance change. It may be noted that Schwarzschild, Spitzer and Wildt (**27**) assume that the metal line strength is proportional to the partial pressure of atoms producing the line divided by the partial pressure of the particles producing the general opacity. It follows therefore that their arguments apply only to weak lines.

It is known (**14**) that a $(U-B)/(B-V)$ plot for the spectroscopically nearly normal giants in NGC 5272 shows an ultra-violet excess which has been interpreted as being due to smaller blanketing in the ultra-violet due to a metal deficiency. This appears quite likely since although the strong lines are relatively unaffected, a metal abundance deficiency by a factor 10 will reduce the equivalent widths of the faint lines proportionally and a significant change in blanketing should occur.

Finally consider the case of the subgiant branch of a globular cluster and take the colour index C.I. $= +0{\cdot}64$ as representative of this group of stars in NGC 5272. Assuming $T_e = 5495°$, $T_i = 5040°$ and $M_{bol} = +1{\cdot}2$, we may solve equations (13), (19) and (20) for $\Delta \log W$ with different assumed metal/hydrogen ratios. We then have:

$A^{-1} = 4 \times 10^{-5}$	$y = 1{\cdot}41 \times 10^{-5}$	$p = 0{\cdot}75$
10^{-5}	$1{\cdot}95 \times 10^{-5}$	$0{\cdot}44$
5×10^{-6}	$2{\cdot}04 \times 10^{-5}$	$0{\cdot}32$

where p is the factor by which a strong metal line is weakened relative to a star of the same colour and luminosity but with solar metal abundance ($A^{-1} = 10^{-4}$). It will be noticed that the weakening becomes large when $y > A^{-1}$; that is when the hydrogen supplies more electrons than the metals. It is thus seen that a metal deficiency which will produce little change in the spectra of the giant stars (as in group A clusters) may produce significant weakening of the metal lines in the subgiants. Since the subgiants contribute a considerable fraction of the integrated cluster light, we shall in the next section try to confirm this by considering the integrated spectra of clusters.

3. *The interpretation of the integrated spectra*

3.1. *The integrated spectrum of NGC 5272.*—Let us consider the formation of an absorption line in the integrated spectrum of a cluster. The cluster may be considered to consist of n groups of stars so that for the ith group the equivalent width of a given line is the same (W_i^*) for all stars in the group. We shall in fact assume that all stars in the group have the same spectrum. Then if α_i is the fraction of the total light of the cluster emitted by the ith group in photographic wave-lengths, the observed equivalent width of the line in the integrated spectrum will be

$$\sum_{i=n} \alpha_i W_i^*. \tag{23}$$

At present this calculation can only be attempted directly for one cluster (NGC 5272) for which Sandage (**24**) has found the luminosity function. For each 0·2 range of absolute photographic magnitude M_{pg} to $M_{pg} + 0{\cdot}2$ corrected according to Johnson and Sandage (**14**), the photographic luminosity function

$\phi(M_{pg})$ is given by Sandage. The total contribution in photographic light from M_{pg} to $M_{pg}+0{\cdot}2$ thus equals

$$\alpha(M_{pg}, M_{pg+0{\cdot}2}) = [\phi(M_{pg})10^{-0{\cdot}4M_{pg}}] / \sum_{i=n} \alpha_i \qquad (24)$$

where the summation of α on the r.h.s. of equation (22) is over the whole range of magnitudes of stars in the cluster. The plot of α against M_{pg} (cf. Fig. 1 in (**24**)) shows a sharp peak around $M_{pg}=0$ which is produced by the stars of the horizontal branch. It is possible to assume that the contribution to α from the giant branch varies smoothly in this region and so the different contributions of the giant and horizontal branches may be separated in this range ($-0{\cdot}4 < M_{pg} < +0{\cdot}8$). The colour magnitude diagram (**14**) allows us to assign a colour to each group of stars within it and using Johnson and Morgan's data (**13**), each group may thus be given a spectral type. As mentioned in Section 2.3 an approximate equivalent width (W_i) may be assigned to each line for a given spectral type and therefore for each group from the data of Pannekoek (**22**), Wright (**31**) and Hiltner and Williams (**10**) if the stars have normal spectra. For abnormal spectra, a factor p must be applied which is appropriate to the given line. We can then find $W_i^* = pW_i$ and knowing α_i from (24) find the equivalent width of the line in the integrated spectrum from (23). The equivalent width may then be converted back to a spectral type corresponding to the absolute intensity of the line for comparison with the observed spectrum.

TABLE III

The contributions to the equivalent widths of hydrogen and metal lines in the integrated spectrum of NGC 5272 when spectra of stars are normal for colours

	Group of Stars	Contribution to photographic light of cluster per cent	Contribution to equivalent width of H lines per cent	Contribution to equivalent width of metal lines per cent
1.	Giant branch $B-V>+0{\cdot}8$	20·8	5·8	36·3
2.	Subgiant branch and main sequence for $B-V<+0{\cdot}8$	50·2	29·1	52·0
3.	Horizontal branch	27·1	64·7	3·9
4.	Main sequence $B-V>+0{\cdot}8$	1·9	0·4	7·8

Table III gives in condensed form the results of this calculation for NGC 5272, assuming that the spectra are normal, i.e. that they correspond to the colours. In the actual calculation the cluster was divided into twenty-one groups of stars but the condensed table with four groups is sufficient to show where the main contributions to the lines in the integrated spectra originate. Equivalent widths of different metal lines will, of course, show a different dependence on spectral type: the present results refer to the strong Fe I lines λ4325 and λ4383 which are representative of those used to obtain Radcliffe and McDonald (Fe) types.

We consider two extreme cases. In the first the spectra correspond to the colours throughout the cluster and there is therefore no line weakening. In this case the (H) type for NGC 5272 is F7 and the (Fe) type is G2. In the second case, we assume that stars with $(B-V)>+0{\cdot}8$ have normal spectra while those with $(B-V)<+0{\cdot}8$ (i.e. the subgiants, horizontal branch and upper part of the

main sequence) have normal hydrogen lines but no metal lines at all. In this case the (Fe) type is F2 while the hydrogen type is of course unchanged (F7). We may compare these types with those observed by Morgan which are (H) = F8 and (Fe) = F1. It is seen that the observed spectrum agrees well with the case in which *the metal lines in the subgiants are very weakened.* This was the prediction for these subgiants (given at the end of the previous section) if the metal/hydrogen ratio was less than about 0·1 of the solar value. We conclude therefore from our discussion of the integrated spectrum of a cluster of Group A that the metal/hydrogen ratio is $\leqslant 0{\cdot}1$ of the solar value and not higher as would have been possible from a consideration of the giant stars alone.

3.2. *The integrated spectra of other clusters.*—Although NGC 5272 is the only cluster for which a full luminosity function is available, one can attempt some interpretation for other clusters using the data on the luminosity function of the giant and horizontal branches of four clusters given by Arp (2, Tables III and IV). It is assumed that the relative fractions of light coming from the giant, subgiant and main sequences are the same in all clusters and that only the contribution from the horizontal branch changes. The contributions to the total light from the horizontal branch of these clusters relative to that in NGC 5272 and from the rest of the cluster relative to that in NGC 5272 can be calculated and are given in Table IV. The cluster NGC 6356 of late integrated type is also considered. According to provisional unpublished data,* this cluster has only a weak stub on the red side of the normal position of the horizontal branch, i.e. in the region $(B-V) = +0{\cdot}4$. It has therefore been assigned a horizontal branch of the same strength as that in NGC 6205 (whose horizontal branch is also weak) at $(B-V) = +0{\cdot}4$.

TABLE IV

Calculated and observed integrated spectral types for five globular clusters

NGC	5904	6205	7089	7078	(6356)
Spectral group (giant stars)	A	A	B	C	A
Photographic contribution to horizontal branch relative to NGC 5272	0·78	0·37	0·50	0·76	0·37
Photographic contribution to giant branch relative to NGC 5272	1·08	1·23	1·18	1·09	1·23
(H) type:					
calculated	F5–6	F8–9	F8	F8	G1
observed	F8 (M)	F8 (M)	F8 (R)	F6–8 (MR)	G2 (M)
(Fe) type:					
calculated	F5	F6	A9–F0	A4	G5
observed	F0 (M)	F0 (M)	F0 (R)	(0) (MR)	G5 (M)

Observed type M = McDonald. R = Radcliffe

Spectral types have been calculated for the hydrogen and metal lines in five clusters by the method described in Section 3.1 under the following assumptions:

(1) *For NGC* 6356, the spectra correspond to the colours of the stars, i.e. the abundances are sufficiently normal for no metal line weakening to occur.

(2) *For Group A clusters NGC* 5904 *and* 6205, the spectra correspond to the colours of the stars for $(B-V) > +0{\cdot}8$ but metal lines are absent in stars to the blue of this limit.

*I am indebted to Dr A. R. Sandage for kindly telling me this in a private discussion.

(3) *For the Group B cluster NGC* 7089, the metal lines have 60 per cent of the normal strength for the star's colour for $(B-V)>+0{\cdot}8$ and are absent to the blue of this limit.

(4) *For the Group C cluster NGC* 7078, the metal lines have 30 per cent of the normal strength for the star's colour for $(B-V)>+0{\cdot}8$ and are absent to the blue of this limit.

Table IV gives the calculated and observed (H) and (Fe) types for these five clusters. The agreement between observation and calculation must be considered as good as could be expected considering the drastic simplifying assumptions which have been made. The greatest discrepancy is for the (Fe) types of NGC 6205 and 5904; it may be noted that these clusters belong to the group of intermediate (CH/Hγ) type in which there appear to be systematic differences between Radcliffe and McDonald observations.

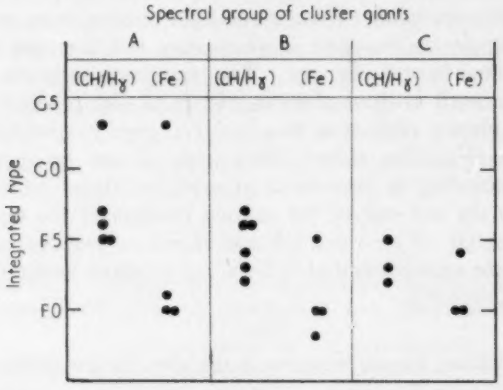

FIG. 5.—*The integrated spectral types (CH/Hγ) and (Fe) associated with the spectral groups of the cluster giants A, B and C.*

Fig. 5 shows the relations between the integrated (CH/Hγ) and (Fe) types and the spectral group (A, B or C) of the cluster giant stars. The clusters containing giants of Group A are seen to have a wide range in the (Fe) type of their integrated spectra. This may be understood since we have seen that a wide range of metal abundance may produce practically normal spectra for the brighter giant stars. Such a range of metal abundance will however produce quite different metal line strengths in the subgiants which contribute at least half the photographic light of the cluster and so have a considerable influence on the integrated spectrum. Other differences in the integrated spectrum are likely to originate in the different relative populations of the horizontal branches of different clusters; it does not seem as though it is necessary to assume any large differences in the luminosity functions of the giant, subgiant and main sequences in different clusters apart from a scale factor.

The present calculations contain many simplifications which later work should remove. To do this, however, more cluster luminosity functions together with photometric and spectrophotometric data on both clusters and normal disk stars will be needed before an accurate understanding of the composition of globular cluster stars is possible. It is not unlikely, for example, that the relative

abundances of different metals or their abundance relative to carbon or nitrogen is variable but investigations of this point are beyond the scope of this paper.

We conclude, however, that the metal/hydrogen ratios relative to the Sun $A_{\oplus}^{-1}/A_{\odot}^{-1}$ derived here should be of the correct order of magnitude; they are summarized for different kinds of cluster below:

Spectral group of cluster giant stars	Integrated type (CH/Hγ)	$A_{\oplus}^{-1}/A_{\odot}^{-1}$
A	G5–G0	> 1/10
	G0–F5	< 1/10
B	F7–F2	> 1/100
C	F5–F2	< 1/100

4. *Correlations between spectral type and other parameters*

4.1. *Spectral type and distance from the galactic plane.*—Mayall (19) noticed originally that the clusters of later spectral type occurred near the galactic centre. Baade (3) has recently shown that Mayall's spectral types show a correlation with the distance (Z) of the cluster from the galactic plane. He suggests that

TABLE V

The spectral type (CH/Hγ) of integrated spectrum, distance from the galactic plane ($|Z|$) and distance from galactic centre projected onto the galactic plane (R_c) in kpc. Assumed distance of Sun from galactic centre equals 8·2 kpc

NGC	(CH/Hγ)	$\|Z\|$	R_c	NGC	(CH/Hγ)	$\|Z\|$	R_c
104	G3	4·1	6·8	6333	F3–4	1·2	0·9
362	F8	12·6	8·4	6341	F2	6·1	9·6
1261	F8	23	19·9	6356	G5	1·6	2·4
1851	F7	9·3	19·0	6388	G3	1·8	5·1
1904	F6	6·2	18·2	6397	F5	0·5	6·2
2298	F7	7·8	33	6402	F8	1·6	3·0
2419	F5	31	69	6440	G5	0·2	3·9
2808	F8	1·5	10·1	6441	G4	0·9	1·0
4147	F2	26	10·9	6541	F6	0·9	4·2
4590	F2	6·9	8·7	6544	F9	0·4	3·3
5024	F4	19·6	4·8	6584	F7	3·9	4·9
5139	F7	1·2	6·4	6624	G4	2·0	4·2
5272	F7	13·4	6·1	6626	F8	0·6	3·7
5286	F8	2·0	8·4	6637	G5	1·5	1·2
5634	F5	17·0	7·8	6638	G2	2·2	5·6
5694	F3	20	30	6652	G2	3·6	7·2
5824	F5	16	36	6656	F5	0·5	5·2
5904	F5	6·0	2·5	6681	G0–1	4·8	11·2
5927	G2	0·2	5·8	6712	G4	0·6	3·7
5986	F8	3·1	6·7	6715	F7	4·2	6·4
6093	F7	3·3	2·6	6723	G2	3·3	1·3
6139	F8	1·3	5·3	6752	F6	2·9	3·8
6171	G0–1	1·1	5·4	6779	F5	1·9	12·2
6205	F5	4·4	7·0	6838	G5	0·6	6·8
6218	F6	2·4	3·4	6864	F8	10·9	14·0
6229	F7	15·7	24	6934	F7	5·7	12·4
6254	F8	1·9	3·9	6981	G0–1	10·2	9·6
6266	F8	0·7	1·6	7006	F3–4	20	53
6273	F4	1·0	1·4	7078	F3	7·1	12·3
6284	F9	2·6	8·2	7089	F3	9·5	10·2
6293	F3	1·7	6·1	7099	F3	9·4	3·9
6304	G2	0·4	2·4				

clusters may be divided into two groups: those with integrated spectral type G3–5 which have a strong concentration to the plane and those of A5–Go which are a halo group which show very little concentration to the plane.

Table V gives the integrated spectral type (CH/Hγ) and the galactocentric distance projected onto the galactic plane (R_c) for 63 clusters. The clusters are divided *for convenience* into three groups according to spectral type: G5–Go, F9–F6 and F5–F2. As we have seen in Section 3, these groups are roughly in order of decreasing metal/hydrogen ratio. Fig. 6 shows the distribution of $|Z|$ and R_c for the three groups and shows the decrease in $|Z|$ as the spectral type gets later. On the simplifying assumption that Z has a normal distribution about the galactic plane, we may find the variance $\sum Z^2/n-1$ for each group. Snedecor's variance ratio test then shows that the probability that any two of the observed variances could have come by chance from the same parent population is less than one in one hundred. We should consider whether the observed relation could be produced by a variation in the absolute magnitude of the RR Lyrae stars (upon which the distances are based) with integrated spectral type. This is unlikely since Baade (*loc. cit.*) has shown that a similar relation holds between spectral type and galactic latitude. Moreover, if the pulsation hypothesis of the RR Lyrae stars is correct, the assumed absolute magnitudes of these stars in clusters of earliest type are too faint and so the distances of these clusters are too small; a correction for this effect will therefore accentuate the spectral type-$|Z|$ relation found above.

It is seen in Fig. 6 that the ratio mean R_c/mean $|Z|$ increases as the integrated spectral type gets later which is an indication that the clusters of later type form a more flattened system than those of earlier type as distinct from a spherical system of smaller mean radius. This result is only tentative since there are likely to be many clusters (particularly of later type) which are unobserved because of obscuration. Schmidt (**26**), however, attempts to allow for this observational selection by effectively considering only high latitude clusters and also finds a systematic decrease in the flattening of the cluster system outwards.

Whilst the largest difference in distribution undoubtedly exists between the groups of type G5–Go and those of F5–F2, we do not think that it can be assumed (as by Baade) that the intermediate group is merely a mixture of the two extreme groups produced by inaccurate spectral types. These inaccuracies must not be underestimated but the present spectra of both stars and integrated cluster light do show the presence of *intermediate spectral types*; so that some intermediate spatial distribution of these clusters is not unlikely. Observational selection undoubtedly influences the observed frequency distribution of clusters with spectral type. This may be roughly corrected by assuming (after Baade, *loc. cit.*) that the number of clusters with $|b|<19^\circ$ should be tripled. We then have:

	Range in spectral type		
	G5–Go	F9–F6	F5–F2
Observed frequency	17	26	20
Corrected frequency	45	56	32

After correction, the intermediate group is still the largest which lends support to the hypothesis that a *continuous range of spectral types exists and not two groups.*

4.2. *Spectral type and the RR Lyrae stars.*—Arp (**2**) suggested that a correlation exists between the giant star spectra and the mean period of the RR Lyrae stars of type *ab* in a cluster: the giant stars of more normal spectral type (Group A) being associated with the variables of shorter mean period. Fig. 7 shows a plot of mean period against giant star spectral group (A, B or C) and also against integrated spectral type. The spread in periods among type *ab* variables in a cluster is of the order of 0·1 days or more so that only clusters containing ten or more variables to define a mean period have been used. The present meagre data give some support to Arp's conclusion but clearly more data are required.

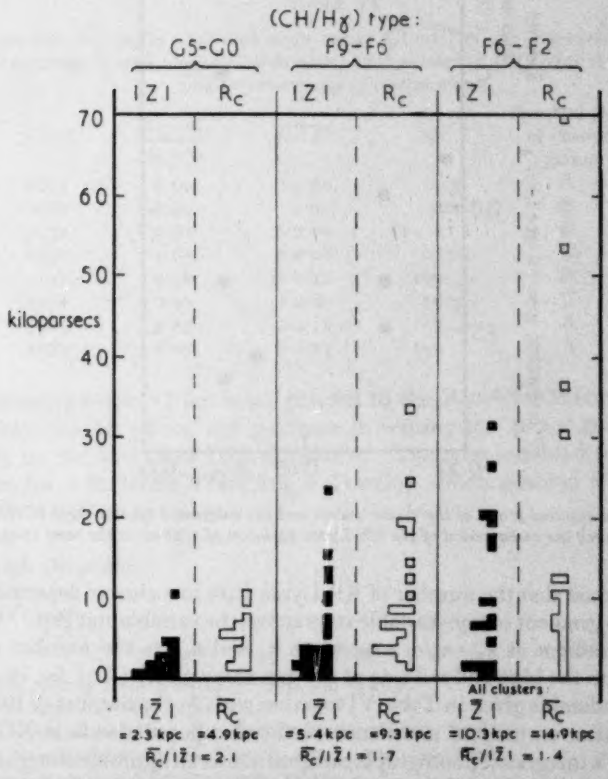

FIG. 6.—*The distance from the galactic plane* ($|Z|$) *and the galactocentric distance projected on the plane* (R_c) *in kpc as a function of the integrated spectral type* ($CH|H\gamma$).

Iwanowska (**12**) finds a relation between the period of field RR Lyrae stars and their spectral type so a correlation is not unlikely between the periods of cluster RR Lyrae stars and the spectra of stars in the same cluster. The pulsation hypothesis (**15, 25**) predicts that the absolute magnitude of these variables should be a function of both colour and period. Thus if the absolute magnitude of the horizontal branch is related to the spectral group of the cluster giants, the mean period of the RR Lyrae stars should be also if their mean colour is constant. Arp's data (*loc. cit.*) shows that the gradient of population of non-variable stars

across the RR Lyrae gap is not the same for all clusters and so the mean colour of the variables is probably not constant*. This may partly explain the scatter in Fig. 7, but actual colours of RR Lyrae stars in clusters are needed to make this certain.

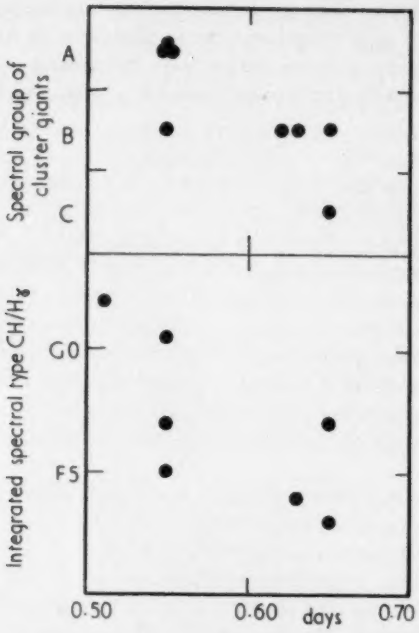

FIG. 7.—*The spectral group of the cluster giants and the integrated spectral type (CH/Hγ) plotted against the mean period of the RR Lyrae variables of type ab in the same cluster.*

Arp also noted that the number of RR Lyrae stars in a cluster depended upon the population gradient of non-variable stars across the variable star gap. We may express this gradient as n_1-n_2/n_1+n_2, when n_1 and n_2 are the number of non-variable stars on the blue and red side of the gap respectively (Arp, *loc. cit.*, Table IV). The gradient is given in Table VI together with N, the number of RR Lyrae stars in the cluster normalized to the same total stellar population as in NGC 5272 using Christie's integrated photographic magnitude as an approximate measure of the total population. Table VI also shows that the relative number of variables is large when the mean colour of the non-variable stars in the horizontal branch $\overline{B-V}$ lies in or near the zone of instability ($0{\cdot}17 < B-V < 0{\cdot}39$) and is few when $\overline{(B-V)}$ is well outside these limits. Neither $\overline{(B-V)}$ nor the gradient n_1-n_2/n_1+n_2, however, show any correlation with the spectral group of the cluster giants.

To summarize: the present classification of the spectra of cluster giants agrees with that of Deutsch. The classification of the integrated spectra in general confirms that of Mayall and Morgan at lower dispersion although small systematic

* I am indebted to Dr A. R. Sandage for pointing this out to me.

differences are present. An analysis of the spectra shows that the metal/hydrogen ratio probably ranges from less than 0·01 to greater than 0·1 of the solar value. Clusters with the lowest metal abundance show an extended spherical galactic distribution, and the greater the metal abundance, the more the clusters are concentrated to the galactic plane. More photometric and spectrophotometric data of both cluster giants and subgiants are needed to find more accurate metal abundances. Also more data on cluster RR Lyrae stars are needed to confirm the suspected correlation between their mean period and cluster spectral type.

TABLE VI

Density gradient (n_1-n_2/n_1+n_2) *and mean colour* $\overline{(B-V)}$ *of the non-variable stars in the horizontal branch compared with normalized number of RR Lyrae stars* (N) *and spectral group of cluster giants*

NGC	$\frac{n_1-n_2}{n_1+n_2}$	$\overline{B-V}$	N	Spectral group of cluster giants
6205	1·00	−0·02	4·5	A
7089	0·90	0·00	9·2	B
6254	0·82	+0·09	0	B
6341	0·63	+0·08	20·6	C
4147	0·58	+0·11	160	B
7078	0·47	+0·17	55·7	C
5904	0·45	+0·16	113	A
5272	0·07	+0·24	169	A

Acknowledgments.—I am most grateful to the Radcliffe Observer (Dr A. D. Thackeray) for his advice and guidance in writing this paper and to Dr A. R. Sandage for his lively and helpful interest. I am also indebted to the Radcliffe Trustees for a Radcliffe Travelling Fellowship which enabled this work to be undertaken at Pretoria.

Radcliffe Observatory,
Pretoria :
1959 *February.*

References

(1) J. Ph. Alania, *Bull. Abastuman Obs.*, **23**, 1, 1958.
(2) H. C. Arp, *A.J.*, **60**, 317, 1955.
(3) W. Baade, *Pont. Acad. Sci. Scripta Varia*, **16**, 303, 1958.
(4) S. Chandrasekhar and G. Münch, *Ap. J.*, **104**, 446, 1946.
(5) A. J. Deutsch—private communication.
(6) A. J. Deutsch, Principes. Fondamentaux de Classification Stellaire, 25, CNRS, Paris 1955.
(7) J. L. Greenstein. Draft reports of I.A.U. (Moscow), p. 262, 1958.
(8) C. B. Hazelgrove and F. Hoyle, *M.N.*, **118**, 519, 1958.
(9) H. L. Helfer, G. Wallerstein and J. L. Greenstein, *Ap. J.* (in press).
(10) W. A. Hiltner and R. C. Williams, Photometric Atlas of Stellar Spectra, Univ. of Michigan, 1946.
(11) F. Hoyle and M. Schwarzschild, *Ap. J. Supplement No.* 13, Vol. II, 1, 1955.
(12) W. Iwanowska, *Torun. Bull.* III, No. 2, 1, 1953.
(13) H. L. Johnson and W. W. Morgan, *Ap. J.*, **117**, 313, 1953.
(14) H. L. Johnson and A. R. Sandage, *Ap. J.*, **124**, 379, 1956.
(15) T. D. Kinman, *M.N.*, **119**, 135, 1959.
(16) T. D. Kinman, *M.N.*, **119**, 157, 1959.

(17) R. R. Kippenhahn, St. Temesváry and L. Biermann, *Zs. f. Ap.*, **46**, 257, 1958.
(18) G. P. Kuiper, *Ap. J.*, **88**, 429, 1938.
(19) N. U. Mayall, *Ap. J.*, **104**, 290, 1946.
(20) W. W. Morgan and P. C. Keenan, *Astrophysics* (ed. Hynek) p. 20, McGraw Hill (1951).
(21) W. W. Morgan, *P.A.S.P.*, **68**, 509, 1956.
(22) A. Pannekoek, *Dom. Astr. Obs. Victoria*, **8**, 141, 1951.
(23) D. M. Popper, *Ap. J.*, **105**, 204, 1947.
(24) A. R. Sandage, *A.J.*, **59**, 162, 1954.
(25) A. R. Sandage, *Pont. Acad. Sci. Scripta Varia*, **16**, 41, 1958.
(26) M. Schmidt, *B.A.N.*, **13**, 15, 1956.
(27) M. Schwarzschild, L. Spitzer, Jnr. and R. Wildt, *Ap. J.*, **114**, 398, 1951.
(28) S. Ueno, *Publ. Astr. Soc. of Japan*, **1**, 138, 1949.
(29) A. Unsöld, *M.N.*, **118**, 3, 1958.
(30) S. E. A. van Dijke, *Ap. J.*, **104**, 27, 1946.
(31) K. O. Wright, *Dom. Astr. Obs., Victoria*, **8**, 281, 1951.

GLOBULAR CLUSTERS, III. AN ANALYSIS OF THE CLUSTER RADIAL VELOCITIES

T. D. Kinman

(Communicated by the Radcliffe Observer)

(Received 1959 April 20)

Summary

The solar motion found from the radial velocities of 70 globular clusters is 167 ± 30 km/s with an apex which does not deviate from the direction of the Sun's galactic rotation. A small and scarcely significant apparent contraction of the system is found which could be produced by systematic errors in the velocities found from low dispersion spectra. The radial velocities provide no conclusive evidence for differential motion in the cluster system either as a function of galactocentric distance or of integrated spectral type: large errors are inherent in these solutions, however, because of the small samples of clusters available, their unfavourable galactic distribution and large peculiar motions.

It is shown that field RR Lyrae stars of the *same period range* as those occurring in globular clusters have the same solar motion and velocity dispersion as the clusters; it is suggested that these stars and the clusters have a common origin.

A scatter diagram of the ratio of the radial velocity to the circular velocity against the angle subtended at the cluster by the Sun and the galactic centre confirms von Hoerner's conclusion that the cluster orbits are mainly highly eccentric. A high eccentricity ($e = 0{\cdot}8$) is also found by considering the mean galactic rotation of the cluster system.

A simple model is used to determine the distribution of mass in the Galaxy from the cluster motions. The results are consistent with Schmidt's model except possibly at galactocentric distances beyond 12 kpc.

The mean angular momentum per unit mass of the cluster system and of the rest of the Galaxy is shown to be the same. The bearing of this on the origin of the cluster system is briefly discussed.

Introduction.—Recent analyses of the radial velocities of globular clusters have been based on Mayall's (**11**) velocities of 50 clusters. After correction for local solar motion, Mayall found a solar motion with respect to the cluster system of 175 ± 25 km/s from the mean of four solutions. He considered that this result was probably influenced by the absence of velocities for southern clusters and that the probable value for the solar motion was 200 ± 25 km/s. Since he found from other evidence (motions of the extragalactic nebulae and the Oort galactic rotation constants) that the Sun's galactic rotation velocity was 280–300 km/s, he suggested that the cluster system must have a rotational velocity of the order of 80–100 km/s. However, he was unable to find any satisfactory evidence for a differential or general rotation of the clusters from the peculiar velocities of the clusters themselves. Later, Parenago (**17**) and also Perek (**18**) claimed to have found differential rotation in the cluster system but Schmidt (**21**), using the same observations, has been unable to find any evidence for this, although (on the assumption of a solar galactic rotation of 216 km/s) he finds a mean rotational velocity of 80 km/s for the cluster system.

In the first paper in this series (**8**) radial velocities were given for 30 southern globular clusters, 10 of which had been observed previously. Radial velocities are thus available for 70 globular clusters (or roughly two-thirds of the total numbers of clusters known) and the effects of observational selection should be much reduced. It is therefore appropriate to attempt a fresh analysis to try to resolve the conflicting results found previously. In the first section we consider various solutions for the solar motion with respect to the cluster system as a whole, while in the second section the motion of different groups of clusters is discussed in an attempt to detect differential motion. In the third section the motions of the globular clusters are compared with those of some other high velocity galactic objects and the galactic orbits of the globular clusters are considered in a fourth section. In a fifth section an attempt is made to determine the mass of the Galaxy from globular cluster motions while the brief concluding section deals with the origin of the system of globular clusters.

1. *The solar motion of the system of globular clusters.*—We may use the radial velocities of the clusters to determine the motion of the clusters as a whole relative to the Sun. It is more useful, however, to refer the cluster motion to a coordinate system which has the same motion as the nearby stars. The heliocentric cluster radial velocities were therefore corrected for the local solar motion relative to these stars. The standard local solar motion of 20 km/s towards $\alpha = 18^h$ and $\delta = +30°$ is of sufficient accuracy because of the dispersion and accuracy of the cluster velocities. This corrected velocity V_c for a cluster with equatorial coordinates (α, δ) is related to the component cluster velocities X, Y and Z by

$$X \cos\alpha \cos\delta + Y \sin\alpha \cos\delta + Z \sin\delta = V_c \qquad (1)$$

where X, Y and Z are directed towards $(0^h, 0°)$, $(6^h, 0°)$ and $(+90°)$ respectively. 1950·0 coordinates have been used throughout. A least squares solution for the 70 clusters then gives the following solution:

$$X = -73 \pm 33 \text{ km/s};$$
$$Y = +93 \pm 22 \text{ km/s};$$
$$Z = -119 \pm 28 \text{ km/s}.$$

Unless otherwise stated, the errors quoted in this paper are r.m.s. errors. The total cluster motion (U) relative to the nearby stars is thus $(X^2 + Y^2 + Z^2)^{1/2}$ which equals 168 ± 27 km/s. The apex of this cluster motion is

$$\alpha = (21^h\,27^m) \pm (26^m); \quad \delta = (+45°\,08') \pm (6°\,08').$$

Converting to epoch 1900·0 and using the Lund galactic coordinate tables (**13**), which are of sufficient accuracy for this purpose, the galactic coordinates of the apex are:

$$l = 57°{\cdot}8 \pm 7°{\cdot}5; \quad b = -4°{\cdot}6 \pm 7°{\cdot}6.$$

The apex of cluster motion therefore shows no deviation from the direction in the galactic plane at right angles to the galactic centre ($l = 58°$, $b = 0°$) within the errors of the solution. No attempt has been made to weight the cluster velocities in this solution or later ones, since the errors in the component velocities are largely due to the actual dispersion in the cluster velocities rather than to observational errors. Mayall, in a similar solution for 50 clusters (**11**, p. 312, solution 6), found $U = 168 \pm 34$ km/s and $l = 51°{\cdot}3 \pm 10°{\cdot}1$, $b = +8°{\cdot}2 \pm 13°{\cdot}0$

for the apex (Harvard = Lund pole); Mayall's probable errors have been changed to r.m.s. errors for comparison purposes. *It is seen that an increase in the number of clusters together with a more uniform distribution over the sky has produced no change in the value of the solar motion although the errors are slightly reduced.* In all the following solutions we shall assume that the apex is in fact at right angles to the galactic centre and in the galactic plane ($l = 58°$, $b = 0°$). Let us also introduce a K term of motion of the clusters relative to the Sun. The equation of condition for a cluster with galactic coordinates (l, b) is then

$$U \cos A + K = V_c \qquad (2)$$

where $\cos A = \sin (l - 328°) \cos b$. A least squares solution for the 70 clusters then gives:

$$U = 172 \pm 31 \text{ km/s}; \quad K = -16 \pm 15 \text{ km/s}.$$

We find, in agreement with Mayall, that the K term relative to the Sun is of the same order as its error. It is therefore omitted in the next solution, leaving as the equation of condition

$$U \cos A = V_c \qquad (3)$$

for which the least squares solution is

$$U = 167 \pm 30 \text{ km/s}.$$

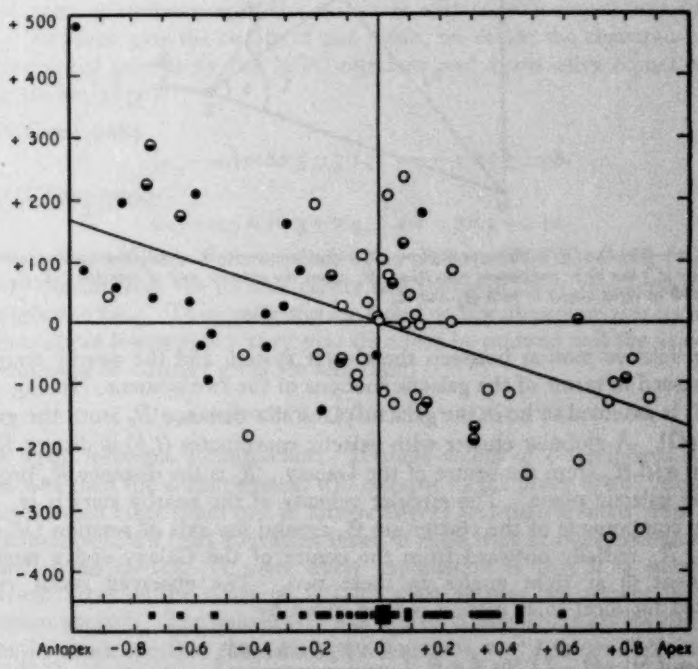

FIG. 1.—*The ordinate is the cluster radial velocity (corrected for local solar motion) in km/s and the abscissa is the cosine of the apical distance. New velocities are shown by filled circles and previously known velocities by open circles. Previously known velocities corrected by new observations are shown by half-filled circles. The solar motion solution $U = 167 = \pm 30$ km/s is shown by the line. The apical distances of clusters with unknown velocities are shown by the filled squares along the abscissa axis.*

Following Mayall (*loc. cit.*, Fig. 3), this solution may be represented as a straight line in Fig. 1 which is a plot of the cluster velocity against the cosine of the apical distance (A). Clusters with previously known velocities are shown by open circles, clusters with new Radcliffe velocities are shown by filled circles and clusters with both previously known and Radcliffe velocities are shown by half-filled circles. The apical distances of the 35 clusters in Miss Sawyer's catalogue (**20**) with unknown velocities are indicated along the abscissa axis: these are mainly faint clusters near the galactic centre and only a few have a sufficiently large apical distance to affect a solar motion solution.

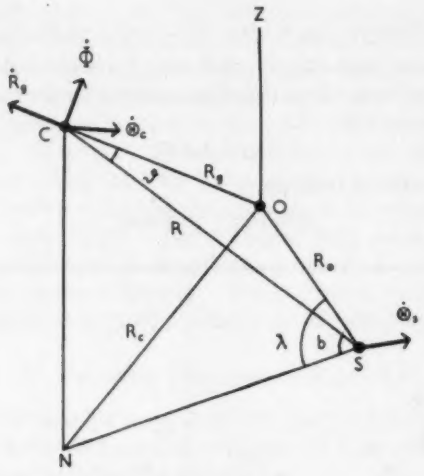

FIG. 2.—*The Sun (S) in the galactic plane has a circular velocity $\dot{\Theta}_s$ about the galactic centre (O). A cluster (C) has three component velocities: $\dot{\Theta}_c$ about the galactic axis of rotation OZ, $\dot{R}_g$ along OC and $\dot{\Phi}$ at right angles to both $\dot{\Theta}_c$ and $\dot{R}_g$.*

The relative motion between the cluster system and the nearby stars may be expressed in terms of the galactic motions of the two systems. In Fig. 2, the Sun (S) is assumed to be in the galactic plane at a distance R_0 from the galactic centre (O). A globular cluster with galactic coordinates (l, b) is distant R from the Sun and R_g from the centre of the Galaxy. R_c is the distance R_g projected onto the galactic plane. The circular velocity of the nearby stars is $\dot{\Theta}_s$. The velocity components of the cluster are $\dot{\Theta}_c$ around the axis of rotation OZ of the Galaxy, $\dot{R}_g$ radially outward from the centre of the Galaxy and a tangential component $\dot{\Phi}$ at right angles to these two. The observed radial velocity corrected for local solar motion is then given by

$$V_c = \left(\dot{\Theta}_s - \dot{\Theta}_c \frac{R_0}{R_c}\right) \cos A + \dot{R}_g \left(\frac{R - R_0 \cos\lambda \cos b}{R_g}\right) + \dot{\Phi} \frac{\sin b}{R_g} \left(R_c - \frac{R}{R_c}(R\cos b - R_0 \cos\lambda)\cos b\right) \qquad (4)$$

where $\cos A = \sin\lambda \cos b$ as before and $\lambda = l - l_0$, with $l_0 = 328°$.

It seems reasonable to assume that with a sufficiently large number of clusters, the tangential component $\dot{\Phi}$ will average zero and this term may therefore be omitted. We now see that equation (3) above implies that for all clusters:

(*a*) $\sum \dot{R}_g = 0$, i.e. that there is no expansion or contraction of the cluster system;

(*b*) $\dot{\Theta}_c(R_0/R_c) = \text{constant}$, i.e. that the cluster system rotates as a solid body with angular velocity $\omega_c = \dot{\Theta}_c/R_c$.

Equation (3) may thus be written as

$$V_c = R_0(\omega_s - \omega_c)\cos A, \tag{5}$$

where ω_s is the angular velocity of the nearby stars. On these assumptions and taking $R_0 = 8{\cdot}2$ kpc, the difference in angular velocity between the cluster system and the nearby stars is $20{\cdot}4 \pm 3{\cdot}7$ km/s kpc.

Let us now remove assumption (*a*) and assume that the cluster system expands so that $\dot{R}_g = \epsilon R_g$ where ϵ is constant. The equation of condition is then

$$V_c = (\omega_s - \omega_c)R_0 \cos A + \epsilon(R - R_0 \cos\lambda \cos b) \tag{6}$$

and a least squares solution for 70 clusters gives (in km/s kpc)

$$(\omega_s - \omega_c) = 20{\cdot}5 \pm 3{\cdot}6; \quad \epsilon = -1{\cdot}48 \pm 0{\cdot}85.$$

The velocity of contraction of the system is only slightly larger than its r.m.s. error. To investigate the reality of this result, we divide the clusters arbitrarily into two equal groups by the NGC numbers and again solve equation (*b*) to obtain (in km/s kpc)

NGC 104–6284

$$(\omega_s - \omega_c) = 20{\cdot}5 \pm 5{\cdot}1; \quad \epsilon = -1{\cdot}21 \pm 1{\cdot}08.$$

NGC 6293–7099

$$(\omega_s - \omega_c) = 16{\cdot}9 \pm 7{\cdot}4; \quad \epsilon = -2{\cdot}93 \pm 2{\cdot}12.$$

Both solutions indicate a contraction. The clusters NGC 2419 and NGC 7006 are very distant from the galactic centre and they will have considerable weight in the solution for ϵ. Their velocities are based on low dispersion spectra however and thus are of low weight; they may therefore be omitted and the solution for the remaining 68 clusters gives (in km/s kpc)

$$(\omega_s - \omega_c) = 20{\cdot}0 \pm 3{\cdot}8; \quad \epsilon = -1{\cdot}76 \pm 1{\cdot}12,$$

which again indicates a contraction. If these values of ϵ are indeed due to a contraction then the cluster system will collapse in the order of 10^9 years. This implies a much more rapid rate of kinetic energy loss than is likely from Spitzer and Schwarzschild's (**22**) relaxation times of such stars in their encounters with interstellar gas clouds. A more likely explanation is that it is caused by a systematic error of the order of 10 km/s such as may be present in the low dispersion spectra. The calcium H line which is blended with Hϵ has a large weight in these spectra. Its true wave-length is 0·35 A bluer for clusters of late integrated type than for those of early type (Paper I (**8**), Table VI), which corresponds to a velocity difference of 25 km/s. No allowance for this effect is mentioned in Mayall's paper; if a mean wave-length was in fact used for all clusters, then the clusters of late type will show a spurious velocity of recession and those of early type will show a spurious velocity of approach. Since the

late type clusters occur predominantly near the galactic centre (Paper II (**9**)), this will produce a spurious contraction of the whole system. Ten clusters of early type observed by Mayall do show a mean velocity of approach of 4 ± 8 km/s compared with the Radcliffe observations (Paper I (**8**)), but since none of these Mayall velocities is wholly based on low dispersion spectra, the effect may be reduced in this case.

It is thus concluded that the observed contraction of the cluster system could be produced by systematic errors in the velocities such as could be produced by errors in the standard wavelengths in the low dispersion spectra. Only the first term on the r.h.s. in equations (4) and (6) will therefore be retained in future solutions.

2. *Differential motion in the system of globular clusters.*—In the previous section it was assumed that the cluster system rotates as a solid body; the linear rotational velocity $\dot{\Theta}_c$ of a cluster is thus proportional to its distance (R_c) from the galactic axis of rotation. In the simple case of circular orbits about a central point mass, this circular velocity should be inversely proportional to the square root of the radius of the orbit. We should therefore expect $\dot{\Theta}_c$ to decrease with galactocentric distance. Since, however, the eccentricity and major axes of the cluster orbits are unknown and the central point mass approximation is only valid for the clusters which are most distant from the galactic centre, it is inadvisable (as Schmidt (**21**) points out) to try to fit the observed velocities to an analytical form. We therefore proceed empirically and divide the cluster system into two groups, each rotating as a solid body: 51 clusters for which the projected galactocentric distance $R_c < 9$ kpc and 19 clusters for which $R_c > 9$ kpc, and solve equations (3) or (5) for both groups. The division at 9 kpc was chosen to give both solutions nearly equal weight; many more clusters were therefore needed in the first group because $\cos A$ is small for clusters near the galactic centre. The solution of equation (5), assuming $R_0 = 8{\cdot}2$ kpc, gives the following differences in angular velocity between the two groups of clusters and the nearby stars:

$R_c < 9$ kpc	$R_c > 9$ kpc
$(\omega_s - \omega_c) = 18{\cdot}2 \pm 5{\cdot}0$ km/s kpc	$(\omega_s - \omega_c) = 22{\cdot}4 \pm 6{\cdot}2$ km/s kpc

while the difference in linear rotational velocity $U = (\dot{\Theta}_s - \dot{\Theta}_c R_0/R_c)$ found from equation (3) is:

$R_c < 9$ kpc	$R_c > 9$ kpc
$U = 149 \pm 41$ km/s	$U = 183 \pm 51$ km/s

The difference in U between the two groups is thus 34 ± 65 km/s. Although the difference in rotational motion between the two groups is in the expected sense, i.e. the outer group have the larger solar motion and thus rotate more slowly, the errors of the solution are too large for the result to be statistically significant. There seems little point in attempting further solutions with a finer subdivision of R_c, partly because of the uncertainties in the values of R_c and partly because decreasing the number of clusters in each group would increase the already large errors in the solution for each group. We conclude that, although differential motion is very likely to exist, the errors produced by the peculiar motions of the clusters preclude its detection.

In Paper II (9) it was shown that the galactic distribution of the globular clusters depends on their integrated spectral type; those of earliest type have an extended spherical distribution and those of latest type have a distribution which is flattened to the galactic plane. In this case, we might expect on dynamical grounds that the clusters of later type should have a larger rotational velocity and hence smaller solar motion than those of earlier type. To test this, the clusters were divided into two groups according to their spectral type: Group I consisting of 17 clusters of spectral type G5–Go and Group II consisting of 46 clusters of spectral type F9–F2. The division was made to give the largest difference in spatial distribution between the two groups. Least squares solutions for U and $(\omega_s - \omega_c)$ on the assumption $R_0 = 8{\cdot}2$ kpc then give:

	Group I G5–Go	Group II F9–F2
$(\omega_s - \omega_c)$	$9{\cdot}8 \pm 10{\cdot}0$ km/s kpc	$19{\cdot}8 \pm 4{\cdot}4$ km/s kpc
U	80 ± 82 km/s	162 ± 36 km/s

The difference in U between the two groups $= 82 \pm 90$ km/s. It is seen that the difference in the solar motions of the two groups is in the expected sense, i.e. the groups of later spectral type have the smaller solar motion and hence the larger galactic rotation, but again the errors of the solution are too large for the result to have statistical significance. The large errors in the solution for Group I are caused by the majority of the clusters of this group lying near the galactic centre and so having small values of $\cos A$. Thus while differential motions of the kind indicated between clusters of different spectral type are very likely to exist, they are largely masked by the errors introduced by the peculiar motions of the clusters.

3. *A comparison of the solar motion of globular clusters with other galactic objects.*—Large radial velocities are found for several other classes of galactic objects besides the globular clusters and together with the globular clusters these form the galactic halo. However it is necessary to restrict the discussion to such classes of objects which may be distinguished as belonging to the halo by some physical parameter (such as spectrum or light variation) other than high velocity. Clearly, the analysis of the velocities of a group of objects selected on the grounds of high velocity will yield a spurious solar motion. In this section we shall therefore deal only with the RR Lyrae stars and, rather briefly, with the subdwarfs.

3.1. *The RR Lyrae stars.*—Oort (14) analysed the radial velocities of 67 RR Lyrae stars and found a solar motion of 130 ± 21 km/s towards $l = 53° \pm 12°$, $b = +12° \pm 12°$. Since then velocities of more of these stars have become available so that a new analysis is possible. This was made for 129 stars whose velocities are either given in Wilson's General Catalogue (27) or by Joy (7) and assuming an apex of $l = 58°$, $b = 0°$. After correction for local solar motion, this gave a solar motion U of 134 ± 20 km/s. It was noticed by Struve (24) that the solar motion of the RR Lyrae stars increases with increasing period but he failed to discriminate between variables of the Bailey types *ab* and *c*. Such discrimination must be made, however, since the variables of Bailey type *c* of period 0·3–0·4 days are known to be associated in clusters with those of type *ab* of period 0·5–0·6 days. In the present analysis, the 129 RR Lyrae stars were divided into five groups according to period and Bailey type and for which the following solar motions (U) were found:

Bailey type	Period range	Mean period	U	No. of stars
c	$0^d.25 - 0^d.35$	$0^d.296$	89 ± 29 km/s	14
ab	$0^d.20 < P < 0^d.40$	$0^d.369$	30 ± 27	11
ab	$0^d.40 < P < 0^d.50$	$0^d.460$	105 ± 29	37
ab	$0^d.50 < P < 0^d.60$	$0^d.548$	167 ± 30	46
ab	$0^d.60 < P < 0^d.75$	$0^d.666$	205 ± 45	21

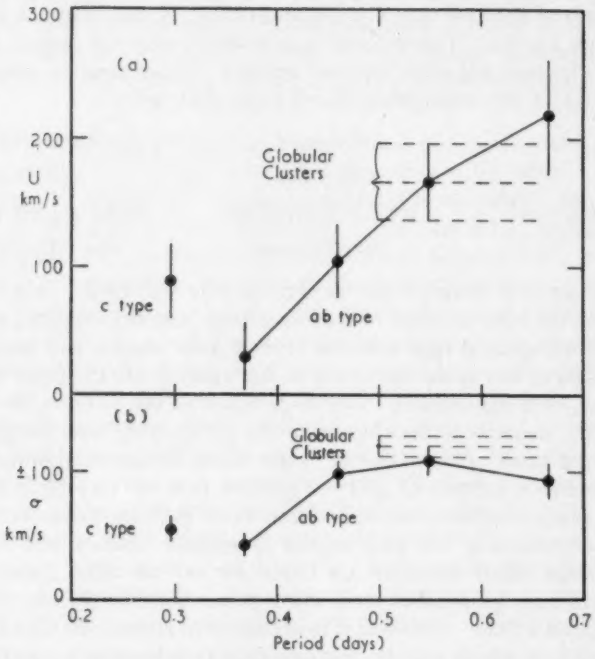

FIG. 3.—*(a) Solar motion (U) in km/s of field RR Lyrae stars as a function of their period in days. (b) r.m.s. random sight-line velocity (σ) in km/s after removal of solar motion component for field RR Lyrae stars as function of their period in days. The corresponding quantities for globular clusters are also shown.*

These results are also given in Fig. 3*a*, which shows the marked increase of the solar motion with increasing period. The mean periods of the *ab* type variables in different globular clusters lie roughly in the range $0^d.50$–$0^d.65$ (see Fig. 4*a*). It is seen that the solar motion of the RR Lyrae stars of this period range corresponds closely to that found for the globular clusters (167 ± 30 km/s). Furthermore, the r.m.s. random sight-line velocity (σ) after removal of the solar motion is also the same within the quoted errors (Fig. 3*b*) for the field RR Lyrae stars of the period range $0^d.50$–$0^d.65$ as for the globular clusters.

There is therefore reason to believe that the RR Lyrae stars of a given period have essentially similar galactic motions whether they occur in globular clusters or in the general field. This is contrary to the findings of Oort (*loc. cit.*) who found a significant difference between the solar motions of the globular clusters and the RR Lyrae stars of *all* periods and therefore concluded that the field RR Lyrae

stars could not have escaped from the clusters. The present results however support a common origin for RR Lyrae stars of a given period and Bailey type in both clusters and the general field. Either the field variables result from the disruption of globular clusters or, more generally, their presumed origin from the interstellar medium occurred at the same epoch as for the clusters and with the same galactic distribution.

These results suggest that the globular clusters whose RR Lyrae variables of type *ab* have the longest mean periods may be expected to have the greatest solar motion. They will therefore have a nearly spherical galactic distribution and a large mean distance ($|Z|$) from the plane; hence, according to Section 4.1 of Paper II they will have the earliest spectral type. It was shown in Section 4.2 of Paper II that the few available observations tend to confirm this.

In the previous section, we were unable to demonstrate convincingly that a difference in solar motions does exist between clusters of different spectral types: this was due to the small number of clusters available and their unfavourable distribution in the sky for solar motion solutions. While it is unlikely that the number of spectroscopically observable clusters can be greatly increased in the near future, this is not the case with the RR Lyrae variables. Moreover, their distribution in the sky for a solar motion solution is relatively more favourable on account of their greater spatial density near the Sun. We must aim therefore to improve the solar motion of the field RR Lyrae stars of *longest* period and this should prove the best method of obtaining a lower limit to the Sun's galactic rotation velocity.

Fig. 4*a* shows the period–frequency function for the type *ab* RR Lyrae stars in globular clusters (taken from Sawyer's catalogue (**20**)). The same function is shown in Fig. 4*b* for the type *ab* variables with galactic latitude $b < \pm 30°$ (taken from the *General Catalogue of Variable Stars* (**4**) but omitting those due to Gaposchkin (**3**) at the galactic centre). It is seen that variables with periods less than $0^d{\cdot}45$ are much more numerous in the latter group which lie near the galactic plane; this is in accord with the small solar motion of this group (cf. van den Bergh (**25**), Oosterhoff (**16**) and Kukarkin (**10**)).

It is possible that variables with periods $\sim 0^d{\cdot}45$ and less may occur in globular clusters of late integrated spectral type (G3–5) which lie close to the galactic plane. Variables have been found in those clusters of this type which have been searched (NGC 104, 6356, 6712 and 6833 (**20**)) but as yet no periods have been published. Relatively few of such clusters are available for searching: no doubt some are not observed because of obscuration. It is also possible that such clusters were more numerous in the past but, lying near the plane, they have been broken up by the tidal action of interstellar clouds: a mechanism which has been discussed by Spitzer (**23**) to account for the scarcity of "galactic" clusters with ages $> 10^9$ years.

3.2. *The subdwarfs.*—Fricke (**2**) has analysed the radial velocities of 78 subdwarfs and has found a solar motion of 148 ± 28 km/s towards $l = 75° \pm 8°$ and $b = -2° \pm 9°$. Apart from an unexplained deviation of the apex in longitude, this is similar to the solar motion found for *all* the RR Lyrae stars taken together. It seems likely that, as in the case of the RR Lyrae stars, we are dealing with a mixture of different kinds of stars; indeed it is reported (**5**) that Greenstein has found that the space velocity dispersion in the subdwarfs depends on their metal line weakening: the stars with the weakest lines having the greatest velocity

dispersion and hence presumably the greatest $|Z|$. This is in qualitative agreement with what was found for the globular clusters in Paper II: the clusters with the weakest metal lines (earliest integrated spectral type) have the greatest $|Z|$. By analogy with the RR Lyrae stars we might expect that globular clusters containing subdwarfs with a given line weakening (or metal/hydrogen ratio) will have the same galactic motions and hence presumably the same origin as subdwarfs of the same physical characteristics in the general field. The same should also hold for all the constituent stars of globular clusters although, apart from the RR Lyrae stars and subdwarfs, it may not be so easy to identify the field stars with the same physical characteristics as their counterparts within clusters. In some cases it is possible that groups of the field stars having the same origin as globular clusters may retain a loose dynamical association by which they could be identified: they would thus exist as a very loose cluster. It is interesting to note in this connection that Eggen* has recently found that RR Lyrae itself is a member of a group of stars with a common motion.

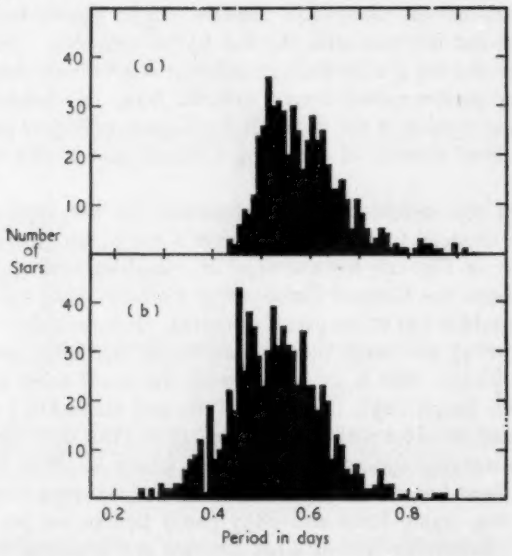

FIG. 4.—*Frequency of occurrence of RR Lyrae variables of Bailey type ab as a function of period*
(a) in globular clusters
(b) in the general field for $|b| < 30°$.

4. *The galactic orbits of the globular clusters.*—The eccentricities of the cluster orbits have been discussed by von Hoerner (**26**) and Perek (**19**) on the basis of Mayall's velocities. Contrary to an earlier discussion by Edmondson (**1**), using only 26 clusters, they both conclude that the cluster orbits are highly eccentric. Von Hoerner considers the ratio u_0 between the radial velocity of a cluster (u) (corrected for the Sun's galactic rotation and for local solar motion) to the circular velocity at the cluster. He assumes a point mass for the Galaxy at the galactic centre such that the circular velocity at the Sun is 260 km/s and

* I am grateful to Dr Eggen for giving me this information in advance of publication.

R_0 is taken as 9 kpc; in this case $u_0 = u\sqrt{(R_g)/780}$, where R_g is the distance from the galactic centre to the cluster. If ϑ is the angle subtended at the cluster by the Sun and the galactic centre (see Fig. 2), then in order that a globular cluster should not escape from the Galaxy:

for circular orbits, $u_0 < \sin\vartheta$;

for straight line orbits through the galactic centre, $u_0 < \sqrt{2}\cos\vartheta$;

for elliptical orbits, $u_0 < \sqrt{2}$,

since the escape velocity on this model equals $\sqrt{2}$ times the circular velocity. Von Hoerner excludes clusters nearer to the centre than 6 kpc so that the point-mass model of the Galaxy may be approximately valid; he then finds, with only two exceptions, that $u_0 < \sqrt{2}.\cos\vartheta$ so that the orbits must be highly eccentric.

Apart from the approximate nature of the point-mass assumption, the distances of the globular clusters are poorly determined (Paper I (8), Table VIII): probable errors of the order of 30–50 per cent being common. These errors will therefore introduce considerable uncertainty in the calculated values of ϑ, particularly for clusters near the galactic centre, while, since u_0 depends upon $\sqrt{R_g}$, this will also be affected but to a lesser degree. Von Hoerner's calculations have been repeated assuming $R_0 = 8{\cdot}2$ kpc and $\dot{\Theta}_g = 216$ km/s, so that

$$u_0 = \frac{u\sqrt{R_g}}{619};$$

clusters with $R_g < 6$ kpc have again been omitted.

The results are shown in Fig. 5 in which u_0 is the ordinate and ϑ is the abscissa; the scatter of points again favours the highly eccentric as opposed to circular orbits. The horizontal lines indicate probable errors in ϑ for selected clusters determined from the probable errors in the distances alone (Paper I (8), Table VIII), while the vertical lines indicate probable errors in u_0 determined from the probable errors in the distances and radial velocities alone.

The only cluster which appears to be necessarily escaping from the Galaxy is NGC 5694; the distance of this cluster is very uncertain however, and its velocity is based only upon low dispersion spectra so that this result must be treated with reserve. NGC 3201, whose velocity and distance are relatively well-determined, deserves special mention. It is situated 11° from the solar antapex of galactic motion and has the large velocity of recession (corrected for local solar motion) of 481 km/s. It therefore appears that for any reasonable value of the circular velocity of the nearby stars this cluster must have a *retrograde orbit*.

The accuracy of this analysis is clearly not high but does show that the values $\dot{\Theta}_g = 216$ km/s and $R_0 = 8{\cdot}2$ kpc are at least compatible with few if any of the clusters having velocities in excess of the velocity of escape and the majority having highly eccentric orbits. One would not expect to find clusters with velocities in excess of the escape velocity. As remarked earlier, there is probably little energy exchange between the clusters and the rest of the Galaxy; hence if, as is thought, the cluster ages $\sim > 10^9$ years, any cluster whose original velocity was excessive would have escaped long ago.

Schmidt (21) has pointed out that many highly elongated orbits would be expected *a priori* since the dispersion in the cluster velocities is of the same order as the circular velocities. Let us take a very simplified model in which a cluster

describes an elliptic orbit of semi-major axis a and eccentricity e around a point mass M. If p is its constant angular momentum per unit mass, then we have:

$$e = \sqrt{\left(\frac{2(1-\lambda)}{\lambda+2}\right)} \quad \text{where} \quad \lambda = \frac{p^2}{GM\bar{R}}.$$

Here $\bar{R}$ is the time averaged mean radial distance of the cluster from the mass M, and taking the mean value of $R_\odot$ for all the clusters may be put as 11·8 kpc. Since the orbits may be inclined at random to the galactic plane, we put p equal to $\sqrt{2}.\dot{\Theta}_c.R_\odot$, where $\dot{\Theta}_c$ is the linear rotational velocity about the galactic axis of rotation. We have found that

$$\left(\dot{\Theta}_\odot - \dot{\Theta}_c \frac{R_0}{R_c}\right) = 167 \text{ km/s}$$

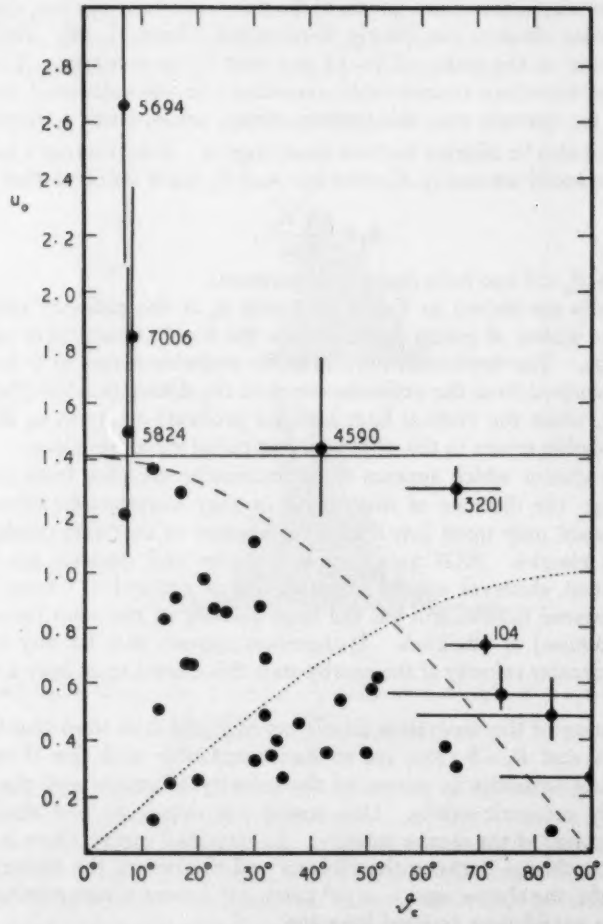

FIG. 5.—*The ordinate (u_ϑ) is the ratio of the cluster radial velocity after removal of the component due to the Sun's galactic rotation, divided by the circular velocity at the cluster. The abscissa (ϑ) is the angle subtended at the cluster by the Sun and the galactic centre.*
The solid horizontal line at $u_\vartheta = \sqrt{2}$ is the limit for elliptical orbits.
The dotted line ($u_\vartheta = \sin\vartheta$) is the limit for circular orbits.
The dashed line ($u_\vartheta = \sqrt{2}.\cos\vartheta$) is the limit for straight-line orbits.

and so assuming $\dot{\Theta}_g = 216$ km/s, $R_0 = 8{\cdot}2$ kpc and $R_c = 11{\cdot}5$ kpc (which is the mean value weighted according to $\cos A$), we have $\dot{\Theta}_c = 69$ km/s. The quantity GM is equal to $\dot{\Theta}_g^2 R_0$ and hence we find that the eccentricity equals 0·8, i.e. the orbits are highly eccentric.

It is interesting to note that Newkirk (**12**) also finds highly eccentric orbits for the field RR Lyrae stars: out of 50 stars discussed on the basis of proper motions and radial velocities, only 12 were found to have eccentricities less than 0·6. This lends further support to a common origin for the field RR Lyrae stars and the globular clusters.

5. *The mass of the Galaxy from globular cluster motions.*—Consider a cluster moving in a Keplerian orbit of eccentricity e and semi-major axis a about a point mass galaxy of mass M. The perimeter of this orbit is

$$2\pi a\left(1-\frac{e^2}{4}-\frac{3}{64}e^4-\frac{5}{256}e^6-\ldots\right)$$

while the period is $2\pi a^{3/2}/\sqrt{(GM)}$. The time averaged mean galactocentric distance of a cluster ($\bar{R}_g$) equals $a(1+\frac{1}{2}e^2)$, so that the mean square velocity of the cluster in its orbit (v^2) is

$$\frac{GM}{\bar{R}_g}(1+\tfrac{1}{2}e^2)\left(1-e^2-\frac{3}{64}e^4-\frac{5}{256}e^6-\ldots\right)^2.$$

The coefficient containing e is unity for a circular orbit, 0·88 for $e = 0{\cdot}8$ and 0·61 for a straight line orbit; following the conclusions of the last section we shall take the coefficient 0·88.

Since only the radial velocity and not the space motion of the clusters are known, the mean square velocity has been deduced on two assumptions. If v is the residual radial velocity of a cluster after removing local solar motion and a solar galactic motion of 216 km/s, we assume either:

(1) the peculiar motions of the cluster are random so that

$$v^2 = \frac{\sum_n 3v^2}{n}$$

for a group of n clusters;

(2) the peculiar motions are along the line through the cluster passing through the galactic centre which makes an angle ϑ with the line joining the cluster to the Sun. In this case, weighting according to $\cos\vartheta$ and omitting clusters with $\cos\vartheta < 0{\cdot}3$,

$$v^2 = \frac{\sum_n \frac{v^2}{\cos^2\vartheta}\cdot\cos\vartheta}{\sum_n \cos\vartheta}$$

for a group of n clusters.

In order to consider approximately homogeneous groups, the clusters were divided into 4 groups according to spectral type: G5–G3, G2–G0, F9–F6 and F5–F2. The results are shown in Fig. 6, in which the mass calculated on the two assumptions is plotted against $\bar{R}_g$. The open circles are for assumption (1) (random motion) and the filled circles are for assumption (2) (straight line motion). The increase in M as the mean galactocentric distance of the group increases is

likely to be due to the greater part of the galactic mass encompassed by the clusters with greater $\bar{R}_g$. For comparison, the solid curve gives the mass of the Galaxy within a distance R_g of the centre computed from Schmidt's model (**21**, Table 5).

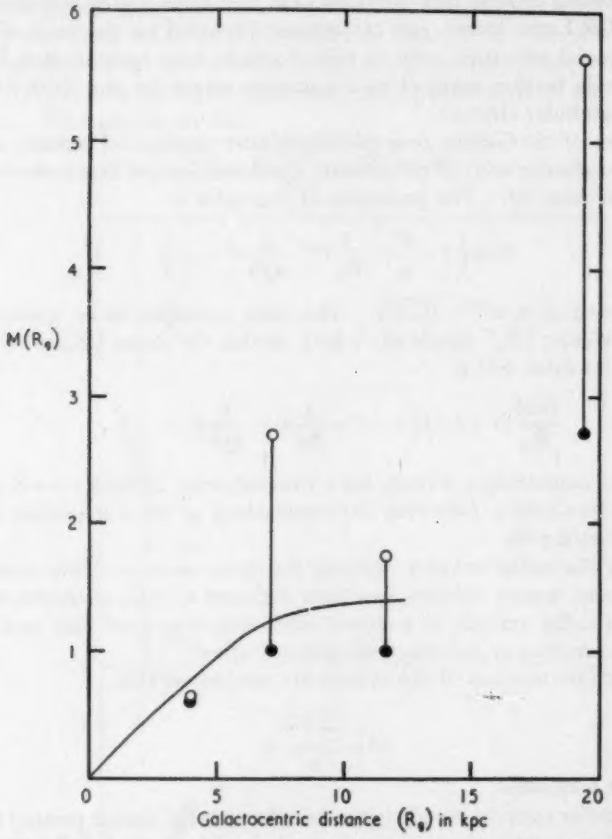

FIG. 6.—*The galactic Mass $M(R_g)$ within a galactocentric distance R_g (in units of 10^{44} gm) as a function of R_g.*

The smooth curve from Schmidt's model

The filled circles are masses deduced assuming that the clusters have straight line orbits through the galactic centre.

The open circles are found on the assumption of randomly oriented orbits.

Within the range of Schmidt's model ($0 < R_g < 12{\cdot}3$ kpc) the agreement is satisfactory considering the approximate nature of the present analysis and suggests that straight line orbits are a better approximation than random motions. The same solar circular velocity (216 km/s) is however used in both Schmidt's model and the present analysis and so the two results are not completely independent. The presence of a substantial galactic density for $R_g > 12$ kpc suggested by the group of twenty clusters with spectral type F5–F2 on either assumption is surprising. Whilst it is difficult to assess just how trustworthy

this result may be, in view of the very simple model which has been used and also the uncertainties in the cluster distances and the solar circular velocity, it is suggested that it should be treated with reserve.

6. *The origin of the globular clusters.*—We can find the *mean* angular momentum per unit mass of the cluster system ($\bar{p}_c$) about the axis of galactic rotation since this equals the product of the mean linear rotational velocity ($\bar{\Theta}_c$) and the mean galactocentric distance projected onto the galactic plane ($\bar{R}_c$) of the clusters. Using values of $\bar{\Theta}_c$ and $\bar{R}_c$ which are given in Section 4, we have

$$\bar{p}_c = 794 \text{ km/s kpc.}$$

We may also find the corresponding quantity for the rest of the Galaxy ($\bar{p}_g$) using Schmidt's model (**21**). The angular momentum of an annular zone of the Galaxy of mass $m(r)$, circular velocity $\Theta(r)$ and radius r is $r \cdot m(r) \cdot \Theta(r)$, so that the mean angular momentum per unit mass is

$$\bar{p}_g = \frac{\sum r \cdot m(r) \cdot \Theta(r)}{\sum m(r)} = 800 \text{ km/s kpc.}$$

The agreement between $\bar{p}_g$ and $\bar{p}_c$ is very striking; it is better than could have been expected from the limited accuracy of the data available although it may be noted that the same solar circular velocity (216 km/s) has been used to find both $\bar{p}_g$ and $\bar{p}_c$ and that an error in this velocity will produce an error in both $\bar{p}_g$ and $\bar{p}_c$ in the same sense.

Thus, although the galactic distribution of the cluster system differs markedly from that of the disk population (which largely determines $\bar{p}_g$), the mean angular momentum per unit mass of the two systems is the same and this must also have been true of the media from which these systems were formed. It seems likely therefore that the clusters were formed from representative samples of the same medium as the rest of the Galaxy. This lends some support to the proposal (cf. Oort (**15**)) that the Galaxy originated in a large turbulent gas cloud. This cloud contracted as the turbulent velocities decayed and, since angular momentum was conserved, formed the present rotating disk of gas and stars. The globular clusters are considered to have been formed from the gas when its distribution was still nearly spherical and since little energy exchange can have taken place between the clusters and the rest of the Galaxy since then (see Section 1), their present distribution and motion must reflect that of the original gaseous cloud at the time of their formation. It has been shown (Paper II) that the clusters with the most extended and spherical galactic distribution have the earliest spectral type and hence a lower metal/hydrogen ratio than clusters with a less extended and flatter distribution. One possibility is that the clusters with low metal content were formed first when the primordial gas was most extended and the clusters with higher metal content later when the cloud had contracted and flattened somewhat. In this case, the metal content of the Galaxy must have increased with time—possibly by a mechanism such as that considered by Hoyle (**6**). Alternatively, the clusters may have been formed nearly simultaneously but the metals (perhaps in the form of dust) may have contracted to the plane more rapidly than the gas. This latter alternative might be rejected if it could be shown conclusively that the interaction between gas and dust were sufficient for no separation to be possible in the time required for the gas to contract to the plane.

To summarize:

The cluster system shows a solar motion of 167 ± 30 km/s with no deviation of the apex. Differential motion in the cluster system is expected from differences in galactic distribution of clusters of different spectral types; it has not been possible to confirm this from the radial velocities because the small samples of clusters available, their unfavourable galactic distribution and large peculiar motions produce large errors in the solutions.

Field RR Lyrae stars of the same period range as those occurring in globular clusters have the same solar motion and velocity dispersion as the clusters; it is suggested that these stars and the clusters have a common origin.

It is confirmed that the clusters probably have highly eccentric orbits as is expected from the low galactic rotation of the cluster system. An attempt to find the distribution of galactic mass from the peculiar motions of the clusters gives results which are, in general, consistent with Schmidt's model within their limited accuracy.

The mean angular momentum per unit mass of the cluster system is the same as the mean for the rest of the Galaxy. This is in accord with the hypothesis that the clusters were formed in a spherical gas cloud which was in the process of contracting to form the galactic disk.

Unfortunately, it is unlikely that the number of cluster radial velocities can be greatly increased in the near future and hence any improvement made in the present solar motion solution. As was pointed out in Section 3, however, the number of radial velocities of RR Lyrae stars of long period ($> 0^d.6$) may be increased (particularly if new stars are discovered) and these should give a solar motion which is a better approximation to the Sun's galactic circular velocity. A radial velocity programme which includes such stars in the Southern Hemisphere is at present being undertaken at the Radcliffe Observatory.

Acknowledgments.—I am very grateful to the Radcliffe Observer (Dr A. D. Thackeray) for his encouragement and advice in writing this paper and also to Dr A. J. Wesselink for some helpful discussions. This work was carried out partly with the aid of a Radcliffe Travelling Fellowship and partly with the aid of a grant by the Department of Scientific and Industrial Research to the Radcliffe Trustees.

Radcliffe Observatory,
Pretoria:
1959 *March*

References

(1) F. K. Edmondson, *A.J.*, **45**, 1, 1935.
(2) W. Fricke, *A.N.*, **278**, 121, 1950.
(3) S. Gaposchkin, *Var. Stars*, **10**, 337, 1956.
(4) *General Catalogue of Variable Stars*, B. V. Kukarkin, P. P. Parenago, Yu. I. Efremov and P. N. Khopolov, Moscow, 1958.
(5) J. L. Greenstein, reported in *Trans. I. A. U.*, **9**, 394, 1955.
(6) F. Hoyle, *Pont. Acad. Sci. Scripta Varia*, **16**, 279, 1958.
(7) A. H. Joy, *P.A.S.P.*, **67**, 420, 1955.
(8) T. D. Kinman, *M.N.*, **119**, 157, 1959 (Paper I).
(9) T. D. Kinman, *M.N.*, **119**, 538, 1959 (Paper II).
(10) B. V. Kukarkin, reported in *Trans. I.A.U.*, **8**, 502, 1952.
(11) N. U. Mayall, *Ap. J.*, **104**, 290, 1946.
(12) J. M. Newkirk, *H.B.*, **921**, 15, 1952.

(13) J. Ohlsson, *Ann. Obs. Lund.*, **3**, 1932.
(14) J. H. Oort, *B.A.N.*, **8**, 337, 1939.
(15) J. H. Oort, *Pon. Acad. Sci. Scripta Varia*, **16**, 415, 1958.
(16) P. Th. Oosterhoff, reported in *Trans. I.A.U.*, **8**, 502, 1952.
(17) P. P. Parenago, *A.J.* (U.S.S.R.), **24**, 167, 1947.
(18) L. Perek, *Ann. d'Ap.*, **11**, 185, 1948.
(19) L. Perek, *Contr. Ast. Inst. Masaryk Univ.*, **1**, No. 12, 1954.
(20) H. B. Sawyer, *Publ. David Dunlap Obs.*, II, 35, 1955.
(21) M. Schmidt, *B.A.N.*, **13**, 15, 1956.
(22) L. Spitzer, Jnr. and M. Schwarzschild, *Ap. J.*, **114**, 385, 1952.
(23) L. Spitzer, Jnr., *Ap. J.*, **127**, 17, 1958.
(24) O. Struve, *P.A.S.P.*, **62**, 217, 1950.
(25) S. van der Bergh, *A.J.*, **62**, 334, 1957.
(26) S. von Hoerner, *Zs. f. Ap.*, **35**, 255, 1955.
(27) R. E. Wilson, *General Catalogue of Stellar Radial Velocities*, Carnegie Inst. Washington, 1953.

Note added in proof.—Two RR Lyrae stars have been identified (A. D. Thackeray, A. J. Wesselink and M. W. Feast (*M.N.*, in press)) as belonging to NGC 104 (47 Tuc) which has an integrated spectral type G3; one of type *ab* has a period 0·74 days and the other of type *c* a period of 0·37 days. Although this is a small sample, the discovery of such long periods in a cluster of late integrated type weakens the correlation between period and integrated spectral type discussed here and in Paper II.

SOME FORMULAE CONNECTING HARVARD x AND y EQUATORIAL COORDINATES AND STANDARD COORDINATES FOR THE MAGELLANIC CLOUDS

A. J. Wesselink
(Communicated by the Radcliffe Observer)

(Received 1959 March 2)

Summary

The paper deals with the essentially practical problem of identification of stars in the Magellanic Clouds. Formulae are given which convert Harvard x and y equatorial coordinates and standard coordinates into each other. Their use for the identification of objects and for the ruling of prints is described. In order to simplify the vast amount of future work that is likely to be concerned with the Magellanic Clouds, the advantages of the systems of standard coordinates in preference to the Harvard x, y systems are pointed out.

Notation and definition

x, y: the rectangular coordinates introduced by the Harvard Observatory in *H.A.*, **60**, IV. Each Magellanic Cloud has its own system. In the first instance a system is defined by a negative of the corresponding Magellanic Cloud on which the square net of a reticule has been photographed. The original plates were taken with the 24 inch Bruce Telescope at the former Harvard Station at Arequipa, Peru, and are of size 14×17 inches. The reproductions published in *H.A.*, **60**, IV are about half this size.

α, δ: equatorial coordinates referred to 1875·0. The epoch 1875·0 was chosen as this is the epoch of the CPD and the AGC. In the derivation of the formulae AGC positions have been used. For future application and use, the CPD positions seem to be the most useful.

α_0, δ_0: the equatorial coordinates of the centres of the Harvard plates as used in the present investigation. The coordinates differ slightly from the centres published in *H.A.*, **60** and are rounded off values of the latter. We have (again for 1875·0)

Small Magellanic Cloud	Large Magellanic Cloud
$\alpha_0 = 0^h50^m00^s{\cdot}0$	$\alpha_0 = 5^h26^m00^s{\cdot}0$
$\delta_0 = -73^\circ15'00''$	$\delta_0 = -69^\circ00'00''$

$$\Delta\alpha = \alpha - \alpha_0.$$

Standard coordinates.—The standard coordinates as used here comply with the definition in general use. The origin of the coordinates are the positions α_0, δ_0 as given above. ξ and η are expressed in seconds of arc. The η-axis is directed towards the pole of 1875·0.

The problem of identification.—There are essentially two methods of identifying celestial objects. In the one method, charts are used showing the object

and the stars in its immediate neighbourhood. This method is usually quite satisfactory but when many objects, widely spread over a large area of the sky, have to be identified and when moreover the background is crowded, many separate charts are required. The other method is followed by the Harvard Observatory in the Magellanic Clouds. It defines the relevant object by its rectangular coordinates x and y (see above). There is little doubt that the method works quite satisfactorily both in assigning x and y to a new object, and in finding the star when x and y are given, when the original plates, with the imprinted mesh system, are at hand. However, practice shows that the investigator who has no access to these original plates is confronted with almost insuperable difficulties in the same problem. For this problem, then, the investigator could until now make use of: (1) the two published reproductions of both clouds as given in *H.A.*, **60**; (2) Tables I and III, also of *H.A.*, **60**; and (3) the HDE which gives for a large number of CPD stars Harvard x and y in the LMC.

Though the reproductions mentioned above show the reticule lines clearly, they are useful only for the identification of the brighter objects in the least crowded areas.

The use of Tables I and III of *H.A.*, **60**, for the identification on photographs obtained with large telescopes by interpolation, fails on account of the small number of these standard stars available on the same photograph.

The HDE can be used in identifying LMC objects by interpolation between the CPD stars with known coordinates x and y. But this cannot be done in the SMC and in those regions of the LMC which are outside the HDE.

The formulae presented in the present paper in Tables I and II permit (among other things) the calculation of Harvard x and y from equatorial coordinates and vice versa for any object for which the one set of data is known. Since reproductions of photographs obtained with even the larger telescopes usually contain a sufficient number of CPD stars, it is now easy to rule these prints in x and y. In this way it has been found possible to identify objects given by their x and y in any part of the Clouds.

Derivation of formulae.—For 28 AGC stars near the Small Magellanic Cloud, Harvard coordinates x and y are given in Table I, p. 89, of *H.A.*, **60**. The table contains, though in an implicit manner, the most accurate definition of the x, y system of the SMC available.

Standard coordinates were calculated for the 28 stars mentioned above, using the 1875·0 positions as given by the AGC.

Then least square solutions were made of the following form:—

$$a_1\xi + b_1\eta + c_1 = x - \xi$$
$$a_2\xi + b_2\eta + c_2 = y - \eta$$
$$a_3x + b_3y + c_3 = x - \xi$$
$$a_4x + b_4y + c_4 = y - \eta.$$

The results are presented as formulae (5), (6), (7) and (8) in Table I of the present paper. As a further check formulae (7) and (8) were derived from (5) and (6) by transformation.

In the course of this work it was found that the data of *H.A.* **60** (Table I, p. 89) were discordant for the stars AGC 193 and 1449. They were excluded from the solutions. In a similar manner, the data given in Table III (p. 98) for 21 AGC

stars near the Large Magellanic Cloud were treated. The results of the computations will be found as formulae (5), (6), (7) and (8) in Table II of the present paper. As in the case of the SMC the results for the LMC were further checked by transformation.

The discordant star AGC 6746 was excluded from the solutions.

The residuals in the various solutions for both the SMC and the LMC are of the same order of magnitude. The mean error of a single equation of condition was found $\pm 2''$ generally.

Formulae (1)–(4) were adapted from the formulae as given by Smart (1). Formulae (9)–(12) were derived from the formulae (1)–(8) by substitution and rearrangement.

The formulae as presented in Tables I and II were all checked on several stars having known equatorial, standard and x, y coordinates. The standard coordinates of these latter stars were computed in a manner independent of formulae (1) and (2).

It may be found useful to note that formula (1), (2), (9) and (10), (3) and (4); and (11) and (12) have the same denominator.

The formulae transform to an accuracy of about one second of arc.

Preference of standard coordinates over Harvard x and y.—The question arises what the uses of these coordinate systems for future work could be. To dispense with rectangular systems altogether, and to confine oneself to the sole

TABLE I

Small Magellanic Cloud

$$\xi = \frac{10^6 \sin \Delta\alpha}{1{\cdot}39721 \cos \Delta\alpha + 4{\cdot}64244 \tan(-\delta)} \tag{1S}$$

$$\eta = \frac{957571 \cos \Delta\alpha - 288196 \tan(-\delta)}{1{\cdot}39721 \cos \Delta\alpha + 4{\cdot}64244 \tan(-\delta)} \tag{2S}$$

$$\tan \Delta\alpha = \frac{\xi}{59445 + 0{\cdot}95757\eta} \tag{3S}$$

$$\tan(-\delta) = \frac{197513 - 0{\cdot}28820\eta}{59445 + 0{\cdot}95757\eta} \cos \Delta\alpha \tag{4S}$$

$$x = +12740 + 1{\cdot}00694\xi + 0{\cdot}00108\eta \tag{5S}$$

$$y = +10423 - 0{\cdot}00135\xi + 1{\cdot}00677\eta \tag{6S}$$

$$\xi = -12642 + 0{\cdot}99312x - 0{\cdot}00108y \tag{7S}$$

$$\eta = -10370 + 0{\cdot}00133x + 0{\cdot}99332y \tag{8S}$$

$$x = \frac{1007116 \sin(\Delta\alpha + 4^m 17^s{\cdot}2) + 58834 \tan(-\delta)}{1{\cdot}39721 \cos \Delta\alpha + 4{\cdot}64244 \tan(-\delta)} \tag{9S}$$

$$y = \frac{978618 \cos(\Delta\alpha + 0^m{\cdot}19^s{\cdot}0) - 241759 \tan(-\delta)}{1{\cdot}39721 \cos \Delta\alpha + 4{\cdot}64244 \tan(-\delta)} \tag{10S}$$

$$\tan \Delta\alpha = \frac{-12642 + 0{\cdot}99312x - 0{\cdot}00108y}{49515 + 0{\cdot}00127x + 0{\cdot}95115y} \tag{11S}$$

$$\tan(-\delta) = \frac{200502 - 0{\cdot}00038x - 0{\cdot}28626y}{49515 + 0{\cdot}00127x + 0{\cdot}95115y} \cos \Delta\alpha \tag{12S}$$

TABLE II

Large Magellanic Cloud

$$\xi = \frac{10^6 \sin \Delta\alpha}{1{\cdot}73742 \cos \Delta\alpha + 4{\cdot}52612 \tan(-\delta)} \qquad (1L)$$

$$\eta = \frac{933580 \cos \Delta\alpha - 358368 \tan(-\delta)}{1{\cdot}73742 \cos \Delta\alpha + 4{\cdot}52612 \tan(-\delta)} \qquad (2L)$$

$$\tan \Delta\alpha = \frac{\xi}{73919 + 0{\cdot}93358\eta} \qquad (3L)$$

$$\tan(-\delta) = \frac{192565 - 0{\cdot}35837\eta}{73919 + 0{\cdot}93358\eta} \cos \Delta\alpha \qquad (4L)$$

$$x = +12140 + 1{\cdot}00642\xi + 0{\cdot}01104\eta \qquad (5L)$$

$$y = +10610 - 0{\cdot}01111\xi + 1{\cdot}00631\eta \qquad (6L)$$

$$\xi = -11945 + 0{\cdot}99349x - 0{\cdot}01091y \qquad (7L)$$

$$\eta = -10676 + 0{\cdot}01096x + 0{\cdot}99362y \qquad (8L)$$

$$x = \frac{1006910 \sin(\Delta\alpha + 7^{m}08^{s}{\cdot}9) + 50991 \tan(-\delta)}{1{\cdot}73742 \cos \Delta\alpha + 4{\cdot}52612 \tan(-\delta)} \qquad (9L)$$

$$y = \frac{957969 \cos(\Delta\alpha + 2^{m}39^{s}{\cdot}5) - 312607 \tan(-\delta)}{1{\cdot}73742 \cos \Delta\alpha + 4{\cdot}52612 \tan(-\delta)} \qquad (10L)$$

$$\tan \Delta\alpha = \frac{-11945 + 0{\cdot}99349x - 0{\cdot}01091y}{63952 + 0{\cdot}01023x + 0{\cdot}92762y} \qquad (11L)$$

$$\tan(-\delta) = \frac{196391 - 0{\cdot}00393x - 0{\cdot}35608y}{63952 + 0{\cdot}01023x + 0{\cdot}92762y} \cos \Delta\alpha \qquad (12L)$$

use of an equatorial system, might seem attractive were it not that, due to the curvature of the mesh lines of that system, it is rather inconvenient to rule prints accurately. Nor is it, for the same reason, so convenient and accurate to make measurements of position as a rectangular system. If then, for these reasons, it is advantageous to continue using a rectangular system, the author favours the use of the systems of standard coordinates in preference to the x, y systems because of the greater simplicity in the relations with α, δ of the ξ, η (see Tables I and II of the present paper). Since transformation between α, δ and the rectangular coordinates and vice versa may become a frequent occupation, this choice in favour of the standard coordinates may merit serious consideration.

It is a pleasure to thank Mr D. Lodge for his efficient help in calculating standard coordinates for a number of stars. I am indebted to Mr J. v. B. Lourens of the Royal Observatory, Cape, for advice on the approximate methods (2) in working out standard coordinates.

Radcliffe Observatory,
Pretoria:
1959 *February* 24.

References

(1) W. M. Smart, *Spherical Astronomy*, p. 282 ff, 1931.
(2) C. Vick, *Hamburg Mitteilungen*, Bd. 5, No. 19, p. 93.

A SURVEY OF RADIO SOURCES AT A FREQUENCY OF 159 Mc/s*

D. O. Edge, J. R. Shakeshaft, W. B. McAdam, J. E. Baldwin and S. Archer

Summary

The Cambridge four-element interferometer has been used at a frequency of 159 Mc/s to determine positions and flux densities for 471 radio sources lying between declinations $-22°$ and $+71°$. Information concerning the angular diameters of some of the brighter sources has also been obtained and the majority of these have diameters less than 6′.

Most sources have an isotropic distribution but there is a concentration of the intense ones towards the galactic plane. There is also evidence for an excess of sources in the region of the belt of background radiation crossing the galactic plane at $l=0°$.

If the number-flux density distribution is compared with that expected from a uniform distribution of sources in space, a deficit of the more intense sources is found.

THE POSITIONS, FLUX DENSITIES AND ANGULAR DIAMETERS OF 64 RADIO SOURCES OBSERVED AT A FREQUENCY OF 178 Mc/s*

B. Elsmore, M. Ryle and Patricia R. R. Leslie

Summary

Measurements have been made at a frequency of 178 Mc/s of the position, flux densities and angular diameters of 64 radio sources between declinations $+65°$ and $-06°$, both to provide a system of reference sources and to aid in a further search for optical identifications.

The observations were made with a transit interferometer in which one aerial had dimensions 1450 ft × 65 ft; this element was separated by 2570 ft from a second smaller aerial mounted on a North–South railway track 1000 ft in length. In the present measurements, observations of each source were made with eight different positions of the movable aerial and the declination was derived from the relative phases of the interference patterns recorded with the different positions. The right ascension was determined in the usual way from the mean of the observed phases.

The average probable errors of the 64 positions are $\pm 1^s{\cdot}5$ in R.A. and $\pm 1'{\cdot}5$ of arc in declination. The optical identification of six of the sources has been confirmed by these observations.

* The full text of these papers is published in *Memoirs of the R.A.S.*, **68**, Part II, 1959.

РЕЗЮМЕ ДОКЛАДОВ, В ПЕРЕВОДЕ НА РУССКИЙ ЯЗЫК

ДВИЖЕНИЯ В СОЛНЦЕ НА УРОВНЕ ФОТОСФЕРЫ. VIII. ВРАЩЕНИЕ СОЛНЦА И ФОТОСФЕРНАЯ ЦИРКУЛЯЦИЯ

Г. Х. Пласкетт

По спектрограммам, полученным 21–23 апреля 1953 г., были измерены в 332 точках видимой поверхности Солнца скорости по лучу зрения. Для каждой точки лучевая скорость может быть выражена как линейная функция компонентов скорости, направленных к западу и к северу. Решения по способу наименьших квадратов таких наблюдательных уравнений для различных широт указывают на асимметрию вращательных скоростей в экваториальной зоне и на наличие меридиональных течений. Эти движения указывают на существование в фотосфере циркуляции, аналогичной циркуляции, имеющейся в верхней атмосфере Земли. Эта гипотеза рассматривается в свете исследования Лайтхилла, и предлагается наблюдательный метод ее проверки.

ИНТЕНСИВНОСТЬ СОЛНЕЧНОГО ИЗЛУЧЕНИЯ У 11 μ

Ф. Сайеди и Р. М. Гуди

Наблюдение излучения центра солнечного диска вблизи $\lambda = 11{,}10\,\mu$ (901 $см^{-1}$) путем непосредственного сравнения с излучением черного тела при 1300 °К было произведено весной 1958 г. Интенсивность солнечного излучения была приближенно редуцирована к излучению черного тела при помощи вращающегося сектора, и отношение интенсивностей было затем измерено при помощи калиброванного электрического ослабителя, т.е. система была независима от линейности приемника. Единственные вспомогательные измерения, которые требовались, это измерения абсолютной отражательной способности одного зеркала и изменения отражательной способности с изменением угла отражения другого зеркала.

Ширина щели $0{,}031\mu$ или 2,5 $см^{-1}$ была достаточно мала, чтобы впустить лишь атмосферное "окно", для которого поглощение описывается законом Ламберта, что позволяет провести экстраполяцию к интенсивности вне Земли.

Среднее взвешенное из пяти измерений центральной интенсивности составляет

$$I_{\odot}(11{,}10\,\mu) = 2{,}408 \pm 0{,}016 \times 10^{10}\ эрг/см^2\ стерадиан\ .\ сек$$

(в 1см интервала длин волн). Это значение эквивалентно цен тральной температуре $T_{\odot}(11{,}10\,\mu) = 5036 \pm 30$ °К.

МАГНИТНОЕ И ДИНАМИЧЕСКОЕ ПОЛЯ ВНЕ ПРОТОЗВЕЗДЫ

Л. Местел

Сжимающаяся протозвезда, формирующаяся в магнитном облаке, сохраняет свой магнитный поток, если только плотность плазмы не становится слишком низкой. В этой статье исследуется структура внешнего поля и его влияние на течение вещества. Предполагается, что центробежная сила все время пренебрежимо мала, а звезда в облаке неподвижна. Поле в звезде и на бесконечности считается однородным, а поток—изотермическим.

Возможные равновесные поля включают в себя:

1. Полоидальное поле, со всеми силовыми линиями, уходящими в бесконечность, но с небольшим тороидальным компонентом, достаточно сильным, чтобы сохранить центробежное поле слабым несмотря на втекание вещества. Это поле слабо на экваторе, но силовые линии претерпевают там резкие извивы, порождая самофокусирующийся экваториальный разряд.

2. Полоидальное поле с частью линий конечной протяженности, отделенных кольцом нейтральных точек типа X от бесконечных линий поля, которое имеет структуру, подобную полю, описанному в п. 1.

3. Скрученное без скручивающего усилия и почти бессиловое поле, ограниченное конечной поверхностью S, и почти безвихревое поле вне S.

Если поле облака первоначально содержит тороидальный поток, пронизывающий полоидальные петли, то получается поле типа 3; в противном случае типы 1 и 2 будут равновесными полями.

Наличие поля несколько изменяет проблему аккреции. Существуют решения как со сверхзвуковыми, так и с дозвуковыми скоростями на бесконечности, обуславливающие соответственно повышенную и пониженную скорости аккреции. При отсутствии на бесконечности сильного внешнего поля давления система, по-видимому, приближается к состоянию с более низкой скоростью, т.е. наличие поля существенно уменьшает скорость аккреции по сравнению с величиной, вычисленной Бонди.

ЗАМЕЧАНИЕ О МАГНИТНОМ ТОРМОЖЕНИИ ВРАЩАЮЩЕЙСЯ ЗВЕЗДЫ

Л. Местел

Произвольное полоидальное магнитное поле, соединяющее быстро вращающуюся звезду с медленно вращающейся оболочкой, будет так закручено, что будет переносить угловой момент через промежуточную область с низкой плотностью. Поле будет создавать равные и противоположно направленные пары сил, приложенные соответственно к звезде и к оболочке. В промежуточной области поле, вероятно, не будет создавать больших сил сжатия и будет приближенно бессиловым. В отличие от *абсолютно* бессилового поля, рассмотренного в предыдущей работе автора, которое не может возникать в результате деформации полоидального поля, в данном случае не будет возникать тороидального потока, замыкающего полоидальную петлю, а электрический ток не будет течь в том же самом направлении во всех точках петли.

ЗВЕЗДНЫЕ ГРУППЫ. IV. ГРУППА ЗВЕЗД С БОЛЬШИМИ СКОРОСТЯМИ ГРУМБРИДЖ 1830 И ЕЕ СВЯЗЬ С ШАРОВЫМИ СКОПЛЕНИЯМИ

О. Дж. Эгген и А. Р. Сандидж

Имеющиеся данные о собственных движениях и лучевых скоростях были использованы для доказательства существования движущейся группы субкарликов (группа звезд Грумбридж 1830), включающей звезду RR Lyr. На основании существующей зависимости между наблюденным ультра фиолетовым избытком и смещением ниже нормальной главной последовательности субкарлики в группе Грумбридж 1830 были отождествлены как звезды главной последовательности шаровых скоплений. Это отождествление приводит к значению модуля $m-M=14^{m},2$ для шарового скопления M13, в результате чего оказывается что для двух переменных типа RR Lyr $Mv\sim+0^{m},5$, а для наиболее ярких звезд скопления, $Mv=-2^{m},3$. Показывается, что сама звезда RR Lyr, для которой на основе группового параллакса мы имеем $Mv\sim+0^{m},8$, удовлетворяет соотношению период-амплитуда для переменных в скоплении M3 и что она имеет цветовой избыток (покраснение), равный $0^{m},05$ по отношению к этим звездам. Приравнивая светимость RR Lyr к средней светимости переменных в M3, мы получаем для модуля скопления значение $m-M=15^{m},0$. Мы не произвели определение модуля обычным логическим способом путем совмещения главных последовательностей в M3 и группе Грумбридж 1830, так как показатели цвета звезд главной последовательности в M3 могут содержать систематическую ошибку.

Так как присутствие переменных типа RR Lyr в звездных группах может давать единственную возможность точного определения светимостей этих звезд, представляется важным произвести систематические поиски таких групп. Мы привели в таблице имеющиеся данные относительно (1) всех звезд, отнесенных к субкарликам на основании особенностей в их спектрах, (2) звезд, которые, судя по их наблюденным ультрафиолетовым избыткам, по всей вероятности являются крайними субкарликами, хотя и считаются объектами главной последовательности, и (3) звезд, которые могут быть либо гигантами, либо субгигантами, либо звездами горизонтальной ветви шаровых скоплений. Пространственные скорости звезд этих трех категорий были вычислены с параллаксами, определенными при помощи ($Mv, B-V$)-диаграммы для скопления M13, прокалиброванной используя группу Грумбридж 1830. Показано, что с большой степенью вероятности некоторое число этих звезд обладает общим движением в пространстве и что с привлечением дополнительного материала удается обнаружить ряд групп, аналогичных группе Грумбридж 1830. Так же точно показано, что пространственные скорости четырех переменных типа RR Lyr с относительно хорошо определенными собственными движениями совпадают с движениями некоторых окрестных субкарликов, что дало $Mv\sim+0^{m},6$ для этих четырех переменных.

О СУЩЕСТВОВАНИИ СУБКАРЛИКОВ НА ДИАГРАММЕ (M_{Bol}, $\log T_e$)

А. Р. Сандидж и О. Дж. Эгген

Рассматривается влияние ослабления фраунгоферовых линий на наблюдаемые показатели цвета звезд. Учтены задержка непрерывного излучения линиями и обусловленное линиями изменение температурного распределения в солнечной атмосфере. Если бы все источники, создающие линии, были удалены с Солнца, то изменение наблюдаемых показателей цвета, согласно теории, составляло бы $\Delta(U-B)=0^{m},32$ и $\Delta(B-V)=0^{m},17$. Эти изменения определяют " линию тепличного эфекта " (" blanketing line ") на диаграмме ($U-B, B-V$),

из которой поправка к наблюдаемому показателю цвета $B-V$, обусловленная ослаблением линиями, может быть найдена из наблюдаемого ультрафиолетового избытка $\delta(U-B)$.

Приведены звездные величины и цвета субкарликов, лежащих более чем на $0^m,25$ ниже нормальной главной последовательности. Поправки за цвет, выведенные из наблюдаемых ультрафиолетовых избытков, приданы к наблюдаемым показателям цвета $B-V$. Эти поправки являются достаточными, чтобы передвинуть умеренные субкарлики на главную последовательность Гиад. Делается вывод, что большинство субкарликов находится ниже главной последовательности на диаграмме (M_V, $B-V$) только вследствие влияния слабых фраунгоферовых линий на их наблюдаемые цвета.

Члены движущейся группы Грумбридж 1830 не полностью восстанавливаются в главной последовательности и, возможно, что эти звезды действительно лежат ниже главной последовательности на диаграмме (M_{Bol}, $\log T_e$). Предварительные заключения из этих данных следующие: (1) непрозрачность субкарликов скорее, по-видимому, обусловлена свободно-свободными переходами H и He, чем фотоэлектрическим поглощением тяжелыми элементами; (2) отношение H/He для звезд группы Грумбридж 1830 может немного отличаться от аналогичного отношения для звезд скопления Гиад.

Тепличная (*blanketing*) модель дает соотношение между разностью звездных величин любой звезды от главной последовательности Гиад и наблюдаемым УФ-избытком цвета. Это соотношение применяется к звездам в различных галактических скоплениях и к звездам общего поля, откуда получаются результаты: (1) метод подгонки главных последовательностей для определения модуля расстояний галактических скоплений ошибочен, если не внесены поправки за различные УФ-избытки; (2) наблюдаемый разброс в $0^m,10$ в УФ-избытках звезд поля, которые обычно называются "карликами главной последовательности", показывает, что полная истинная ширина главной последовательности, определяемая этими звездами, составляет по крайней мере $0^m,60$. Так как звезды поля с сильными линиями, субкарлики и звезды различных галактических скоплений образуют континуум на диаграмме ($B-V$), ($U-B$), то представляется вероятным, что (а) субкарлики образуют континуум на диаграмме (M_V, $B-V$), объединяясь с более нормальными звездами с сильными линиями, и (б) существуют различия между содержанием тяжелых элементов в отдельных звездах поля и в звездах различных галактических скоплений.

РАДИОИЗЛУЧЕНИЕ НОРМАЛЬНЫХ ГАЛАКТИК. I. НАБЛЮДЕНИЯ M31 И M33 НА ЧАСТОТЕ 158 И 237 МГЦ.

Р. Х. Браун и С. Хазард

Было проведено изучение радиоизлучения ярких нормальных галактик на частоте 158 Мгц. В данной статье сообщается о результатах, относящихся к M31 и M33. Интегральные радиовеличины (m_r) этих двух галактик были измерены и сравнены с их фотографическими величинами (m_p); найдено, что разность (m_r-m_p) почти одинакова для обеих галактик.

Распределение интенсивности поперек M31 указывает на наличие двух главных компонентов: диска и короны. Корона обусловливает 90% общего излучения, имеет отношение видимых осей, равное примерно 0,6; ее большая ось примерно в три раза длиннее большой оси видимой туманности. Результаты показывают, что M33 также имеет корону; эллиптичность, излучение и размеры короны по отношению к видимой туманности весьма близки к значениям, найденным для M31.

Сравнение M31 и M33 с нашей Галактикой указывает на то, что излучение короны Галактики существенно сильнее, чем изучение корон указанных двух галактик.

КОСМОЛОГИЯ СТАЦИОНАРНОГО СОСТОЯНИЯ, РАССМОТРЕННАЯ СОГЛАСНО ОБЩЕЙ ТЕОРИИ ОТНОСИТЕЛЬНОСТИ

В. Дэйвидсон

Интерпретация космологии стационарного состояния с точки зрения общей теории относительности, начатая Мак-Кри, в данной работе продолжена путем исследования внешней и внутренней метрик для статического наложения сферически симметричной сконцентрированной или разреженной массы на "стационарную" среду.

Найдено, что постоянная полная плотность ρ_0 и отрицательное давление p_0 ($=-\rho_0$), по-видимому, представляют собой характеристики естественного состояния относительной

устойчивости стационарной среды. Исследование показывает, что это состояние может существовать между галактиками в стационарной модели Вселенной. Рассмотрение мировых линий среды в окрестности статического возмущения приводит к выводу, что подобное возмущение обладает способностью либо противодействовать космическому отталкиванию, либо усиливать его в зависимости от того представляет ли оно концентрацию или разрежение материи по отношению к естественному состоянию. Предлагается механизм зарождения материи, при котором скорость зарождения сильно зависит от локального гравитационного влияния; она оказывается положительной там, где среда расширяется, и отрицательной (аннигиляция) там, где она сжимается.

Определены пределы размеров и плотности для статических возмущений естественного состояния. Показано, что в возмущенной среде знак гравитационного поля зависит от локального состояния среды и в случае разрежения плотность инерции, в ньютоновском смысле, оказывается отрицательной. Указаны теоретические условия, необходимые для относительной устойчивости естественного состояния.

NOTICE TO AUTHORS

Presentation of Papers at Meeting

At some meetings of the Society the background and conclusions of selected papers are presented and then discussed. In order to assist the Secretaries in the selection of papers for such meetings, authors are asked to let the Society know, when submitting papers, whether they would be willing to give an account of their paper, if requested.

The attention of authors resident abroad is drawn to the fact that the Society welcomes information about their work. The Secretaries would be happy to consider having such work described at a meeting, in accordance with the author's wishes, either by a Secretary or other Fellow.

Publication of Papers

1. *General.*—It is the aim of the Society to be of the greatest possible service in disseminating astronomical results and ideas to the scientific community with the utmost possible speed. Contributors are accordingly urged to give the most careful consideration to the presentation of their work, for attention to detail will assuredly result in a substantial saving of time.

It is the practice of the Society to seek a referee's opinion on nearly every paper submitted for publication in *Monthly Notices*; experience has shown that frequently the comments of referees have enabled authors to improve the presentation of their work and so increase its scientific value.

2. *Communication.*—Papers must be communicated to the Society by a Fellow. They should be accompanied by a summary at the *beginning* of the paper summarizing briefly the content of the paper, and drawing attention to important new information and to the main conclusions. The summary should be intelligible to itself, without reference to the paper, to a reader with some knowledge of the subject; it should not normally exceed 200 words in length. Authors are requested to submit both MSS. in duplicate. These should be typed using double spacing and leaving a margin of not less than one inch on the left-hand side. Corrections to the MSS. should be made in the text and not in the margin. By Council decision, MSS. of accepted papers are retained by the Society for one year after publication; unless their return is then requested by the author they are destroyed.

3. *Presentation.*—Authors are allowed considerable latitude, but they are requested to follow the general style and arrangement of *Monthly Notices*. References to literature should be given either in the traditional form of a numbered list at the end of the paper or as prescribed in *Notes on the Preparation of Papers to be Communicated to the Royal Society*.

4. *Notation.*—For technical astronomical terms, authors should conform as far as the recommendations of Commission 3 of the International Astronomical Union (Trans. *I.A.U.*; Vol. VI, p. 345, 1938). Council has decided to adopt the I.A.U. abbreviations for constellations where contraction is desirable (Vol. IV, p. [illegible]). In general matters, authors should follow the recommendations in *Symbols, Units and Abbreviations* (London: Royal Society, 1951) except where these conflict with I.A.U. practice.

5. *Diagrams.*—These should be designed to appear upright on the page and be about twice the size required in print and prepared for direct photographic reproduction except for the lettering, which should be inserted [illegible]. Legends should be given in the manuscript indicating where in the text the diagrams should appear. Blocks are retained by the Society for 10 years; unless the author requires them before the end of this period they are then destroyed. Duplicates or prints of the diagrams should accompany each manuscript.

6. *Tables.*—These should be arranged so that they can be printed [illegible].

7. *Proofs.*—Authors are liable for costs of alteration exceeding [illegible] composition. It is therefore in their own and the Society's interest [illegible] maximum conciseness and simplification of symbols and equations consistent [illegible]

устойчивости стационарной среды. Исследование показывает, что это состояние может существовать между галактиками в стационарной модели Вселенной. Рассмотрение мировых линий среды в окрестности статического возмущения приводит к выводу, что подобное возмущение обладает способностью либо противодействовать космическому отталкиванию, либо усиливать его в зависимости от того представляет ли оно концентрацию или разрежение материи по отношению к естественному состоянию. Предлагается механизм зарождения материи, при котором скорость зарождения сильно зависит от локального гравитационного влияния; она оказывается положительной там, где среда расширяется, и отрицательной (аннигиляция) там, где она сжимается.

Определены пределы размеров и плотности для статических возмущений естественного состояния. Показано, что в возмущенной среде знак гравитационного поля зависит от локального состояния среды и в случае разрежения плотность инерции, в ньютоновском смысле, оказывается отрицательной. Указаны теоретические условия, необходимые для относительной устойчивости естественного состояния.

NOTICE TO AUTHORS

Presentation of Papers at Meeting

At some meetings of the Society the background and conclusions of selected papers are presented and then discussed. In order to assist the Secretaries in the selection of papers for such meetings, authors are asked to let the Society know, when submitting papers, whether they would be willing to give an account of their paper, if requested.

The attention of authors resident abroad is drawn to the fact that the Society welcomes information about their work. The Secretaries would be happy to consider having such work described at a meeting, in accordance with the author's wishes, either by a Secretary or other Fellow.

Publication of Papers

1. *General.*—It is the aim of the Society to be of the greatest possible service in disseminating astronomical results and ideas to the scientific community with the utmost possible speed. Contributors are accordingly urged to give the most careful consideration to the presentation of their work, for attention to detail will assuredly result in a substantial saving of time.

It is the practice of the Society to seek a referee's opinion on nearly every paper submitted for publication in *Monthly Notices*; experience has shown that frequently the comments of referees have enabled authors to improve the presentation of their work and so increase its scientific value.

2. *Communication.*—Papers must be communicated to the Society by a Fellow. They should be accompanied by a summary at the *beginning* of the paper conveying briefly the content of the paper, and drawing attention to important new information and to the main conclusions. The summary should be intelligible in itself, without reference to the paper, to a reader with some knowledge of the subject; it should not normally exceed 200 words in length. **Authors are requested to submit MSS. in duplicate.** These should be typed using double spacing and leaving a margin of not less than one inch on the left-hand side. Corrections to the MSS. should be made in the text and not in the margin. By Council decision, MSS. of accepted papers are retained by the Society for one year after publication; unless their return is then requested by the author they are destroyed.

3. *Presentation.*—Authors are allowed considerable latitude, but they are requested to follow the general style and arrangement of *Monthly Notices*. References to literature should be given either in the traditional form of a numbered list at the end of the paper, or as prescribed in *Notes on the Preparation of Papers to be Communicated to the Royal Society*.

4. *Notation.*—For technical astronomical terms, authors should conform closely to the recommendations of Commission 3 of the International Astronomical Union (*Trans. I.A.U.*; Vol. VI, p. 345, 1938). Council has decided to adopt the I.A.U. 3-letter abbreviations for constellations where contraction is desirable (Vol. IV, p. 221, 1932). In general matters, authors should follow the recommendations in *Symbols, Signs and Abbreviations* (London: Royal Society, 1951) except where these conflict with I.A.U. practice.

5. *Diagrams.*—**These should be designed to appear upright on the page, drawn about twice the size required in print and prepared for direct photographic reproduction except for the lettering, which should be inserted in pencil.** Legends should be given in the manuscript indicating where in the text the figure should appear. Blocks are retained by the Society for 10 years; unless the author requires them before the end of this period they are then destroyed. **Rough copies or prints of the diagrams should accompany each manuscript.**

6. *Tables.*—These should be arranged so that they can be printed upright on the page.

7. *Proofs.*—Authors are liable for costs of alteration exceeding 5 per cent of composition. It is therefore in their own and the Society's interests to seek the maximum conciseness and simplification of symbols and equations consistent with clarity.

CONTENTS

Printed in London by Taylor & Francis, Ltd., 1959 December